University of Tennessee, Knoxville
TRACE: Tennessee Research and Creative Exchange

Doctoral Dissertations | Graduate School

6-1986

# Development and Applicability of a Mathematical Model for the High Speed Melt Spinning of Crystallizable Polymers

Kenneth F. Zieminski
*University of Tennessee - Knoxville*

Follow this and additional works at: https://trace.tennessee.edu/utk_graddiss

Part of the Engineering Commons

## Recommended Citation

Zieminski, Kenneth F., "Development and Applicability of a Mathematical Model for the High Speed Melt Spinning of Crystallizable Polymers. " PhD diss., University of Tennessee, 1986.
https://trace.tennessee.edu/utk_graddiss/2522

This Dissertation is brought to you for free and open access by the Graduate School at TRACE: Tennessee Research and Creative Exchange. It has been accepted for inclusion in Doctoral Dissertations by an authorized administrator of TRACE: Tennessee Research and Creative Exchange. For more information, please contact trace@utk.edu.

To the Graduate Council:

I am submitting herewith a dissertation written by Kenneth F. Zieminski entitled "Development and Applicability of a Mathematical Model for the High Speed Melt Spinning of Crystallizable Polymers." I have examined the final electronic copy of this dissertation for form and content and recommend that it be accepted in partial fulfillment of the requirements for the degree of Doctor of Philosophy, with a major in Polymer Engineering.

Joseph E. Spruiell, Major Professor

We have read this dissertation and recommend its acceptance:

D. C. Bogue, E. S. Clark, L. Wadsworth

Accepted for the Council:

Carolyn R. Hodges

Vice Provost and Dean of the Graduate School

(Original signatures are on file with official student records.)

To the Graduate Council:

I am submitting herewith a dissertation written by Kenneth F. Zieminski entitled "Development and Applicability of a Mathematical Model for the High Speed Melt Spinning of Crystallizable Polymers." I have examined the final copy of this dissertation for form and content and recommend that it be accepted in partial fulfillment of the requirements for the degree of Doctor of Philosophy, with a major in Polymer Engineering.

Joseph E. Spruiell, Major Professor

We have read this dissertation
and recommend its acceptance:

Donald R. Bogue

Edward S. Clark

Larry C. Wadsworth

Accepted for the Council:

Vice Provost
and Dean of The Graduate School

# DEVELOPMENT AND APPLICABILITY OF A MATHEMATICAL MODEL FOR THE HIGH SPEED MELT SPINNING OF CRYSTALLIZABLE POLYMERS

A Dissertation

Presented for the

Doctor of Philosophy

Degree

The University of Tennessee, Knoxville

Kenneth F. Zieminski

June 1986

ACKNOWLEDGMENTS

The author would like to thank his advisor, Professor Joseph E. Spruiell, for his guidance during the past four years. I would also like to thank Professors D. C. Bogue, E. S. Clark and L. Wadsworth for serving on my committee. I appreciate all of the advice, although not always welcome, from my fellow graduate students, both past and present, in the Materials Science and Engineering and Chemical Engineering Departments at the University of Tennessee.

This project would not have been completed without the help of Ted and Ron from the electronics shop and Tommy, Jack and Doug from the machine shop.

I would also like to thank the financial sponsorship of the Material Science and Engineering Department and to acknowledge the contribution of processing equipment and suggestions from Dr. J. Southern and Mr. W. Nunning of the Monsanto Fibers and Intermediates Company in Pensacola, Florida.

ABSTRACT

A mathematical model was developed to describe the high speed melt spinning behavior of crystallizable polymers. This model included the effects of acceleration, gravity and friction on the kinematics of the process, temperature and molecular orientation on the crystallization kinetics of the polymer and temperature, molecular weight and crystallinity on the elongational viscosity of the material. Experimental online diameter, birefringence and temperature profiles were obtained for a 12000 Mn nylon-66 at 2.5 gm/min spun at take-up speeds ranging from 2800 to 6600 meters/minute. These profiles were qualitatively and reasonably quantitatively in agreement with the predicted profiles. They indicated that orientation induced crystallization occurs at spinning speeds greater than 4000 meters/minute. The experimental diameter and birefringence profiles were compared to those predicted by the model using Avrami indices of 3, 2 and 1. There was a small increase in the crystalline index at the lower speeds with decreasing index. The effect of the strain hardening was more significant at the higher speeds, this being shown by decreasing the exponent in the relationship for the crystallinity on the elongational viscosity.

The model was also applied to two polypropylenes of different molecular weight. There was very good agreement between the predicted and experimental diameter and birefringence profiles for both molecular weights. There was some differences in the temperature profile comparisons, but there was good agreement between the predicted and

experimental temperatures and positions where the crystallization is first observed. The position and duration of the temperature plateaus were qualitatively in good agreement with those predicted.

The model developed in this study indicates that high spinning speeds provide a high stress environment which increases the molecular orientation within the fiber. It is this higher molecular orientation which is the driving force for rapid crystallization on the spinline. This rapid crystallization causes a strain hardening preventing any further drawdown in the fiber diameter and an abrupt rise in the birefringence. This behavior closely corresponds to the observed spinline profiles.

TABLE OF CONTENTS


| CHAPTER | | PAGE |
|---|---|---|
| 1 | INTRODUCTION | 1 |
| 2 | LITERATURE REVIEW | 6 |
| | Melt Spinning Process | 6 |
| | Dynamics | 6 |
| | Rheology | 9 |
| | Heat Transfer | 10 |
| | Crystallization and Orientation | 13 |
| | Structure Development | 17 |
| | Mathematical Modeling | 21 |
| | High Speed Spinning | 25 |
| | Crystallization Kinetics | 32 |
| | Nylon-66 | 39 |
| | Synthesis | 39 |
| | Chemical Behavior | 40 |
| | Physical Properties | 41 |
| | Crystallography | 42 |
| | Crystallization Kinetics | 44 |
| | Structure | 45 |
| | Effect of Moisture | 47 |
| 3 | DEVELOPMENT OF FUNDAMENTAL EQUATIONS | 50 |
| | Force Balance | 50 |
| | Energy Balance | 55 |
| 4 | SIMULATION OF THE MELT SPINNING PROCESS | 58 |
| | Mathematical Model | 58 |
| | Force Balance | 58 |
| | Energy Balance | 60 |
| | Birefringence and Molecular Orientation | 61 |
| | Crystallization Kinetics | 62 |
| | Physical Properties | 63 |
| | Nylon-66 | 63 |
| | Polypropylene | 66 |
| | Continuous System Modeling Program (CSMP) | 67 |

CHAPTER PAGE

5 EXPERIMENTAL APPARATUS AND PROCEDURE . . . . . 68

Melt Spinning Operations . . . . . 68

Description of the Apparatus . . . . . 68
Experimental Procedure . . . . . 72

Diameter and Birefringence Measurement . . . . . 74

Temperature Measurement . . . . . 75

Spinline Force Measurement . . . . . 77

Characterization of Nylon-66 Fibers . . . . . 78

Dilute Solution Viscosity . . . . . 78
Capillary Rheometry . . . . . 80
Wide Angle X-ray Scattering . . . . . 81
Crystalline Orientation Functions . . . . . 81
Small Angle X-ray Scattering . . . . . 82
Density . . . . . 82
Differential Scanning Calorimetry . . . . . 82
Mechanical Properties . . . . . 83

6 DATA ANALYSIS . . . . . 84

Diameter and Birefringence . . . . . 84

Crystalline Index . . . . . 84

Density . . . . . 84
Differential Scanning Calorimetry . . . . . 85

Small Angle X-ray Scattering . . . . . 85

Crystalline and Amorphous Orientation Functions . . . . . 86

Mechanical Properties . . . . . 88

7 RESULTS AND DISCUSSION . . . . . 90

Predictions of the Model for Nylon-66 . . . . . 90

Online Experimental Results for Nylon-66 . . . . . 107

Comparison of Model Predictions and Online Experimental

Profiles for Nylon-66 . . . . . 119

Structure and Properties of Conditioned Nylon-66 Fibers . . 134

CHAPTER PAGE

Application of the Model to the Melt Spinning of Polypropylene . . . . . 142

8 CONCLUSIONS AND RECOMMENDATIONS . . . . . 159

REFERENCES . . . . . 161

APPENDIXES . . . . . 175

A. CSMP Program for Nylon-66 Melt Spinning . . . . . 176

B. CSMP Program for Polypropylene Melt Spinning . . . . . 179

VITA . . . . . 182

LIST OF TABLES


| TABLE | | PAGE |
|---|---|---|
| 5.1 | Specification of Monsanto dies. . . . . | 70 |
| 5.2 | Intrinsic viscosity of Monsanto nylon-66. . . . . | 79 |
| 5.3 | Shear viscosity of Monsanto nylon-66. . . . . | 80 |
| 6.1 | Directional cosines for nylon-66 unit cells. . . . . | 88 |
| 7.1 | Summary of experimental processing conditions. . . . . | 90 |
| 7.2 | Polypropylene spinning conditions (12). . . . . | 146 |

LIST OF FIGURES


| FIGURE | | PAGE |
|---|---|---|
| 3.1 | Schematic representation of the melt spinline. . . . . | 51 |
| 5.1 | Schematic of the experimental apparatus. . . . . | 69 |
| 5.2 | Schematic diagram of the Monsanto spinneret. . . . . | 71 |
| 5.3 | Schematic of the temperature measuring apparatus. . . . . | 76 |
| 7.1 | Predicted velocity profiles for nylon-66 with a mass throughput of 2.5 gm/min and n = 3. . . . . | 91 |
| 7.2 | Predicted diameter profiles for nylon-66 with a mass throughput of 2.5 gm/min and n = 3. . . . . | 93 |
| 7.3 | Predicted birefringence profiles for nylon-66 with a mass throughput of 2.5 gm/min and n = 3. . . . . | 94 |
| 7.4 | Predicted crystalline index profiles for nylon-66 with a mass throughput of 2.5 gm/min and n = 3. . . . . | 95 |
| 7.5 | Predicted temperature profiles for nylon-66 with a mass throughput of 2.5 gm/min and n = 3. . . . . | 97 |
| 7.6 | Predicted stress profiles for nylon-66 with a mass throughput of 2.5 gm/min and n = 3. . . . . | 98 |
| 7.7 | Predicted amorphous orientation function profiles for nylon-66 with a mass throughput of 2.5 gm/min and n = 3. . | 100 |
| 7.8 | Predicted rheological, drag, inertial and gravitational force profiles for nylon-66 at a spinning speed of 2800 meters/minute. . . . . | 101 |
| 7.9 | Predicted rheological, drag, inertial and gravitational force profiles for nylon-66 at a spinning speed of 3200 meters/minute. . . . . | 102 |
| 7.10 | Predicted rheological, drag, inertial and gravitational force profiles for nylon-66 at a spinning speed of 4000 meters/minute. . . . . | 103 |
| 7.11 | Predicted rheological, drag, inertial and gravitational force profiles for nylon-66 at a spinning speed of 5400 meters/minute. . . . . | 104 |

FIGURE PAGE


7.12 Predicted rheological, drag, inertial and gravitational force profiles for nylon-66 at a spinning speed of 6300 meters/minute. . . . . 105

7.13 Predicted rheological, drag, inertial and gravitational force profiles for nylon-66 at a spinning speed of 6600 meters/minute. . . . . 106

7.14 Predicted velocity profiles for nylon-66 with a mass throughput of 2.5 gm/min and n = 1. . . . . 108

7.15 Predicted temperature profiles for nylon-66 with a mass throughput of 2.5 gm/min and n = 1. . . . . 109

7.16 Predicted crystalline index profiles for nylon-66 with a mass throughput of 2.5 gm/min and n = 1. . . . . 110

7.17 Experimental diameter profiles for nylon-66 with a mass throughput of 2.5 gm/min. . . . . 111

7.18 Experimental birefringence profiles for nylon-66 with a mass throughput of 2.5 gm/min. . . . . 113

7.19 Experimental temperature profiles for nylon-66 with a mass throughput of 2.5 gm/min. . . . . 114

7.20 Experimental temperature profiles for nylon-66 with a mass throughput of 2.8 gm/min. . . . . 115

7.21 Experimental temperature profiles for nylon-66 with a mass throughput of 4 gm/min. . . . . 116

7.22 Experimental temperature profiles for nylon-66 with a mass throughput of 5.2 gm/min. . . . . 117

7.23 Experimental temperature profiles for nylon-66 with a mass throughput of 5.2 gm/min with transverse air flow. . 118

7.24 Comparison of predicted and experimental diameter profiles for nylon-66 with n = 1. . . . . 120

7.25 Comparison of predicted and experimental diameter profiles for nylon-66 with n = 2. . . . . 121

7.26 Comparison of predicted and experimental diameter profiles for nylon-66 with n = 3. . . . . 122

7.27 Comparison of predicted and experimental birefringence profiles for nylon-66 with n = 1. . . . . 123

FIGURE PAGE

7.28 Comparison of predicted and experimental birefringence profiles for nylon-66 with n = 2. . . . . 124

7.29 Comparison of predicted and experimental birefringence profiles for nylon-66 with n = 3. . . . . 125

7.30 Comparison of predicted and experimental diameter profiles for nylon-66 using a value of 2 for the exponent in the relationship for the effect of crystallinity on the elongational viscosity. . . . . 126

7.31 Comparison of predicted and experimental birefringence profiles for nylon-66 using a value of 2 for the exponent in the relationship for the effect of crystallinity on the elongational viscosity. . . . . 127

7.32 Predicted crystalline index profiles for nylon-66 using a value of 2 for the exponent in the relationship for the effect of crystallinity on the elongational viscosity. . 129

7.33 Predicted temperature profiles for nylon-66 using a value of 2 for the exponent in the relationship for the effect of crystallinity on the elongational viscosity. . . . . 130

7.34 Final fiber birefringence as a function of spinning speed for nylon-66. . . . . 135

7.35 Final fiber density as a function of spinning speed for nylon-66 at a mass throughput of 2.5 gm/min. . . . . 136

7.36 Final fiber crystalline index as a function of spinning speed for nylon-66 at a mass throughput of 2.5 gm/min. . 137

7.37 Crystal perfection index in the final fiber as a function of spinning speed for nylon-66 at a mass throughput of 2.5 gm/min. . . . . 139

7.38 Crystalline and amorphous orientation functions in the final fiber as a function of spinning speed for nylon-66 at a mass throughput of 2.5 gm/min. . . . . 140

7.39 Long period in the final fiber as a function of spinning speed for nylon-66 at a mass throughput of 2.5 gm/min. . 141

7.40 Final fiber modulus as a function of spinning speed for nylon-66. . . . . 143

7.41 Final fiber tenacity as a function of spinning speed for nylon-66. . . . . 144

FIGURE PAGE

7.42 Final fiber elongation to break as a function of spinning speed for nylon-66. . . . . 145

7.43 Comparison of predicted and experimental diameter profiles for a 178,000 Mw polypropylene with a mass throughput of 1.68 gm/min. . . . . 147

7.44 Comparison of predicted and experimental birefringence profiles for a 178,000 Mw polypropylene with a mass throughput of 1.68 gm/min. . . . . 148

7.45 Comparison of predicted and experimental temperature profiles for a 178,000 Mw polypropylene with a mass throughput of 1.68 gm/min. . . . . 150

7.46 Comparison of the predicted and experimental temperatures at which crystallization is first observed for the 178,000 Mw polypropylene. . . . . 151

7.47 Comparison of the predicted and experimental distance from the spinneret at which crystallization is first observed for the 178,000 Mw polypropylene. . . . . 152

7.48 Comparison of predicted and experimental diameter profiles for a 237,000 Mw polypropylene with a mass throughput of 1.68 gm/min. . . . . 154

7.49 Comparison of predicted and experimental birefringence profiles for a 237,000 Mw polypropylene with a mass throughput of 1.68 gm/min. . . . . 155

7.50 Comparison of predicted and experimental temperature profiles for a 237,000 Mw polypropylene with a mass throughput of 1.68 gm/min. . . . . 156

LIST OF SYMBOLS

| | | | |
|---|---|---|---|
| $a$ | - | Crystallographic axis | (meters) |
| $A$ | - | Area | (meters$^2$) |
| $b$ | - | Crystallographic axis | (meters) |
| $c$ | - | Crystallographic axis | (meters) |
| $C_d$ | - | Drag coefficient | (-) |
| $C_{op}$ | - | Stress optical coefficient | (pascals) |
| $C_p$ | - | Specific heat | (joules/kg-kelvin) |
| $D$ | - | Diameter | (meters) |
| $D_0$ | - | Crystallization rate halfwidth | (kelvins) |
| $E$ | - | Modulus | (pascals) |
| $E_0$ | - | Modulus of dry fiber | (pascals) |
| $E_1$ | - | Modulus of wet fiber | (pascals) |
| $F_{drag}$ | - | Force due to skin friction | (newtons) |
| $F_{ext}$ | - | Force supplied by the take-up device | (newtons) |
| $F_{grav}$ | - | Force due to gravation | (newtons) |
| $F_{inert}$ | - | Force due to acceleration | (newtons) |
| $F_{rheo}$ | - | Force within the fiber | (newtons) |
| $F_{surf}$ | - | Force due to surface tension | (newtons) |
| $f$ | - | Nucleus size distribution | (-) |
| $F$ | - | Free energy | (joules) |
| $f_a$ | - | Amorphous orientation function | (-) |
| $g$ | - | Gravitation constant | (meters/second$^2$) |
| $G_i$ | - | Crystal growth rate | (meters/second) |
| $Gr$ | - | Grasoff number | (-) |

| | | | |
|---|---|---|---|
| $h$ | - | Heat transfer coefficient | (joules/kg $m^2$ K) |
| $H$ | - | Radius of curvature | (meters) |
| $k$ | - | Rate constant | (seconds$^{-1}$) |
| $K$ | - | Rate constant | (seconds$^{-1}$) |
| $k_f$ | - | Shape factor | (-) |
| $k_{max}$ | - | Maximun rate constant | (seconds$^{-1}$) |
| $K'$ | - | Flory Huggins constant | (-) |
| $K''$ | - | Kramer constant | (-) |
| LP | - | Long period | (meters) |
| $M_w$ | - | Weight average molecular weight | (daltons) |
| $n$ | - | Avrami index | (-) |
| $N_i$ | - | Nucleation rate | (seconds$^{-1}$) |
| $N_0$ | - | Number of nuclei | (-) |
| $N_{ath}$ | - | Athermal nucleation rate | (seconds$^{-1}$) |
| $N_{th}$ | - | Thermal nucleation rate | (seconds$^{-1}$) |
| Nu | - | Nusselt number | (-) |
| $p$ | - | Pressure | (pascals) |
| $P$ | - | Pressure | (pascals) |
| Pr | - | Prandlt number | (-) |
| $q$ | - | Heat flux | (joules/meter$^2$-sec) |
| $r$ | - | Radius | (meters) |
| rh | - | Relative humidity | (%) |
| $R$ | - | Radius | (meters) |
| Re | - | Reynolds number | (-) |
| $R^*$ | - | Critical radius of nucleus | (meters) |
| $S^*$ | - | Distribution of nuclei | (-) |

| | | | |
|---|---|---|---|
| $t$ | - | Time | (seconds) |
| $t_{cr}^{1/2}$ | - | Crystallization halftime | (seconds) |
| $t_{or}^{1/2}$ | - | Orientation halftime | (seconds) |
| $T$ | - | Temperature | (kelvins) |
| $T_a$ | - | Ambient temperature | (kelvins) |
| $T_m$ | - | Equilibrium melting temperature | (kelvins) |
| $T_g$ | - | Glass transition temperature | (kelvins) |
| $T_{g0}$ | - | Glass transition temperature of dry fiber | (kelvins) |
| $T_{gl}$ | - | Glass transition temperature of wet fiber | (kelvins) |
| $T_{max}$ | - | Temperature at maximum crystallization rate | (kelvins) |
| $v$ | - | Crystal growth velocity | (meters/sec) |
| $V$ | - | Velocity | (meters/sec) |
| $V_c$ | - | Air cross flow velocity | (meters/sec) |
| $V_f$ | - | Fiber velocity | (meters/sec) |
| $W$ | - | Mass throughput | (kg/sec) |
| $W_i$ | - | Weight fraction | (-) |
| $z$ | - | Distance | (meters) |
| $\alpha$ | - | Crystallographic angle | (°) |
| $\alpha_e$ | - | Surface tension | (pascals) |
| $\alpha_s$ | - | Surface tension | (pascals) |
| $\alpha_{\parallel}$ | - | Polarizability parallel to chain axis | (-) |
| $\alpha_{\perp}$ | - | Polarizability perpendicular to chain axis | (-) |
| $\beta$ | - | Crystallographic angle | (°) |

| | | | |
|---|---|---|---|
| $\gamma$ | - | Crystallographic angle | (°) |
| $\delta$ | - | Transition parameter | (-) |
| $\Delta H$ | - | Heat of fusion | (joules/kg) |
| $\Delta_c^0$ | - | Crystalline intrinsic birefringence | (-) |
| $\Delta_a^0$ | - | Amorphous intrinsic birefringence | (-) |
| $\Delta n_a$ | - | Amorphous birefringence | (-) |
| $\varepsilon$ | - | Emissivity | (-) |
| $\eta$ | - | Elongational viscosity | (pascal-second) |
| $\xi$ | - | Cooling rate | (kelvin/second) |
| $\Theta$ | - | Crystalline index | (-) |
| $\Theta_\infty$ | - | Maximum crystalline index | (-) |
| $\lambda$ | - | Stephan - Boltzman constant | (watt/meter$^2$ K) |
| $\mu_a$ | - | Viscosity of air | (pascal-second) |
| $\rho$ | - | Density | (kg/meter$^3$) |
| $\rho_a$ | - | Amorphous density | (kg/meter$^3$) |
| $\rho_c$ | - | Crystalline density | (kg/meter$^3$) |
| $\sigma$ | - | Surface tension | (pascals) |
| $\tau_{ij}$ | - | Stress | (pascals) |
| $\phi_{cr}$ | - | Crystallite orientation angle | (°) |
| $\phi_s$ | - | Amorphous orientation angle | (°) |

# CHAPTER 1

## INTRODUCTION

The introduction of synthetic fibers revolutionized the textile industry worldwide. They offered an important alternative to cotton, silk and wool in the clothing and carpet industries. Synthetic fibers derived from polymeric materials offered many technological and economic advantages over the naturally occurring cotton, silk and wool. By controlling the synthesis of the polymer and by introducing various innovations into the fiber spinning process, it was then possible to modify and control the physical properties of the manufactured fiber to meet consumer demands. These synthetic materials also freed producers from the whims of factors over which they had no control, such as the weather, on the quality of their product.

The success of synthetic fibers is not limited to the textile industry. In medicine, they are being used as replacements for ligaments, arteries and veins. Nonwoven fabrics from melt blown polymers are being extensively used in surgical gowns and dressings. In transportation, synthetic fibers are used in the belting of radial tires and nonwoven materials are being introduced into road construction materials. In pollution control, they are used as filter media and in devices to contain and collect chemical and oil spills. Synthetic fibers are used in composite materials in the demanding field of high performance air and spacecraft.

Fibers from polymeric materials are produced by three methods; wet, dry and melt spinning. In wet spinning, the polymer is dissolved

in a solvent to form a spinning dope. This is extruded through a capillary die into a bath containing a liquid which is a nonsolvent for the polymer. As the extruded dope enters the bath the solvent migrates to the bath leaving a solidified fiber. Dry spinning also utilizes a spinning dope but the extruded dope usually enters a chamber containing heated gases where the solvent evaporates leaving behind the solidified fiber.

The most popular method of fiber formation is melt spinning. Solid polymer, usually in pellet form, is melted and pressurized in an extruder and then forced through a capillary die into the ambient air or a quench chamber. The extruded fiber cools and solidifies on its path to the take-up device. As the fiber cools and solidifies the morphological structure of the fiber is formed. This structure determines of the macroscopic physical properties exhibited by the manufactured fiber.

In amorphous materials, this structure is described by the orientation of the molecular chains themselves. In polycrystalline materials the structure is complicated by the degree and orientation of the crystalline regions in conjunction with the remaining amorphous material. There has been a considerable amount of research effort along two avenues in the textile industry; the relationships between the microscopic structure and the macroscopic physical properties of the fiber and the relationships between the processing conditions and the microscopic structure formed. Historically, the major emphasis has been on the relationships between structure and physical properties. The emphasis in this study is on the interrelationships between the

processing conditions and the resulting structure developed within the fiber. In particular the approach has involved the development of a mathematical model to describe the high speed melt spinning of crystallizable polymers. Such a model can provide considerable insight into the nature of the structures produced by a variety of spinning conditions.

The chemical and physical requirements of the finished product along with limitations imposed by the melt spinning process has naturally led to the common industrial use of several types of polymers for fiber production. These include polyolefins, polyesters and polyamides. The majority of previous investigations have centered on the structure - physical property relationships of polyolefins and polyesters. This study involves the relationships between the processing conditions and the development of the structure during processing for a polyamide (nylon-66) at high spinning speeds.

Nylon-66, in contrast to polyesters, exhibits very rapid crystallization kinetics. The physical properties of the polycrystalline fiber produced from nylon-66 are dictated by the structure which is developed by the crystallization phenomenon taking place during the melt spinning process. Shimizu et al. (1) has recently studied some of the relationships between the structure and the physical properties of high speed spun nylon-66 fibers. They noted extensive changes in those physical properties of fibers spun at speeds greater than 3000 meters per minute. Chappel et al. (2) tried experimentally to quantitify the structure development within the spinline at low take-up speeds but

were only partially successful. Lecluse (3) also reported an attempt to perform similar studies at high take-up speeds.

Nylons, in addition to being one of the oldest thermoplastics in use, are the largest group in terms of volume totaling 324 million pounds in 1983. Nylon 6 and 66 account for 90% of the nylon use in the United States. The chemical and physical characteristics of these materials lead to such varied uses as industrial and personal brushes, monofilament for fishing line, string for tennis rackets and musical instruments, sewing threads and woven screens for industrial filtration operations. The growth rate of nylon is anticipated at 8% per year leading to a volume of around four billion pounds by the end of the century (4). They are, and will continue to be, a vital engineering material and an important facet in the development of new products resulting from the commercialization of new technology such as high speed melt spinning.

The online melt spinning behavior of polypropylene will also be examined. Polypropylene is also an important polymer for a range of fiber applications including both woven and nonwoven fabrics. Polypropylene is a material with lower crystallization kinetics than nylon-66 but higher than polyesters.

Koyama and Ishizuka (5-8) have examined the online behavior of polypropylene at low speeds whereas Shimizu et al. (9-11) performed studies on the physical properties of high speed spun fibers. Extensive studies by Lu and Spruiell (12) have made available online experimental diameter, birefringence and temperature data which will be compared to predictions of the model developed.

A mathematical model was developed to help interpret the structure development process which a crystallizable polymer experiences during high speed melt spinning. This model was applied to two polymers which exhibited different online behavior. The applicability of the model was examined in comparisons between online experimental measurement of the diameter, birefringence and temperature profiles and theoretical predictions.

# CHAPTER 2

# LITERATURE REVIEW

## Melt Spinning Process

### Dynamics

The melt spinning process has been the target of extensive research because of its economic and technical value. The initial studies were performed by Carothers and Hill (13) on the relationships between spinning conditions and the structure and properties of the linear aliphatic polyester fiber which was produced. The first theoretical analysis was undertaken in the late 1950's and early 1960's by Ziabicki (14). Using a simple force balance he derived a relationship between the tensile force and the stress in the fiber. Ziabicki and Kedzierska (15) presented a relationship between the fiber diameter and the velocity in the spinline and specified criteria for successful spinning, namely a continuity of flow, a limit on the maximum stress and an increase in the Trouton, or elongational, viscosity along the spinline.

Ziabicki and Kedzierska (16) presented an approach to the die swell at the spinneret exit which is one of the most difficult problems, both conceptually and mathematically, in the analysis of the overall process.

The basic force balance from Ziabicki is

$$F_{rheo} = F_{ext} + F_{inert} + F_{drag} + F_{surf} + F_{grav} \qquad (2\text{-}1)$$

where $F_{ext}$ is the external force supplied by the take-up device, $F_{rheo}$ is the rheological force within the fiber, $F_{drag}$ is the drag force caused by the motion of the fiber through the cooling medium, $F_{inert}$ is the force caused by the fiber's acceleration, $F_{grav}$ is the force due to gravity and $F_{surf}$ is the force due to the surface tension on the exposed fiber-air interface.

The drag force has been neglected in most analyses due to past limitations in the fiber take-up speed. With take-up speeds presently in the 4000-7000 meters per minute range and higher, the drag force has become an increasingly important component of the force balance. In general, the drag force is expressed as

$$F_{drag} = \rho \, C_d \, V^2 \, A \qquad (2\text{-}2)$$

where $\rho$ is the density, V is the velocity, A is an exposed area and $C_d$ is a drag coefficient. In a given situation the physical meaning of $\rho$, V and A are apparent. The evaluation of $C_d$ is more obscure. With regards to melt spinning, Sakiadis (17) performed a laminar and turbulent boundary layer analysis to calculate the drag on a constant diameter cylinder passing through a stationary fluid at a constant velocity. He considered the drag force as a function of the parameter $\xi$, defined by

$$\xi = 8 \, (Re_x^{1/2}/Re) \qquad (2\text{-}3)$$

where $Re_x$ and Re are the Reynolds numbers based on the length and diameter of the cylinder, respectively. Andrews (18) undertook an experimental study of the air drag on a stationary fiber in a wind

tunnel. He obtained the following relationship for the drag coefficient

$$C_d = 1.30\ Re^{-0.61} \tag{2-4}$$

Aoki et al. (19) performed experiments similar to Andrews and obtained

$$C_d = 0.18\ Re^{-0.44} \tag{2-5}$$

Sano and Orii (20) measured tensions at various points along the spin-line and determined that

$$C_d = 0.68 Re^{-0.61} \tag{2-6}$$

Hamana et al. (21) performed similar experiments and found

$$C_d = 0.37\ Re^{-0.61} \tag{2-7}$$

Kwon and Prevorsek (22) performed experimental studies on air drag forces using a technique which involved the air boundary layer surrounding the fiber being spun. Their results indicated that the air drag values obtained from available correlations underestimated the actual drag force. A possible cause was the swaying of the fiber which gave an apparent diameter larger than the actual diameter of the fiber.

Gould and Smith (23) also found that the drag force increased significantly when the fiber was allowed to vibrate freely. Under these conditions compact yarns behaved as a thick fiber of the same surface area. For fiber diameters less than 0.3 millimeters, they obtained

$$C_d = 0.27\ Re^{-0.61} \tag{2-8}$$

From these results, it is obvious that there does not exist a general consensus on the actual numerical values, but there is agreement on the form. The problem lies in the experimental techniques and the manner in which the data are being analyzed.

Rheology

Han and coworkers (24-26) examined the rheological aspects of isothermal spinning by considering elongational viscosity, deformation and heat transfer effects. They arrived at a semi-empirical generalized equation for the elongational viscosity as a function of the elongation rate and temperature. The mathematical model developed was similar to that of Kase and Matsuo (27-29) and required a numerical solution but satisfied the mass, momentum and energy balances. The apparent elongational viscosity was computed for polypropylene (29) and nylon 6 (30) from experimental melt spinning data. Hill and Cuculo (31) performed an experimental study on the melt spinning of poly-(ethylene terephthalate) (PET) which included the effects of molecular weight, temperature and elongation rate on the elongational viscosity. The rheological behavior of the material, introduced in the elongational viscosity, must be an important consideration in any melt spinning process. Chen et al. (32) and Spearot and Metzner (33) considered the influence of viscoelasticity and the deformation history on the process and Acierno et al. (34) performed an investigation on non-Newtonian melt behavior in isothermal spinning. Matovich and Pearson (35) and White (36) have attempted a theoretical analysis of melt

spinning taking a non-Newtonian approach toward the rheology of the fluid involved.

Larson (37) compared the isothermal spinline velocity profiles predicted by a Doi-Edwards and a co-rotational Maxwell constitutive equation. Both models predicted limited spin ability (i.e. short spinlines and low draw ratios) which contrasted with the unlimited spin ability found using an upper-convected Maxwell constitutive equation. The spinning behavior of the Doi-Edwards formulation was dominated by the elongational strain measure rather than the distribution of relaxation times.

Heat Transfer

Andrews (38) used a simplified energy balance to arrive at the fiber temperature as a function of its length (i.e. distance from the spinneret). The solution was difficult to apply to the spinning process because of the two-dimensional nature of the problem: radial and axial temperature gradients were considered. Wilhelm (39) applied Andrews' results to his experimental data and in some cases found good agreement.

Ziabicki and Kedzierska (40) attempted to model this phenomena by considering a hot cylinder immersed in an isothermal cooling fluid. Their analysis included simplifying assumptions to yield a tractable problem, however the results did not agree with experimental data. Kase and Matsuo (27-29) performed an energy balance on a differential element in the spinline. They considered conduction-convection effects while neglecting radiation and the heat of crystallization; they produced correlations for the heat transfer coefficient which included

a transverse quench flow. The theory provided a means of computing the temperature as a function of spinline distance but deviations from experimental data were traced to neglecting the heat of crystallization.

Barnett (41), considering forced and free convection, used numerical analysis to compute the temperature as a function of the fiber length. His analysis included acceleration, radiation and free stream turbulence effects. Copley et al. (42) investigated the effect of fiber attenuation on the axial temperature gradient of the fiber. Morrison (43) also performed a numerical analysis on the cooling and solidification process which included the heat of fusion as well as convective and radiative heat transfer. Acierno et al. (34) probed boundary layer theory applications in melt spinning. Nakamura et al. (44) included the heat of fusion in an energy balance similar to that of Kase and Matsuo and developed expressions which related the crystallinity to the temperature. Two differential equations resulted which had to be solved numerically for an a priori set of boundary conditions. The final result was

$$\frac{d\Theta}{dt} = \frac{R(T-T_a)}{\Delta H} + \frac{C_p}{\Delta H}\frac{\partial T}{\partial t} + V\frac{\partial T}{\partial z} \qquad (2\text{-}9)$$

where

$$R = 2\sqrt{\pi}\, h/\sqrt{A} \qquad (2\text{-}10)$$

and h is the heat transfer coefficient, $C_p$ is the specific heat and $\Delta H$ is the heat of fusion.

The heat transfer coefficient has been shown to be a sensitive parameter in determining the overall temperature profile of the spin-line and there have been many attempts to provide theoretical and empirical relationships between it and the spinning conditions. These results are generally expressed as a Nusselt number which is a function of the Reynolds, Prandtl and/or Grashof numbers. Glicksman (45) found using turbulent boundary layer theory

$$Nu = 0.325\ Re^{0.3} \tag{2-11}$$

for a stationary cylinder in an axial air stream, where Nu is the Nusselt number and Re is the Reynolds number based on the cylinder diameter and the velocity of the air stream. Empirical results for a stationary cylinder in an axial air stream include Mueller (46) who found

$$Nu = 0.516\ Pr^{0.3}\ Re^{0.43} \tag{2-12}$$

where Pr is the Prandtl number. Roberts (47) determined for the same conditions

$$Nu = 0.746\ Re^{0.38} \tag{2-13}$$

while Sano and Nishikawa (48) found

$$Nu = 0.32 + 0.155\ Re^{0.3} \tag{2-14}$$

An empirical relationship for axial motion of the fiber coupled with a transverse air flow was determined by Sano and Yamada (49) as

$$Nu = 0.35 + 0.5\ Re^{0.5} \tag{2-15}$$

where

$$Re = Re_{ef} + (0.3\ Re_{ef}^{0.36} - 0.2)^2 + (1.26\ Gr^{0.7} - 0.7)^2 \quad (2\text{-}16)$$

here $Re_{ef}$ is the Reynolds number based on the transverse air velocity and Gr is the Grashof number. Kase and Matsuo (28) found for these conditions

$$Nu = Nu_0\ [1 + 8(V_c/V_f)^2]^{0.167} \quad (2\text{-}17)$$

where $Nu_0$ is the Nusselt number in the absence of transverse flows and $V_c$ and $V_f$ are the transverse air and fiber velocities, respectively. A general review of heat transfer phenomena in melt spinning was given by Wanger and Fox (50).

Crystallization and Orientation

Ziabicki (51,52) performed a theoretical analysis of crystallization during melt spinning using an isothermal Avrami equation modified for non-isothermal conditions. It was assumed that the rate of transformation from the amorphous phase to the crystalline phase followed first order kinetics. With this assumption, he obtained

$$\Theta = 1 - \exp[-(\int k[T]\ d\tau)] \quad (2\text{-}18)$$

where k[T] is the isothermal rate constant. He also defined the kinetic crystallizability as

$$G = \int k[T]\ dT \quad (2\text{-}19)$$

and the cooling parameter as

$$\xi = dT/dt \tag{2-20}$$

which allowed the degree of crystallinity to be expressed as

$$\Theta = 1 - \exp(G/\xi) \tag{2-21}$$

This formulation resulted in qualitative agreement with experimental data when a constant cooling rate was assumed. Nakamura et al. (44,53) also used a modified Avrami equation and applied numerical techniques to obtain results for melt spinning and non-isothermal quiescient crystallization. They arrived at the following relation

$$\Theta = 1 - \exp[-(\int K[T(\tau)]\ d\tau)^n] \tag{2-22}$$

where $K[T] = k[T]^{1/n}$ and n is the Avrami index. They (54) extended this treatment to include radial temperature gradients. Abbott and White (55) presented a general theory of non-isothermal crystallization including stressed or oriented conditions. A two-dimensional energy balance considered a crystal growth front advancing through the solidifying fiber. The theory contained both hetero- and homogeneous nucleation mechanisms and resulted in a nucleation rate that was a function of temperature and deformation rate. Their result was

$$\Theta = 1 - \exp[-\sum\sum \int K_{kj}(T,\tau)\ d\tau] \tag{2-23}$$

where

$$K_{kj} = \frac{N_{kj}C_j}{\rho_L}\ \beta^{j+\alpha}\ \xi^{j+\alpha} \tag{2-24}$$

the nucleation rate, $N_{kj}$, contained the temperature and deformation rate dependence.

Ishizuka and Koyama (5-8) studied the crystallization kinetics of polypropylene on a running spinline using the following relation for a heterogeneously nucleated system

$$-\ln[1-\Theta/\Theta_\infty] = \rho_a k_f \sum[\sum G_j[T(u),\Delta n_a(u)]\Delta t]N_i[T(\tau),\Delta n_a(\tau)]/\rho_c\Theta_\infty \quad (2\text{-}25)$$

where $\Theta_\infty$ is the maximum crystallinity, $\rho_c$ and $\rho_a$ are the density of the crystalline and amorphous phases respectively, $G_j$ is the time, temperature and orientation dependent linear growth rate and $N_i$ is the temperature and orientation dependent rate of nucleus formation. $\Delta n_a$ is the orientation of the amorphous material and $k_f$ is a shape factor which depends on the dimensionality of the growth. They found that a two-dimensional growth model provided the best fit of the experimental data. The crystallization of polypropylene during melt spinning was dictated by the initial local molecular orientation of the supercooled melt and only highly oriented molecules would be successively incorporated into the growing crystal.

Abhiraman (56) analyzed the crystallization process in terms of the orientation distributions of the crystalline and amorphous phases. It was assumed that the system consisted of distinct crystalline and amorphous phases and no relaxation of the orientation occurred during crystallization. It was also assumed that the orientation of the crystals was the same as that of the nuclei from which they were initiated. Krigbaum and Roe's (57) hypothesis was used to relate the nuclei orientation distribution to that of the amorphous precusor. He

concluded that the crystallization of an oriented precursor would lead to a higher degree of anisotropy than that of the precursor. The depletion of the oriented precursor would lead to an amorphous orientation normal to the initial preferred direction. The overall orientation increases with crystallization. This analysis did not include the effect of free energy changes, a changing amorphous orientation during crystallization or chain folding mechanisms.

Ziabicki (58) performed a theoretical analysis of polymer crystallization which included orientation and non-isothermal effects. His analysis resulted in defining a transition parameter, $\delta$, given by

$$\delta = t_{or}^{1/2} / t_{cr}^{1/2} \qquad (2\text{-}26)$$

where $t_{or}^{1/2}$ and $t_{cr}^{1/2}$ are the orientation and crystallization half-times, respectively. When $\delta$ is small ($\delta \ll 1$) the orientation process is more rapid than the crystallization process and the orientation factor reaches its final value before any significant crystallization can occur. When $\delta$ is large ($\delta \gg 1$) crystallization precedes orientation. In this case the orientation remains at its initial value. When $\delta$ is near unity a complex process involving the interaction of both orientation and crystallization takes place. For PET, $\delta < 1$, and orientation leads crystallization therefore the orientation factor is expected to increase rapidly before crystallization occurs. The crystallization process leads the orientation process for both nylons. This implies that the orientation factor would remain near its initial value after crystallization took place (especially for nylon-66).

## Structure Development

A most significant aspect of melt spinning is the relationship between the processing variables and the properties of the resulting fibers. The fiber properties are determined by the fine structure of the fibers (e.g. orientation, crystallinity, morphology) as well as by the molecular structure of the polymer. Hence, the relationship of processing variables to the structure development is a key aspect to understanding the properties that may be developed during fiber processing. Hearle (59) reviewed the early studies of crystalline structure in fibers but was only interested in the fiber itself and not the conditions under which it was made. Keller (60) and later Vonk (61) showed that lamellar crystals and fibrils formed complex structures which were a consequence of the deformation imposed during the crystallization process. They labelled these as "shish-kebab" structures. Krueger and Yeh (62) examined these shish-kebab structures and concluded that the kebab was not a separate surface growth but was intertwined with the shish by tie molecules passing through the shish. Ziabicki and Kedzierska (63-65) performed a theoretical analysis and collected data on orientation and crystallization in melt spinning. They presented a discussion on the effect of polymer structure on orientation and found that the orientation increased with spinline tension, the difference between the take-up and extrusion velocities and the inverse of the fiber diameter. Furukawa et al. (66) and Kitao et al. (67) carried out studies which emphasized the development of crystallinity in the spinline.

Spruiell and White (68) introduced the continuous cooling transformation (CCT) curve concept and correlated the interaction of stress, temperature and cooling rate. The stress and cooling rate were shown to influence substantially the temperature at which crystallization begins. They also suggested that stress and orientation decreased the free energy of formation of the crystal nuclei which would lead to an observably higher crystallization rate.

Katayama et al. (69) performed online experimental studies on polyethylene, polypropylene and polybutene-1 and found an increased crystallization rate due to molecular orientation and also investigated the interaction of the heat of fusion and the heat transfer rate from the spinline. The morphology they found consisted of lamellar and interlamellar regions stacked normal to the fiber axis. At the University of Tennessee, Knoxville there have been numerous studies on the development of crystallinity in the spinline for polyethylene (70,71), polypropylene (72,73), nylon-6 (74,75) and polyoxymethylene (76).

Aggarwal et al. (77) found that stretching polyethylene initially involved alignment of the a axis with the stretch direction with the b and c axes randomly distributed. Upon further deformation there was a gradual change to alignment of the c axis with the stretch direction. Ishikawa (78) using compression and stretching techniques coupled with x-ray diffraction on polyethylene fibers found a difference in morphology with spinning conditions.

White et al. (79) reported an increase in the Herman's orientation function for polyethylene with take-up speed at constant

extrusion velocity and a decrease with extrusion rate at constant take-up velocity. Abbott and White (55) examined final fiber crystallinity for high and low density polyethylene as a function of spinning speed, extrusion rate and temperature. They found a strong correlation of the mechanical properties of the final fiber with the crystalline orientation. Southern et al. (80) interpreted the high orientation and unusual physical properties of highly crystalline polyethylene fibers in terms of an extended chain morphology. Keller and Machin (81) proposed a model for spherulite growth during melt spinning. A central nuclei consisted of extended or partially extended molecules aligned with the extrusion direction. These constituted fibrils on which lamellae with folded chains grew epitaxially. Dees and Spruiell (71) found that the development of crystallinity in polyethylene fibers was a combination of increased crystallization kinetics, caused by the spinline stress, and a change in any variable that affected the rate of heat transfer. The morphology of the as-spun fiber consisted of row nucleated and twisted lamellar folded chain overgrowth; the quantity of each depended on the spinning conditions. The birefringence was a function of the crystalline orientation only and the mechanical properties correlated well with the crystalline orientation. Fung and Carr (82), using electron microscopy on melt spun polyethylene fibers, found row nucleated structures within the fiber caused by orientation during spinning. The skin-core morphology was produced by a stress effect in the solidifying fiber and gave a higher degree of orientation at the fiber surface and chain tilting with respect to the fiber axis at an angle that varied with the radius.

Binsbergen (83) studied orientation induced nucleation in polypropylene and found that crystalline structures oriented along the lines of strain. Samuels (84) found that orientation increased with drawdown ratio in polypropylene fibers. Garber and Clark (85) found that crystallization under a high stress produced a highly oriented row nucleated morphology in polyoxymethylene. Keller (86) presented a qualitative discussion of crystallinity and orientation in melt spun fibers using x-ray data for nylons, polyethylene and PET. Hamana et al. (21,87) performed the first online birefringence study of PET with take-up speeds up to 1000 meters per minute and found a unique correlation between birefringence and stress. Huisman and Heuvel (88) and Hagler (89) found that PET crystallized in the spinline at speeds greater than 3000 meters per minute.

Chappel et al. (2) performed online x-ray experiments while studying the crystallization of nylon-66, but their results were qualitative in nature. Keller (90) used microphotography to study the effect of an orienting stress on the morphology of nylon-66. He found row structures whose longitudinal axes were parallel to the deformation axis.

Ziabicki and Kedzierska (63-65) derived differential equations for the orientation of rigid ellipsoids and flexible coiled chains in a parallel velocity gradient field. From this analysis a coefficient of fiber orientation was formulated, but the solution required the use of a numerical procedure. Ziabicki (65) later simplified the orientation equations enough to allow an analytical solution and the results were in qualitative agreement with experimental data. The final

orientation was a result of elongational flow and a thermally induced randomization process. Kobayashi (91) suggested a morphology consisting of spiral growth of folded chain lamellae with screw dislocations parallel to the flow direction.

Nishiumi (92), using an analysis similar to Ziabicki's, related the birefringence to several processing variables. Anderson and Carr (93) have proposed a model for flow crystallized polypropylene. Clark (94) and Clark and Spruiell (95) proposed a morphological model for polypropylene where row structures of planar lamellae were interconnected by tie molecules. This gave rise to c axis orientation while the a axis orientation resulted from interlamellar crystal growth that had a special epitaxial relationship with the primary row structure. Sprague (95) proposed morphological models for "hard" elastic fibers such as polypropylene and polyoxymethylene.

## Mathematical Modeling

Kase and Matsuo (27-29) performed the first attempts to mathematically model the melt spinning process. They undertook both a transient and steady state analysis. In the steady state case they arrived at essentially the equations derived by Ziabicki (14), although differences arose in the manner in which they applied their results to experimental data. Prastro and Parrini (97) attempted to define critical spinning parameters for PET by numerically solving the equations of motion, energy and the Newtonian rheological model. They assumed that the specific heat and density were constant and that inertia, gravity and air drag were negligible contributors to the force balance. Under these restrictive assumptions, a correlation of the

critical conditions where fiber breakage would occur was presented. Gagon and Denn (98) introduced a mathematical model to simulate the PET melt spinning process. The Newtonian and Tanner and Phan-Thein constitutive equations were used. They found that the location of the freeze point (the point at which the velocity reached 95% of its final value) was independent of changes in the take-up velocity. Their model was extremely sensitive to the choice of heat transfer expression and this uncertainty did not allow them to discriminate between the Newtonian and viscoelastic models when compared to the experimental data of George (99). They concluded that there was a qualitative difference between the two constitutive equations. The air drag caused an increase in the stress with the Newtonian model, whereas for the viscoelastic model it led to a decrease in the stress which was attributed to the coupling between the stress and the velocity in the viscoelastic fluid. This formulation led to a more descriptive rather than predictive model since there were several boundary conditions which were specified a priori rather than results of the simulation.

George (100) proposed a model for the melt spinning of PET at speeds ranging from 750 to 3500 meters per minute. A comparison of constant and variable tension spinning showed that there was no effect on the temperature and velocity profiles, but there was a 100% increase in the stress at the freeze point for the variable tension model. Correlations were presented for the tenacity, elongation to break and modulus with the birefringence.

Yasuda et al. (101) included a radial temperature gradient which was claimed to be the source of the radial orientation distribution.

Their formulation led to three ordinary and one partial differential equations and the method of solution was not presented. The temperature difference between the center of the fiber and its surface ranged from 2 to 12 °C, but there was an error in the correlation used for the heat transfer coefficient. A relationship between the birefringence and the stress in the fiber, using the computed stress at the freeze point was presented. There was little comparison to experimental data and the data that were given indicated a large amount of scatter. The radial orientation variation increased with velocity, presumably from an increase in the radial temperature gradient. They concluded that increasing the cooling air temperature decreased the radial orientation variation.

Yasuda et al. (102) next proposed a model for the heat transfer in multifilament melt spinning of PET. A variable coefficient was used to relate the flow of air around individual fibers to the take-up velocity. Several coefficients were presented and temperature drops were computed but were not compared to any experimental results. In a subsequent study (103) they applied this to a multifilament spinning process and the simulation indicated that the denier variation was related to the maximum in the velocity gradient and the position where that maximum occurred in the spinline. The birefringence was again compared to the computed stress at the freeze point.

Dutta and Nadkarni (104) used an approach similar to that of Gagon and Denn with a temperature and molecular weight dependent Newtonian viscosity. The effect of several variables on the spinning process was evaluated and they concluded that the extrusion

temperature, melt intrinsic viscosity, mass throughput and take-up velocity were the most significant variables in the process. Shenoy and Nadkarni (105) performed computer simulations with the model of Dutta and Nadkarni on PET. The model used the artificial boundary condition that the final velocity was achieved at the take-up device and the fiber temperature reached the glass transition temperature at the take-up device. They verified the stress optical law for PET using data from several different industrial plants. The utility of these types of simulations was demonstrated by a case study of factors affecting a constant denier product.

In all of the above works it should be emphasized that the models were not applicable to the melt spinning process when structure development processes such as crystallization took place. Kikutani (106) proposed a model which included a crystallinity dependent elongational viscosity along with orientation induced crystallization kinetics for PET melt spinning. This formulation predicted online crystallization at take-up speeds greater than 3000 meters per minute and the appearance of the "necking" phenomenon experimentally observed at high speeds.

Bai (107) compared online experimental diameter, temperature and birefringence profiles to those predicted from Kikutani's model. He found that a reasonable quantitative fit between the experimental data and the model could be obtained by adjusting various parameters within the model so that the appearance of the necking region as predicted by the model coincided with that experimentally observed, this however

led to a discrepancy in the predicted and experimentally observed take-up speeds.

High Speed Spinning

Shimizu and coworkers (9-11,108-115) made extensive use of both an air jet nozzle and a high speed godet to reach take-up velocities of 10,000 meters per minute. Their study of isotactic polypropylene indicated that the fiber diameter reached a limiting value which depended on the distance of the nozzle from the spinneret and the air pressure in the nozzle (9). They found (10) that at take-up speeds greater than 3000 meters per minute, the yield point in stress-strain curves of as-spun fibers had disappeared. The birefringence was independent of extrusion temperature, but the density remained a function of the temperature and the cooling rate. They found a drastic increase in the initial Young's modulus, the thermal contraction and a decrease in the small angle x-ray scattering intensity, in addition to a shoulder melting peak in differential scanning calorimetry (DSC) traces (11). These findings were interpreted in terms of constrained amorphous chains trapped between crystallites when the polymer crystallized under stress. Furthermore, the elastic recovery of the fiber was affected by the spinning conditions (108). The stress-strain behavior was examined in terms of three regions; an elastic modulus I (corresponding to the initial Young's modulus), an elastic modulus II (corresponding to the bending modulus of the lamellae crystal) and an elastic region (corresponding to the extension region where the plastic fracture of the lamellar crystals was neglected).

In another study involving PET (109), they found that below 4000-5000 meters per minute that the fiber structure formation which resulted from orientation induced crystallization took place at lower take-up velocities as a result of increasing elongational viscosity with increasing molecular weight. Also, the degree of crystallinity and the molecular orientation reached limiting values at take-up speeds above 5000 meters per minute. These limiting values decreased with increasing molecular weight from which they inferred that the increase in molecular weight did not lead to the development of fiber structure. Furthermore, for fibers spun near the critical spin ability, there was decreased density and birefringence, a crimping of the fiber and the appearance of a shoulder melting peak in DSC traces which resulted from sliding or scission of the molecules or increased void content. A subsequent study (110) showed that higher take-up speeds were the predominate influence in fiber structure formation. The effect of the mass flow rate, although minor in comparison, was attributed to heat transfer phenomena due to the decrease in fiber diameter rather than the draw ratio. They found, in addition, a disproportional increase in crystallinity at birefringence values of 0.062 - 0.068.

A later study (111) involving PET indicated that at take-up speeds greater than 7000 meters per minute the density and birefringence decreased and the degree of crystallinity achieved a limiting value. The small angle x-ray scattering patterns changed from a four spot X pattern to a two spot meridional pattern. The crystallites were almost completely oriented while the orientation of the amorphous

regions remained low but exhibited a maximum at 6000 meters per minute. At very high take-up speeds, the fibers contained large numbers of voids in the outer skin region. The degree of crystallinity and molecular orientation was higher in the outer skin than in the core and the difference increased with take-up velocity. This effect presumably resulted from large radial stress and temperature gradients within the fiber.

Shimizu et al. (116) used WAXS to examine the crystallite size and imperfection in high speed spun PET fibers. The crystallite size increased in both the chain and lateral dimensions while the imperfection parameter decreased with take-up speed. They (117) proposed the existence of an oriented mesophase in high speed spun PET fibers. This mesophase was postulated to be a highly oriented intermediate between the crystalline and amorphous phases and was used to interpret WAXS patterns obtained from as-spun fibers. The resolution of the WAXS patterns using two amorphous contributions led to higher crystalline orientation factors. The basis upon which the demarcation between the amorphous phase and the mesophase was not clearly explained.

Shimizu (113) observed that above 3000 meters per minute PET exhibited an online "necking" phenomena, an apparent drawdown of the fiber diameter to its final value in a very short distance. He postulated the existence of an oriented mesophase in the "neck" region prior to crystallization. The "neck" region appeared closer to the spinneret with increasing take-up velocity or decreasing mass throughput.

George, Holt and Buckley (118) interpreted experimental birefringence and velocity profiles in terms of the freeze point. They concluded that the interaction of supercooling and stress was the primary driving force in the crystallization of PET on the spinline. They found that a minimum stress (orientation) must be present for crystallization to occur. At intermediate speeds the increase in stress allowed crystallization to occur at higher temperatures. A point was reached where this interaction broke down as a result of the low crystallization rates at the higher temperatures. Their results also implied that the birefringence itself was not indicative of the onset of crystallization.

Bragato and Gianotti (119) used a simplified analysis to interpret the spinline behavior of PET at speeds up to 3500 meters per minute. Their experimental data showed no birefringence at the spinneret, the fibers exhibited no crystalline x-ray diffraction, gave an 8% crystalline index by DSC and the birefringence was linear with stress. They inferred that an elastic zone appeared at a given temperature where the birefringence increased rapidly. Their analysis estimated the molecular orientation and crystallinity in this solidification region. They concluded that the molecular orientation rapidly increased in the elastic zone after the end of the cold crystallization region "neck" and was linearly dependent on the local stress.

In a subsequent paper (120), they examined the crystallization kinetics of the fibers previously obtained using DSC techniques. They found an enormous increase in the kinetic rate with increasing orientation at the same crystallization temperature. The crystallization

temperature decreased with increasing orientation at the same heating rate. They concluded from an Avrami analysis that the mechanism changed from three dimensional growth at low orientations to two (disk) or one (rod) dimensional growth at high orientations.

In their study of nylon 6 spinning, Shimizu et al. (112) found no change in density for fibers spun at take-up speeds less than 3000 meters per minute but extensive changes above that speed. Below 5000 meters per minute, the $\gamma$ and h phases increased while the $\alpha$ phase decreased with increasing take-up speed. Above 5000 meters per minute, the $\gamma$ and h phases decreased while the $\alpha$ increased. The initial Young's modulus and the tenacity showed maxima at 5000 meters per minute. Also, the elongation to break decreased with increasing take-up speed. The transition around 5000 meters per minute reflected the heterogenieties in the fiber cross section.

Shimizu (113) summarized experimental results on high speed spun fibers of PET, nylon 6 and nylon-66. The birefringence of the nylon 6 fibers increased with time after spinning and a normalized differential birefringence decreased with velocity up to 4000 meters per minute to a limiting value. For nylon-66 fibers the transitions occurred around 3000 meters per minute. The birefringence increased and the long period remained constant below 3000 meters per minute. Above 3000 meters per minute, the birefringence and both the crystalline and amorphous orientation functions remained constant while the long period increased. The crystal perfection index remained at 0.60 up to 5000 meters per minute then increased.

Shimizu and coworkers (114) reported findings on an interesting polymorphic response of poly(ethylene - 1,2 - diphenoxyethane - p,p' - dicarboxylate) (PEET) to spinning conditions. PEET exhibited two crystallographic forms labelled α and β. The α form was triclinic and was found in material crystallized from the melt or dilute solutions. When spun at speeds below 3000 meters per minute, the fiber contained only the α form. At speeds between 3000 and 6000 meters per minute, the fiber contained both forms and the β form reverted to the α form on annealing. At speeds greater than 6000 meters per minute, only the β form was found and it would not transform upon annealing.

A later study (115) involved several polymers where the birefringence and stress (as measured by a tensiometer) were determined at several spinning speeds. The drag and inertial stresses were considered. Although the authors claimed a linear relationship between the inertial stresses and the birefringence the data indicated that this was only true for PET, not polypropylene, nylon 6 or nylon-66. They also presented "online" and off line values of the stress optical coefficient for several polymers. The differences between the two were attributed to crystallites in the off line samples, but no crystallinity data were given.

Lecluse (3) performed online x-ray studies of nylon-66 at spinning speeds of 500 to 7000 meters per minute. The x-ray scans were performed on a multifilament line after the fibers were collected into a bundle at temperatures from 110 to 25 °C. The patterns showed no variations along the spinline and only a high temperature γ form, postulated by Colcough and Baker (121), was present. These results are

consistent with the available kinetic data which indicate a maximum crystallization rate at 150 °C, and a Brill transition temperature of 160 °C would indicate a coalescence of the (100) and (110,010) diffraction peaks, thus inferring the γ form. Her emphasis was on the aging behavior of the spun fibers. The γ to α "transition" was dependent on the spinning speed, increased with the level of crystallinity and caused relaxation in the amorphous regions. The "transition" resulted in increased overall birefringence while the differential birefringence decreased between the skin and the core. She concluded that aging caused the fibril crystals to revert to lamellae as a result of epitaxial growth. The original γ crystals converted to the α form and continued to grow in the α form. The internal stresses were relieved by the plasticating action of water. This process was controlled by the relative humidity and molecular orientation.

Ziabicki (122) approached the theoretical aspects of high speed spinning. He concluded that the shear stress from the air drag force was too small to affect the structure formation process. The extremely high elongation rates altered the deformation in the spinline and induced instabilities, especially in conjunction with high cooling rates. The high stresses in the skin region provided a more suitable environment for molecular orientation and crystallization than the higher temperature, lower viscosity and lower stress interior of the fiber. This lead to radial variations in the fiber morphology. There remained the question of low orientation in the amorphous regions. He concluded that the stress in the spinline was the dominant factor in

the crystallization kinetics and that very high crystalline orientations were achieved.

## Crystallization Kinetics

The crystallization of polymers has been characterized as a two step process. The initial step involves the formation of a nucleus of sufficient size to form the basis of a crystal; this step is followed by a growth process whereby material is incorporated into the expanding crystal. Crystallization kinetics attempts to mathematically interpret these processes in a quantitative manner with respect to time.

The formation of a nucleus under isothermal conditions can occur by either a homo- or heterogeneous mechanism. Fisher et al. (123) proposed a theory for polymer crystallization by extending existing theories for nonpolymeric materials. The nucleation step was based on the theory of Becker and Doring (124) for condensed systems. Mandelkern et al. (125) proposed a homogeneous nucleation model to interpret disk and spherulitic shaped nuclei. Mandelkern (126) extended that treatment to cylindrical shaped nuclei. Devoy and Mandelkern (127) used Turnbull's heterogeneous nucleation model (128) and showed that the free energy barrier to nucleation was lower for heterogeneous nucleation than for homogeneous nucleation. Cormia et al. (129) reviewed early experimental studies and concluded that nucleation in polymers was almost entirely heterogeneous.

Avrami (130-132) has been credited with the introduction of the expression which relates the crystalline fraction to the elapsed time,

although the relationship was independently developed by several others (133-135) around the same time period. This relationship is

$$\Theta(t) = 1 - \exp[-E(t)] \tag{2-27}$$

where E(t) is a function whose form depends on the nucleation and growth mechanisms. In the case where there are $N_0$ nuclei formed at the same instant, E(t) is given by

$$E(t) = N_0 \; v(0,t) \tag{2-28}$$

where v(0,t) is the growth velocity. In the case where the nuclei are formed sporadically during the crystallization process, E(t) is

$$E(t) = \int N(s) \; v(s,t) \; ds \tag{2-29}$$

where N(s) is the nucleation rate and v(s,t) is the growth rate of those nuclei formed at time s. The special case of isolated nucleation and growth leads to

$$E(t) = kt^n \tag{2-30}$$

where k is an isothermal rate constant and n is the so-called Avrami index. Equation (2-30) has been extensively used to interpret polymer cystallization phenomena and there have been many theories developed which have attached a significance between the value of n and a particular mechanism. There have been so many of these relationships that a discrimination based on the Avrami index alone is no longer considered unique. Mandelkern (136) modified Avrami's analysis to

account for the amorphous to partially crystalline transformations found in most polymers.

The rate of nucleus formation within a system has been described in terms of two mechanisms. Thermal nucleation results from localized thermal fluctuations in the system about some thermodynamic steady state. Athermal nucleation is a result of changing the entire system from one thermodynamic steady state to another. The thermal nucleation rate for spherical nuclei, as given by Ziabicki (137), is

$$N_{th} = \text{Const}\left[\frac{ckT}{h}\right] \exp\left[\frac{-E_a}{kT}\right] \exp\left[\frac{-16\alpha^3 \, Tm^2}{3(\Delta H \Delta T)^2 kT}\right] \qquad (2\text{-}31)$$

where $E_a$ is the activation energy, $\alpha$ is the surface tension, $\Delta H$ is the heat of fusion, $T_m$ is the melting temperature and $\Delta T$ is the supercooling. For cylindrical nuclei, the nucleation rate is (138,139)

$$N_{th} = \text{Const}\left[\frac{ckT}{h}\right] \exp\left[\frac{-E_a}{kT}\right] \exp\left[\frac{-8\alpha_e \alpha_s^2 Tm^2}{(\Delta H \Delta T)^3 kT}\right] \qquad (2\text{-}32)$$

where $\alpha_e$ and $\alpha_s$ are the surface tensions on the head and side of the cylinder, respectively. The expressions used for the growth rates are of the same form as equations (2-31) and (2-32). Nakamura et al. (44,53) introduced the isokinetic assumption to produce a more tractable equation from Avrami's theory. The time dependence of all growth rates is hypothesized to be the same as that of the nucleation rate

$$N(t) = a\, U(t) \qquad (2\text{-}33)$$

$$G_i(t) = b_i\ U(t) \quad \text{for all } i \tag{2-34}$$

where U(t) was an arbitrary function of time. This gave for E(t)

$$E(t) = c[\int G_1(s)\ ds] \tag{2-35}$$

In the quasi-static assumption the nucleation and growth rates are a function of some parameter of state, $\Phi$, which leads to

$$E(t) = \ln 2\ [\int t_{1/2}[\Phi(s)]^{-1}\ ds]^n \tag{2-36}$$

where $t_{1/2}(\Phi)$ is the crystallization halftime. Ziabicki (140) considered E(t) in terms of a series expansion

$$E(t) = \text{Const}\ S^n[1 + b_1(t)S + b_2(t)S^2 + \ldots\ ] \tag{2-37}$$

where

$$S(t) = \int [N(s)\ G_1(s)\ldots G_{n-1}(s)]^{1/n} ds \tag{2-38}$$

and the $b_i(t)$ are functions of the ratios $N/G_1$, $G_i/G_1$, etc.

For non-isothermal conditions the athermal nucleation must be considered. Ziabicki (141,142) found for the athermal nucleation rate

$$N_{ath} = -\frac{\partial R^*}{\partial T}\frac{dT}{dt}\iint_S f\ ds \tag{2-39}$$

where $R^*$ is the critical radius of the spherical cluster, f is a distribution of cluster sizes and S is the critical size which separates the stable from the unstable nuclei.

The complex nature of non-isothermal polymer cystallization has led to the development of empirical relationships for the temperature

dependence of the rate constant in equation (2-30). This allowed equation (2-30) to be applied to non-isothermal polymer crystallization phenomena. Takayangi and Kusumoto (143) applied a Williams-Landel-Ferry temperature dependence to the activation energy in the expression for the thermal nucleation rate. This produced

$$k(T) = A \exp\left[-\frac{B\,T}{(T - T_g + 51.6)^2 \quad T(T_m - T)}\right] \qquad (2\text{-}40)$$

This expression was restricted to small supercoolings and would lead to large errors at temperatures less than 80% of $T_m$. Ziabicki (142) proposed the following relationship for the temperature dependence

$$k(T) = k_{max} \exp[-4\ln 2(T - T_{max}/D)^2] \qquad (2\text{-}41)$$

where $k_{max}$ is the maximum in the rate-temperature curve, $T_{max}$ is the temperature at $k_{max}$ and D is the half-width of the rate-temperature curve. Equation (2-41) is restricted to temperatures in the range $T_g$ to $T_m$. $T_{max}$, $k_{max}$ and D have been determined for many polymers by various researchers from experimental kinetic data.

The effect of stress, or strain, on the crystallization process was first noted by Katz (144) who found that amorphous natural rubber would crystallize when stretched, but not at rest. Gent (145) studied stress relaxation phenomena caused by crystallization in stretched vulcanized natural rubber. Mitchell (146) found that mechanically milling synthetic rubber before crystallization led to a lowering of the Avrami index and attributed this to a preorientation of the amorphous material. Rabesiaka and Kovacs (147) examined the effect of

nuclei existing above the melting temperature and molecular orientation on the crystallization kinetics of polyethylene. McCord and Spruiell (148) studied the kinetics of strained PET and observed an increased crystallization rate due to an increased number of nuclei and/or an increased nucleation rate which took place during the stretching. Mackley and Keller (149) concluded that preorientation was the cause of long fibrous crystals which were observed in polyethylene melt flows at temperatures above the equilibrium melting temperature.

The effect of molecular orientation on the melting temperature has been the object of several investigations. A thermodynamic approach has been the means by which the effect of deformation on the enthalpy and entropy of the system was evaluated. The entropy contribution was determined for both Gaussian (150,151,57) and non-Gaussian (152,153) chains and always led to an increased melting temperature whereas the enthalpy contribution may have led to a higher or lower melting temperature. Jarecki (154) included rotational isomerism in the enthaply and found a higher melting temperature than Krigbaum and Roe (57) for Gaussian chains.

Molecular orientation affects the thermal nucleation rate through the activation energy and the free energy for nucleus formation. Ziabicki (155) found that

$$E_a(\lambda) = \iint E_a(\phi_{cr},\phi_s)\, W_1(\phi_{cr})\, W_2(\phi_s)\, d\phi_{cr}\, d\phi_s \qquad (2\text{-}42)$$

where the $W_i$ are orientation distributions and $\phi_{cr}$ and $\phi_s$ are the angles of the crystal and the amorphous segments, respectively. The variation of $E_a(\phi_{cr},\phi_s)$ was found to be small and less significant

than the effect of orientation on the melting temperature. The effect of the orientation on the free energy was incorporated through the variation of the melting temperature with orientation. Ziabicki (58) proposed the following expression

$$\frac{dF}{d\lambda} = - \frac{p}{T_m} \frac{\Delta F}{\Delta T} T \frac{dT_m}{d\lambda} \tag{2-43}$$

Ziabicki (155) included an additional term to account for discrimination of amorphous segments which did not have the appropriate orientation with respect to the crystal surface. This indicated that the crystalline orientation distribution would be narrower than that of the original amorphous material. Under non-isothermal conditions, the increased molecular orientation reduced the critical radius needed to form a stable nucleus. The athermal nucleation rate became

$$N_{ath} = - \frac{\partial R}{\partial \lambda} \frac{d\lambda}{dt} \iint_S f \, ds \tag{2-44}$$

Restriction of the effect of orientation to the melting temperature led to

$$\frac{dR}{d\lambda} = \frac{\partial R}{\partial T_m} \frac{\partial T_m}{\partial \lambda} \tag{2-45}$$

and an increased nucleation rate was predicted.

As in the case of the temperature dependence, simplifications and/or empiricisms were necessary to make the theory more amenable to polymer processing applications. Ziabicki (58) expanded the melting temperature in a series expansion

$$T_m = T_m^{\,0} + a_1 f + a_2 f^2 + a_3 f^3 + \ldots \qquad (2\text{-}46)$$

Symmetry and small orientations were assumed and substituting equation (2-46) into the expression for the nucleation rate gave

$$\frac{N(f)}{N(0)} = \exp\left[\frac{\text{Const } f^2}{T_0}\right] \qquad (2\text{-}47)$$

Andrews (156) reported that the principal effect of strain, or orientation, on the crystallization process is in the nucleation step and includes no changes in the growth rate of the once-formed nuclei. Thus it was proposed by Ziabicki (157) that the rate constant can be expressed as

$$\frac{k(f)}{k(0)} = \exp\left(A(T)\ f^2\right) \qquad (2\text{-}48)$$

Combination of equation (2-41) with equation (2-48) produced for the temperature and orientation dependent rate constant

$$k = k_{max} \exp[-4\ln 2(T - T_{max}^{\,0}/D^0)^2 + A(T)\ f^2] \qquad (2\text{-}49)$$

where the superscripted zeros refer to the unoriented state.

## Nylon-66

### Synthesis

Nylon-66 is formed from the polymerization of hexamethylenediamine and adipic acid. By utilizing the free acid, the salt, hexamethylenediammonium, is produced. The stoichiometry of the reaction can then be controlled by the pH. The reactants are dissolved in a

solvent, mixed and then the precipitated salt is collected. In a representative batch process, the salt is dissolved in water and fed to an evaporator where it is concentrated to a liquor containing approximately 75% solids. This liquor is charged to an oxygen purged pressure vessel and heated to a temperature of 210 °C or up to a pressure of 250 psi. Steam is bled off as the temperature reaches 280 °C while maintaining a constant pressure. When the temperature reaches 280 °C the pressure is reduced to 14.7 psi. The polymer is forced out of the vessel by a pressurized inert gas, quenched and cut into chips (158-165).

Nylon-66 can also be manufactured in a continuous process where provisions are made to remove water and prevent dead spots in the flow to maintain consistency in the molecular weight (166-169). Historical reviews are given by Brill (170), Moncrief (171), Hoppf (164) and Sbrolli (172).

## Chemical Behavior

Ammonia has been frequently found as a decomposition product of nylon-66 (173-175) and cyclopentanone, or its derivatives, has also been found among its degradation products (176-180). Nylon-66 has exhibited gel formation after about six hours when heated in nitrogen at 305 °C (181). Although there was no evidence of the reaction of the acid groups there was for the amine groups. The gelation was attributed to the reaction of the thus formed secondary amines which lead to branched structures (182). After heating in steam at 290 °C, there was little change in the solution viscosity. The number of acid groups decreased while the number of amine groups increased. Acid

group loss was attributed to cyclopentanone formation while the amine group increase was caused by hydrolysis. Branching maintained the solution viscosity during the reactions (183). It was discovered that the chromium plating of extruder parts decreased the amount of degradation for nylon-66; oxidation was also a possible factor (184).

Valkok and Chiklis (185) showed that oxidation of nylon-66 fibers in air at 136 to 215 °C resulted in a loss of molecular weight, the number of acid groups remained unchanged and the number of amine groups decreased. In contrast, when heated in nitrogen or in the presence of antioxidents, the molecular weight increased. Numerous researchers (186-190) have found nylon-66 to be sensitive to many types of photo-oxidation processes.

Physical Properties

The melting temperature of nylon-66 is 265 - 270 °C under quiescent conditions (191,192) and is dependent on the cooling conditions in the non-isothermal stressed case. The glass transition temperature of dry nylon-66 is about 58 °C (193), but it is extremely sensitive to the influence of moisture. The density of crystalline nylon-66 depends on the crystal structure. The $\alpha$ form density is 1.226 gm/cm$^3$, the $\beta$ form density is 1.247 gm/cm$^3$ and the $\gamma$ form density is 1.1085 gm/cm$^3$ (194) at 25 °C. The amorphous density is 1.069 gm/cm$^3$ (194) at 25 °C. The melt density as a function of temperature is

$$\rho = [4.86 \times 10^{-4}\ T + 0.751]^{-1} \qquad (2\text{-}50)$$

and the density of solid nylon-66 is

$$\rho = 1.279 - 4.55 \times 10^{-4}\ T \qquad (2\text{-}51)$$

where T is the temperature in Kelvins (195). The thermal conductivity is 0.153 BTU/hr-ft-°F/in at 212 °F (196). Values for the heat of fusion range from 8.79 to 11.2 kcal/mol (197-199), but Wunderlich (200) reported a value of 11.7 kcal/mol. There have been many values of the entropy of fusion (defined as $\Delta H_m/T_m$) reported in the literature, but there is little agreement among them (201-204). Wunderlich (200) reported a value of 0.132 cal/gm °C for the entropy of fusion. Nylon melts are well ordered as a result of the hydrogen bonding effect and the entropy of fusion is a result of an increased volume and rotation about primary bonds in the chain (201-205). The average refractive index of nylon-66 is 1.550 (206) and the difference in polarizabilities ($\alpha_{\parallel} - \alpha_{\perp}$) is 0.00688 (207).

Simpson et al. (208) determined correlations of the tenacity and elongation to break with the amorphous orientation for nylon-66 fibers. Their results were

$$\log(\text{tenacity}) = 0.221 + 1.081\ f_a \qquad (2\text{-}52)$$

and

$$\log(\%\ \text{elongation}) = 2.351 - 1.620\ f_a \qquad (2\text{-}53)$$

Crystallography

Fuller and Frosch (209) performed the first x-ray studies of the crystal structure of nylon-66 and found that the chains are extended into a planar zigzag and that the chemical and crystallographic repeat units are identical.

Bunn and Garner (194) carried out an extensive study of nylon-66 and nylon-610. Nylon-66 was observed to exhibit two different crystalline forms, labelled $\alpha$ and $\beta$, which are different packings of geometrically similar molecules. They found that the $\alpha$ form is dominant. The $\alpha$ form has a one molecule, triclinic unit cell with lattice parameters; a = 4.9 Å, b = 5.4 Å, c = 17.2 Å, $\alpha$ = 48.5°, $\beta$ = 77.0° and $\gamma$ = 63.5°. The perpendicular distance between hydrogen bonded sheets is 3.6 Å and between chains in a hydrogen bonded sheet is 4.2 Å. The $\beta$ form has a two molecule triclinic structure with lattice parameters; a = 4.9 Å, b = 8.0 Å, c = 17.2 Å, $\alpha$ = 90°, $\beta$ = 77° and $\gamma$ = 67°.

Colclough and Baker (121) presented a crystallographic model based on the torsion angles of the carbon atoms adjacent to the amide group. They found that the planar amide group was justified by experimental data. There was also a strong correspondence between the molecular positioning and the intermolecular packing and the packing of the amide groups and the ethylenic groups. In consideration of the $\beta$ form, their model supported the view of Keller and Marradudin (210) that the layer line streaking and additional reflections which appear in nylon-66 are caused by a macroscopic interference effect rather than a different phase.

Brill (211) noted that as the temperature increases the (100) and (110,010) diffraction peaks move toward each other and finally coalesce into a single peak at 160 °C. This is a consequence of the change of the asymmetric packing in the basal plane of the triclinic unit cell to a hexagonal packing. Nuclear magnetic resonance (nmr) studies by Slichter (192) indicated that these crystallographic

changes corresponded to the onset of molecular motion in the parafinic segments. Baker (212) found that the planes of the polar groups remain tilted with respect to the molecular axis in the hexagonal packing. The change in the packing arrangement is accompanied by a change in the unit cell length, this a result of the twisting of the chain segments. It has been postulated that this high temperature form consisted of a three dimensional hydrogen bonded network based on the hexagonal unit cell base and the basal spacing which was typical of hydrogen bonded planes. Cannon et al. (206) disputed this model with optical studies on drawn and rolled nylon-66 fibers. This view was supported by the Colclough and Baker model mentioned previously. The heat driven twisting of the ethylenic segments causes the torsion angles adjacent to the amide groups to change which allows the amide groups to rotate giving rise to the observed changes in the unit cell dimensions. The lattice parameters for this $\gamma$ form are; a = 5.0 Å, b = 5.9 Å, c= 16.23 Å, $\alpha$ = 56.67°, $\beta$ = 80.6°, $\gamma$ = 59.867°.

Crystallization Kinetics

Allen (213) studied the crystallization kinetics of nylon-66 between 245 and 255 °C and melt temperatures of 270 to 300 °C. The crystallization curve consisted of three regions; initially the melt cooled down to the crystallization temperature followed by an induction period of about ten minutes, then the typical S shaped curve appeared. The rate constant was found to vary linearly with temperature. The crystallization rate decreased with increasing melt temperature but increased rapidly with decreasing crystallization temperature. Crystallization had initiated from nuclei that had survived the

melt and from nuclei that had sporadically formed during the crystallization process. The rate of addition to the growing crystal was constant. The induction period was a result of the time necessary for a nucleus to grow to the critical size. At melt temperatures greater than 290 °C there was a marked deviation from the rate equation, perhaps due to degradation.

Savolainen (214) applied the Avrami analysis to the isothermal crystallization of nylon-66 in the range 229 to 236 °C. The Avrami index was between 2.3 and 3 and the activation energy was 149 kcal. Both primary and secondary crystallization phenomena were observed. Magill (215) studied the isothermal crystallization kinetics over a range of temperatures and found that the reciprocal of the crystallization half-times was represented by

$$k(T) = k_{max} \exp[-4\ln 2(T - T_{max}/D_0)^2] \qquad (2\text{-}41)$$

The values for these parameters for nylon-66 are; $T_{max}$ = 150 °C, $k_{max}$ = 1.64 $sec^{-1}$ and $D_0$ = 80 °C. According to Ziabicki (142), the kinetic crystallizability (2-19) establishes the degree of crystallinity when the polymer is cooled from $T_m$ to $T_g$ at a unit cooling rate. For nylon-66, the kinetic crystallizability is 139 °C/sec compared to 1.1 °C/sec for PET, 6.8 °C/sec for nylon 6 and 35 °C/sec for isotactic polypropylene (142).

Structure

Nylon-66 single crystals grown from solution appeared as flat ribbon-like structures (165,173). Koneig and Agboatwalla (216) proposed that chain folding occurred with regular adjacent reentry and

the (010) planes of the unit cell were the preferred fold surface. Dreyfuss and Keller (217) found that these single crystals had a constant lamellae thickness with crystallization temperature of about 59 Å. They attributed this to restrictions imposed by hydrogen bonding. Koneig and Agboatwalla (216) also found that chain folding in melt crystallized nylon-66 was the same as that found in single crystals grown from solution.

Dismore and Statton (218) used SAXS, WAXS, nmr and sonic modulus to study chain folding in oriented nylon-66 fibers. After annealing, the crystallinity and long period increased while the crystalline orientation remained the same. The sonic modulus results indicated that new folds had occurred and the shrinkage behavior was governed by the number of new folds.

Keller and coworkers (219,220) examined the structure of folded chain nylon-66 using x-ray diffraction techniques. It was determined that straight chain stems traversed the entire lamellae thickness which implied sharp chain folds at the surface. This required that a majority of the folds occurred in the acid group. They also found that there were some folds at the surface that went deeper into the crystal than the majority. The spherulitic structures found in nylon-66 have been extensively studied (221-226). In general, below 250 °C, nylon-66 exhibited positively birefringent spherulites composed of fine fibrils grown along the crystallographic a axis. Between 250 and 270 °C, negatively birefringent spherulites were formed. Although highly crystalline, little preferred orientation was exhibited. Magill (224) noted evidence that the crystallographic b axis lies parallel to the

spherulite radius. These spherulites were composed of lamellae rather than fibrils with the plane of the lamellae also parallel to the spherulitic radius.

Effect of Moisture

As a class, polyamides are very susceptible to the influence of moisture. Jones and Porter (227) found that the specific heat of nylon-66 was a constant 1.01 cal/gm-°C over the range 60 to 220 °C at 65% relative humidity (rh), compared to the results of Wilhoit and Dole for dry yarn who found that it ranged from 0.345 at 20 °C to 0.675 cal/gm-°C at 140 °C (228). They also determined that their results were independent of the heating rate in the range 100 to 1000 °C/sec. Adams (229) examined the influence of rh on the shear and Young's modulii. At rh less than 40%, the shear modulus increased with draw ratio, while at rh greater than 40%, it decreased with increasing draw ratio. At a fixed draw ratio, the shear modulus decreased with increasing rh. Young's modulus also decreased with increasing rh, and the difference between the dry and moist cases was greater at higher draw ratios.

Starkweather (230,231) found a large decrease in the modulus in the machine direction but a smaller effect in the transverse modulus. He also discovered a 70 °C decrease in $T_g$ and an increase in density with increasing moisture content. Quistwater and Dunell (232) investigated the effect of water on the dynamic mechanical properties of nylon-66. The storage modulus decreased with increasing moisture content at all frequencies. At 35 and 60 °C, the loss modulus dependence on frequency changed systematically with rh. At low humidities

the loss modulus decreased with frequency, at rh of 35-40% the modulus was independent of frequency and at higher rh the loss modulus increased with frequency. At a fixed temperature an increase in water content caused the maximum in the loss modulus to appear at higher frequencies. They developed a "time - humidity" superposition principle whose utility was limited to rh greater than 58%.

Smith (233) used a pulsed nmr signal to investigate the effect of moisture on the molecular motion in nylon-66 fibers. The temperature at which the mobile component of the nmr signal appeared in the dry fiber was approximately 100 °C. This temperature decreased with increasing moisture content down to around 0 °C at saturation. This phenomena was attributed to the plasticizing effect of the water molecules in the amorphous regions of the fiber. Reimschuessel (234) studied the effect of moisture on the glass transition temperature and Young's modulus for several polymers. The following relationships were found

$$T_g = (T_{g0} - T_{g1}) \exp(-[\ln(T_{g0} - T_{g1})]W/\tau W_1) + T_{g1} \qquad (2\text{-}54)$$

and

$$E = (E_0 - E_1) \exp(-[\ln(E_0 - E_1)] W/\varepsilon W_1) + E_1 \qquad (2\text{-}55)$$

For nylon-66 the following parameters were found; $T_{g0}$ = 97 °C, $T_{g1}$ = 4 °C, $W_1$ = 0.16 and $\tau$ = 0.875. Data was not given for $E_0$, $E_1$ or $\varepsilon$. Brill (211) found that the temperature at which the (100) and (110,010) diffraction peaks coalesced changed from 160 °C in dry fibers to 140 °C for nylon-66 which had been exposed to moisture. McLaren (235)

found that the plasticizing action of water molecules in the amorphous region caused an increase in the rate of crystallization.

Chappel et al. (2), in their study of the melt spinning of nylon-66, concluded that the moisture effect was negligible during the spinning process. They examined the effect of moisture on the crystallinity and orientation of nylon-66 fibers using x-ray and birefringence techniques. Birefringence changes were noted minutes after the fibers were exposed to moisture, whereas no changes in crystallinity from x-ray determination were found up to sixty-six hours after exposure. They concluded that the effect of the water molecules was to change the molecular orientation in the amorphous region without affecting the crystallinity.

Recently, Hunt (236) studied the moisture absorption of nylon-66 and found that it was independent of stress and the thickness and solely a function of rh. The relationship between water content and rh was

$$C = 0.1457R - 3.762\times10^{-3}R^2 + 5.498\times10^{-5}R^3 - 2.34\times10^{-7}R^4 \qquad (2\text{-}56)$$

The diffusion coefficient was found to be primarily dependent on the water concentration but also had a slight dependence on the thickness and shape. There was a slight divergence from Fickian behavior for very small thicknesses.

# CHAPTER 3

## DEVELOPMENT OF FUNDAMENTAL EQUATIONS

The basis of the analysis used in this study was a combination of the equations of continuity, motion and energy along with boundary conditions and assumptions based on the physics of the melt spinline. These will be introduced as needed. The spinline is shown schematically in Figure 3.1, along with the reference axes used.

### Force Balance

The equations of continuity and motion in the cylindrical coordinate system are (237):

Continuity

$$\frac{\partial \rho}{\partial t} + \frac{1}{r}\frac{\partial(\rho r V_r)}{\partial r} + \frac{1}{r}\frac{\partial(\rho V_\theta)}{\partial \theta} + \frac{\partial(\rho V_z)}{\partial z} = 0 \qquad (3\text{-}1)$$

Motion:

r-component

$$\rho\left[\frac{\partial V_r}{\partial t} + V_r\frac{\partial V_r}{\partial r} + \frac{V_\theta}{r}\frac{\partial V_r}{\partial \theta} - \frac{V_\theta^2}{r} + V_z\frac{\partial V_r}{\partial z}\right] = -\frac{\partial P}{\partial r} - \frac{1}{r}\frac{\partial(r\tau_{rr})}{\partial r}$$

$$+ \frac{1}{r}\frac{\partial \tau_{r\theta}}{\partial \theta} - \frac{\tau_{\theta\theta}}{r} + \frac{\partial \tau_{rz}}{\partial z} + \rho g_r \qquad (3\text{-}2)$$

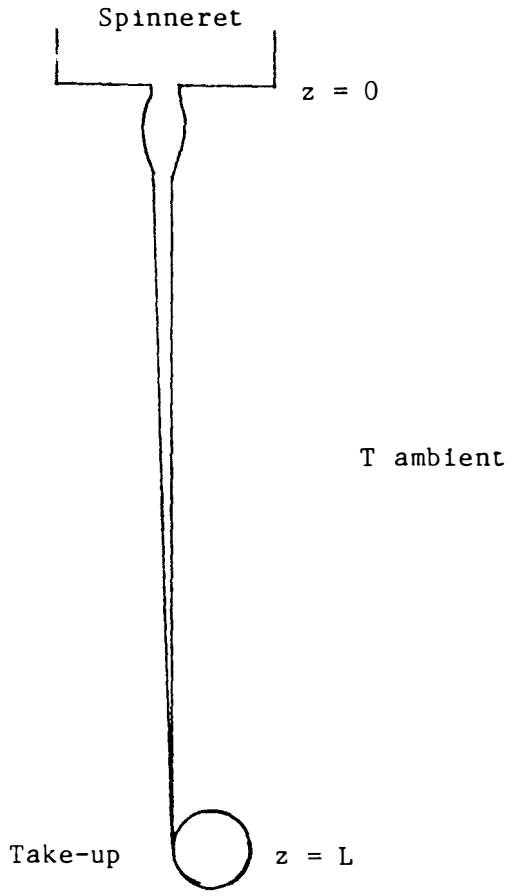


Figure 3.1 Schematic representation of the melt spinline.

θ-component

$$\rho\left[\frac{\partial V_\theta}{\partial t} + V_r\frac{\partial V_\theta}{\partial r} + \frac{V_\theta}{r}\frac{\partial V_\theta}{\partial \theta} + \frac{V_r V_\theta}{r} + V_z\frac{\partial V_\theta}{\partial z}\right] = -\frac{1}{r}\frac{\partial P}{\partial \theta} - \frac{1}{r^2}\frac{\partial(r^2\tau_{r\theta})}{\partial r}$$

$$-\frac{1}{r}\frac{\partial \tau_{\theta\theta}}{\partial \theta} - \frac{\partial \tau_{\theta z}}{\partial z} + \rho g_\theta \qquad (3\text{-}3)$$

z-component

$$\rho\left[\frac{\partial V_z}{\partial t} + V_r\frac{\partial V_z}{\partial r} + \frac{V_\theta}{r}\frac{\partial V_z}{\partial \theta} + V_z\frac{\partial V_z}{\partial z}\right] = -\frac{\partial P}{\partial z} - \frac{1}{r}\frac{\partial(r\tau_{rz})}{\partial r}$$

$$-\frac{1}{r}\frac{\partial \tau_{\theta z}}{\partial \theta} + \frac{\partial \tau_{zz}}{\partial z} + \rho g_z \qquad (3\text{-}4)$$

The spinning operation was assumed to be a steady state process, and symmetry requires that $V_\theta = 0$, in addition, it was assumed that there were no variations of velocity in the r and θ directions. Also it was assumed that there was no radial velocity. These conditions applied to the continuity and motion equations led to

Continuity

$$\frac{\partial(\rho V_z)}{\partial z} = 0 \qquad (3\text{-}5)$$

Motion: z-component

$$V_z\frac{\partial V_z}{\partial z} = -\frac{1}{r}\frac{\partial(r\tau_{rz})}{\partial r} - \frac{\partial \tau_{zz}}{\partial z} + \rho g_z \qquad (3\text{-}6)$$

Integration of the continuity equation yields

$$W = \rho\pi R^2 V \tag{3-7}$$

where W is the mass throughput. Now multiplying the z-component of the equation of motion by the differential area, $2\pi r dr$ and integrating from r = 0 to r = R yields

$$\rho\pi R^2 V \frac{\partial V}{\partial z} = \rho\pi R^2 g + 2\pi r \tau_{rz}\Big|_{r=R} - 2\pi R \frac{dR}{dz} \tau_{zz}\Big|_{r=R} + \pi R^2 \frac{\partial \tau_{zz}}{\partial z} \tag{3-8}$$

where $\tau_{zz}$ indicates the stress averaged over the radial direction. Multiplying by the differential length, dz, produces

$$\rho\pi R^2 V\, dV = \rho\pi R^2 g\, dz + 2\pi R \tau_{rz}\Big|_{r=R} dz - 2\pi R \frac{dR}{dz} \tau_{zz}\Big|_{r=R} dz + \pi R^2\, d\tau_{zz} \tag{3-9}$$

This is the differential force balance which can be written as

$$dF_{rheo} = dF_{inert} + \delta F_{drag} + \delta F_{surf} - dF_{grav} \tag{3-10}$$

where

$$dF_{rheo} = \pi R^2\, d\tau_{zz} \tag{3-11}$$

$$dF_{inert} = \rho\pi R^2 V\, dV = W\, dV \tag{3-12}$$

$$\delta F_{drag} = 2\pi R \tau_{rz}\Big|_{r=R} dz = \rho C_d V^2\, dA = \rho C_d V^2 \pi D\, dz \tag{3-13}$$

$$\delta F_{surf} = 2\pi R \frac{dR}{dz} \tau_{zz}\Big|_{r=R} dz = 4\pi R H \sigma \frac{dR}{dz}\Big|_{r=R} dz \tag{3-14}$$

$$dF_{grav} = \rho\pi R^2 \; g \; dz = \frac{Wg}{V} \; dz \tag{3-15}$$

where $C_d$ is the Reynolds number dependent drag coefficient, $\sigma$ is the surface tension between the polymer and the air and H is the radius of curvature (238) given by

$$H = \frac{1 - RR''}{R[1 + (R')^2]^{3/2}} \tag{3-16}$$

where the primes designate the derivative with respect to z. This differential force balance can be integrated to produce the following macroscopic force balance

$$F_{rheo} = F_{inert} + F_{drag} + F_{surf} - F_{grav} \tag{3-17}$$

where

$$F_{rheo} = \int \pi R^2 \; d\tau_{zz} \tag{3-19}$$

$$F_{inert} = W \; [V_L - V_0] \tag{3-20}$$

$$F_{drag} = 2W \int C_d/R \; dz \tag{3-21}$$

$$F_{surf} = 4\pi\sigma \int HR \left.\frac{dR}{dz}\right|_{r=R} dz \tag{3-22}$$

$$F_{grav} = \pi g \int R^2 \; dz \tag{3-23}$$

The stress profile was computed from

$$\tau_{zz} = F_{rheo}/\text{Area} \tag{3-23}$$

Energy Balance

The energy balance in cylindrical coordinates is (237):

$$\rho C_p\left[\frac{\partial T}{\partial t} + V_r\frac{\partial T}{\partial r} + \frac{V_\theta}{r}\frac{\partial T}{\partial \theta} + V_z\frac{\partial T}{\partial z}\right] = -\frac{1}{r}\frac{\partial(rq_r)}{\partial r} - \frac{1}{r}\frac{\partial q_\theta}{\partial \theta} - \frac{\partial q_z}{\partial z}$$

$$- T\left[\frac{\partial P}{\partial T}\right]_\rho\left[\frac{1}{r}\frac{\partial(rV_r)}{\partial r} + \frac{1}{r}\frac{\partial V_\theta}{\partial \theta} + \frac{\partial V_z}{\partial z}\right]$$

$$- \tau_{zz}\frac{\partial V_r}{\partial r} - \tau_{\theta\theta}\left[\frac{1}{r}\frac{\partial V_\theta}{\partial \theta} + V_r\right] - \tau_{zz}\frac{\partial V_z}{\partial z}$$

$$- \tau_{r\theta}\left[\frac{r\partial(V_\theta/r)}{\partial r} + \frac{1}{r}\frac{\partial V_r}{\partial \theta}\right]$$

$$-\tau_{rz}\left[\frac{\partial V_z}{\partial r} + \frac{\partial V_r}{\partial z}\right] - \tau_{\theta z}\left[\frac{1}{r}\frac{\partial V_z}{\partial \theta} + \frac{\partial V_\theta}{\partial z}\right] \tag{3-24}$$

where $C_p$ is the specific heat at constant pressure. Applying the assumptions introduced in the previous section, in addition to the assumption that $C_p$ is independent of temperature, the temperature is solely a function of z and that the viscous heat generation contribution to the energy balance is negligible, the energy balance becomes

$$\rho C_p V_z \frac{\partial T}{\partial z} = - \frac{1}{r}\frac{\partial (r q_r)}{\partial r} + \frac{\partial q_z}{\partial z} \tag{3-25}$$

Multiplying by the differential area, $2\pi r dr$, and integrating across the radial direction yields

$$\rho \pi R^2 C_p V_z \frac{\partial T}{\partial z} = - 2\pi R q_r \Big|_{r=R} + \pi R^2 \frac{\partial q_z}{\partial z} \tag{3-26}$$

The heat flux in the radial direction at the fiber surface is accomplished by convection and radiation as

$$q_r \Big|_{r=R} = h(T - T_a) + \lambda \varepsilon (T^4 - T_a{}^4) \tag{3-27}$$

where h is the heat transfer coefficient, $\lambda$ is the Stephen-Boltzman constant, $\varepsilon$ is the emissivity and $T_a$ is the ambient temperature. The heat flux in the z direction is a result of conduction and the latent heat given up during the crystallization process within the differential element under consideration

$$q_z = k \frac{dT}{dz} + \rho \Delta H \frac{\partial \Theta}{\partial t} dz \tag{3-28}$$

where k is the thermal conductivity, $\Delta H$ is the heat of fusion and $\Theta$ is the crystalline fraction. Thus the energy balance becomes

$$\rho \pi R^2 C_p V \frac{dT}{dz} = - 2\pi R h(T - T_a) - 2\pi R \lambda \varepsilon (T^4 - T_a{}^4)$$

$$+ \pi R^2 k \frac{d^2 T}{dz^2} + \rho \pi R^2 \Delta H \frac{\partial \Theta}{\partial t} \tag{3-29}$$

There have been studies (39,40) which indicate that the radiation contribution ranges from 20% of the total heat flux near the die and quickly decreases to less than 1% away from the die. Assuming that the radiation and conduction contributions are negligible, the energy balance becomes

$$\rho\pi R^2 C_p V \frac{dT}{dz} = -2\pi Rh(T - T_a) + \rho\pi R^2 \Delta H \frac{\partial\Theta}{\partial t} \tag{3-30}$$

The crystallization rate can be expressed as

$$\frac{\partial\Theta}{\partial t} = \frac{d\Theta}{dt} + V \frac{d\Theta}{dz} \tag{3-31}$$

or at steady-state

$$\frac{\partial\Theta}{\partial t} = V \frac{d\Theta}{dz} \tag{3-32}$$

The energy balance now reduces to

$$\frac{dT}{dz} = -\frac{\pi Dh(T - T_a)}{W C_p} + \frac{\Delta H}{C_p} \frac{d\Theta}{dz} \tag{3-33}$$

# CHAPTER 4

# SIMULATION OF THE MELT SPINNING PROCESS

The melt spinning operation was modeled using a combination of the mass, momentum and energy balances and a mathematical model of the crystallization kinetics which included temperature and orientation effects. This mathematical formulation resulted in a series of eight highly coupled ordinary differential equations. These equations were solved numerically by the Continuous System Modeling Program (CSMP) developed by the International Business Machines Company and available on the University of Tennessee Computer Center's IBM 370 computer system.

## Mathematical Model

The melt spinning model consisted of a combination of ordinary differential equations, which applied to any material, along with various physical property correlations and empiricisms, which were specific to the material. These were then solved simultaneously using CSMP.

### Force Balance

The mass and momentum equations were combined as in Chapter 3 to produce a differential force balance

$$dF_{rheo} = dF_{inert} + \delta F_{drag} - dF_{grav} \tag{4-1}$$

where

$$dF_{inert} = W\ dV \tag{4-2}$$

$$\delta F_{drag} = \rho_a\ C_d\ V^2\ \pi\ D\ dz \tag{4-3}$$

$$dF_{grav} = (Wg/V)\ dz \tag{4-4}$$

Since the drag force was considered as a differential entity, the local drag coefficient rather than an integral drag coefficient must be used. The form used here was derived from boundary layer theory by Sakiadis (17) as

$$C_d = 4/\beta\ Re \tag{4-5}$$

where the parameter $\beta$ was evaluated by integrating from 0 to $\beta$ using

$$\xi^2 = 8 \int \frac{(z-1)\ \exp(2z) + z^2 + 1}{z^2}\ dz \tag{4-6}$$

and

$$\xi^2 = 64\ z/D\ Re \tag{4-7}$$

where Re is the Reynolds number based on the fiber diameter and velocity,

$$Re = \rho_a\ V\ D/\ \mu_a \tag{4-8}$$

The integral in equation (4-6) was performed numerically using CSMP and a table of $\beta$ and $\xi$ was compiled and used as input in the model.

During execution $\xi$ was computed and a table interpolation was performed to acquire a corresponding value of $\beta$ which was then used to compute the local drag coefficient. The density and viscosity of air ($\rho_a$ and $\mu_a$, respectively) were chosen constant with values of $\rho_a$ = $6.62 \times 10^{-5}$ gm/cm$^3$ and $\mu_a = 2.8 \times 10^{-4}$ poise (239).

The stress along the spinline was given by

$$\sigma_{zz} = F_{rheo}/\text{Area} \tag{4-9}$$

and the velocity gradient by

$$\frac{dV}{dz} = \frac{\sigma}{\eta} \tag{4-10}$$

The fiber diameter was evaluated from the continuity equation

$$D = 4\sqrt{W/\rho\pi V} \tag{4-11}$$

Energy Balance

The energy balance, as given in equation (3-30), was used to evaluate the temperature gradient along the spinline. After some rearrangement equation (3-30) becomes

$$\frac{dT}{dz} = \frac{h\pi D\ (T_a - T)}{W\ C_p} + \frac{\Delta H}{C_p}\frac{d\Theta}{dz} \tag{4-12}$$

The heat transfer coefficient has been studied by several groups (28,45-50) and the following relationship was used (28)

$$h = 6.85\text{x}10^{-5}(\rho V^2/W)^{0.259}(1 + (8\ V_y/V_f)^2)^{0.167} \qquad (4\text{-}13)$$

where $V_y$ and $V_f$ are the cross and fiber velocities, respectively.

Birefringence and Orientation

The birefringence and amorphous orientation were modeled by a combination of the stress optical law with a Maxwell element. The stress optical law

$$\Delta n_a = C_{op}\ \sigma \qquad (4\text{-}14)$$

was differentiated with respect to time to yield, assuming that $C_{op}$, the stress optical coefficient, is independent of time

$$\frac{\partial \Delta n_a}{\partial t} = C_{op}\ \frac{\partial \sigma}{\partial t} \qquad (4\text{-}15)$$

The Maxwell element produced for $\partial\sigma/\partial t$

$$\frac{\partial \sigma}{\partial t} = E\ \frac{dV}{dz} - \frac{E\ \sigma}{\eta} \qquad (4\text{-}16)$$

Combination of the two gives

$$\frac{\partial \Delta n_a}{\partial t} = C_{op}\ E\ \frac{dV}{dt} - \frac{C_{op}\ E\ \sigma}{\eta} \qquad (4\text{-}17)$$

Converting the partial derivative with respect to time to the total derivative with respect to position and substituting $\Delta n_a$ for $C_{op}\ \sigma$ gave

$$\frac{d\Delta n_a}{dz} = \frac{C_{op}\ E}{V}\ \frac{dV}{dz} - \frac{E\ \Delta n_a}{V\ \eta} \qquad (4\text{-}18)$$

This relationship was used to compute the amorphous birefringence gradient. The total birefringence was calculated from

$$\Delta n = (1 - \Theta)\ \Delta n_a + \Theta\ f_c\ \Delta^0{}_c \tag{4-19}$$

Previous work (9,10,108-113) has indicated that at the higher take-up speeds the crystalline orientation factor maintained a fairly high and constant value. Thus it was assumed that $f_c = 0.9$ during the spinning process. The amorphous orientation function was calculated from

$$f_a = \Delta n_a / \Delta^0{}_a \tag{4-20}$$

Crystallization Kinetics

The basis of the mathematical expression of the crystallization kinetics was the Avrami analysis (130-132)

$$\Theta(t) = \Theta_\infty [1 - \exp(-[\int K\ d\tau]^n)] \tag{4-21}$$

The temperature (215) and the orientation (157) effects were introduced into the rate "constant" as

$$K = K_{max} \exp[-4\ln 2(T - T_{max}/D_0)^2 + C\ f_a{}^2] \tag{4-22}$$

In order to evaluate the temperature gradient, an expression for the crystallization rate was necessary. This was obtained by differentiating equation (4-21) with respect to time

$$\frac{\partial \Theta}{\partial t} = \Theta_\infty\ n\ K\ (\int K\ d\tau)^{n-1} \exp[-(\int K\ d\tau)^n] \tag{4-23}$$

Since the expressions for the crystalline index (4-21) and the rate (4-23) involved integration with respect to time, it was necessary to convert these integrals so they were compatible with the notion of variation with respect to position. This conversion was accomplished by

$$dt = dz/V \tag{4-24}$$

Thus the equation for the crystalline index becomes

$$\Theta(z) = \Theta_\infty[1 - \exp(-[\int K/V\ dz']^n)] \tag{4-25}$$

and for the crystallization rate

$$\frac{d\Theta}{dz} = \Theta_\infty \frac{n\ K}{V} (\int K/V\ dz')^{n-1} \exp[-(\int K/V\ dz')^n] \tag{4-26}$$

Physical Properties

In order to perform the simulations, several material physical properties were required. Some of these were treated as constants while others were expressed as a function of temperature, molecular weight, crystallinity, etc., depending upon the availability of data in the literature.

Nylon-66. The density of nylon-66 in the melt was taken as (195)

$$\rho = [4.86\text{x}10^{-4}\ T + 0.891]^{-1} \tag{4-27}$$

and in the solid as

$$\rho = \frac{1.1018 - 0.00151\Theta}{1 - 0.128\Theta} - 4.55\times10^{-4}\ T \qquad (4\text{-}28)$$

In equation (4-28) it was assumed that the crystalline density was 1.226 $gm/cm^3$ and the amorphous density was 1.069 $gm/cm^3$ at 25 °C (194).

The elongational viscosity of nylon-66 was evaluated as a function of temperature, molecular weight and crystalline index. The molecular weight dependence was expressed as

$$\eta = k(M_w)^{3.5} \qquad (4\text{-}30)$$

The temperature dependence was divided into two regions; above $T_m$ it was expressed in terms of an Arrhenius expression

$$\eta = k'\ \exp[7548/T + 273] \qquad (4\text{-}31)$$

and below $T_m$ it was expressed in terms of a Williams-Landel-Ferry expression

$$\eta = k''\ \exp[-8.86(T - 100)/(T - 1.6)] \qquad (4\text{-}32)$$

The influence of the crystallinity was expressed as

$$\eta = k'''\ \exp[4.605\ [\Theta/\Theta_\infty]^{12}] \qquad (4\text{-}33)$$

Combination of the preceding expressions gave for the elongational viscosity above $T_m$

$$\eta = 3.31\times10^{-17}(M_w)^{3.5}\ \exp\left[\frac{7548}{T + 273}\right]\ \exp\left[4.605\left[\frac{\Theta}{\Theta_\infty}\right]^{12}\right] \qquad (4\text{-}34)$$

and below $T_m$

$$\eta = 1.1\times10^{-11}(M_w)^{3.5} \exp\left[\frac{-8.86(T - 100)}{T - 1.6}\right] \exp\left[4.605\left[\frac{\Theta}{\Theta_\infty}\right]^{12}\right] \quad (4\text{-}35)$$

It should be noted that the weight averaged molecular weight appears in the expressions for the elongational viscosity but all the information available in the literature for nylon-66 is given in terms of the number averaged molecular weight, so it was used in place of the weight averaged molecular weight in the viscosity expressions.

The specific heat as a function of temperature was evaluated from the data given in reference (240) for nylon-66 as

$$C_p = 0.0014\ T + 0.33 \quad (4\text{-}36)$$

The modulus of nylon-66 was evaluated as a function of temperature by linear interpolation of the data of Starkweather and Jones (241). The thermal conductivity and the stress optical coefficient were assumed constant because of the scant amount of data on the variability with temperature published in the literature. The thermal conductivity was $6.32\times10^{-4}$ cal/gm-°C-cm (196) and the stress optical coefficient was $1.3\times10^{-10}$ $cm^2$/dyne (242). The amorphous and crystalline intrinsic birefringences were assumed equal at 0.090 (206). The heat of fusion was 45 cal/gm (200). Magill (215) reported for nylon-66, values of $T_{max}$ = 150 °C, $D_0$ = 80 °C and $K_{max}$ = 1.62 $sec^{-1}$. The variation of C in equation (4-22) was taken as

$$C = 26000/(T_m - T) \quad (4\text{-}37)$$

Polypropylene. The density of polypropylene in the melt was taken as (243)

$$\rho = [9.03\text{x}10^{-4}\ T + 1.145]^{-1} \tag{4-38}$$

and in the solid as

$$\rho = [9.03\text{x}10^{-4}\ T - 0.102\Theta + 1.148]^{-1} \tag{4-39}$$

In equation (4-39) it was assumed that the crystalline density was 0.936 gm/cm$^3$ and the amorphous density was 0.854 gm/cm$^3$ (244). The elongational viscosity as a function of molecular weight (245), temperature and crystallinity above $T_m$ was

$$\eta = 2.00\text{x}10^{-16}(M_w)^{3.55} \exp\left[\frac{500}{T + 273}\right] \exp\left[9.210\left[\frac{\Theta}{\Theta_\infty}\right]^2\right] \tag{4-40}$$

and below $T_m$

$$\eta = 2.0\text{x}10^{-16}(M_w)^{3.55} \exp\left[\frac{5100}{T + 273}\right] \exp\left[9.210\left[\frac{\Theta}{\Theta_\infty}\right]^2\right] \tag{4-41}$$

The specific heat as a function of temperature was taken as (246)

$$C_p = 2.42\text{x}10^{-3}\ T + 0.3669 \tag{4-42}$$

The modulus was evaluated as a function of temperature by linear interpolation of the data provided by Reding (247). The thermal conductivity was 2.8x10$^{-4}$ cal/gm-°C-cm (243) and the stress optical coefficient was 2.5x10$^{-10}$ cm$^2$/dyne (248). The amorphous and crystalline intrinsic birefringences were 0.060 and 0.0291, respectively (249,250). The heat of fusion was 59 cal/gm (251). Magill (252) found

that $T_{max}$ = 65 °C, $D_0$ = 60 °C and $K_{max}$ = 0.55 $sec^{-1}$. The melting temperature was 180 °C and the glass transition temperature was -20 °C (252).

## Continuous System Modeling Program

CSMP is a Fortran based package developed by IBM which allows scientists and engineers to simulate physical systems with minimum programming of complex numerical schemes such as integration and differentiation. A CSMP program consists of three segments; an Initial segment where constants and initial conditions are specified, a Dynamic segment where the mathematical expressions used to simulate the physical system are described and a Terminal segment where any calculations subsequent to the dynamic computations are performed and the results outputted.

In this study, a system of eight ordinary differential equations (4-1 to 4-4, 4-10, 4-12, 4-18 and 4-24) was used to mathematically model the melt spinning process. Since this system of equations described several physical processes whose solutions were expected to occur at much different time scales a numerical integration scheme designed for stiff equations was employed. CSMP offers several methods of integration and the method designated as STIFF was used in all the simulations in this study. A more detailed description of this and other integration routines along with instructions for using CSMP is given in reference (253). Complete CSMP programs for nylon-66 and polypropylene melt spinning are shown in the Appendixes.

# CHAPTER 5

# EXPERIMENTAL APPARATUS AND PROCEDURE

## Melt Spinning Operations

### Description of the Apparatus

A Fourne extruder (shown schematically in Figure 5.1) coupled to a melt spinning head was used in all experiments. The extruder was a single screw (diameter = 13 millimeters, length = 300 millimeters) machine equipped with a nitrogen-purged hopper. It has two independently controlled band-type heaters along its barrel. The spinning head also has two independently controlled band heaters similar to those on the barrel. Cooling water was provided to the throat of the extruder to prevent melted polymer from backwashing into the hopper feed section.

A Dynisco pressure transducer (Model PT441AE-10M-6/30) was mounted in the spinning head between the extruder exit and the Zenith gear pump. This pump (Type HPB-4647) was a positive displacement type which used counter-rotating intermeshing gears to deliver a constant mass throughput to the spinneret. The actual mass throughput was determined by the density of the material, size of the gears and the rotational speed of the gears.

In addition to the thermocouples associated with the band heaters, two resistance temperature detectors were placed in the spinning head, one between the pressure transducer and the gear pump and the other between the gear pump and the spinneret. These were mounted so that the actual melt temperature could be determined.

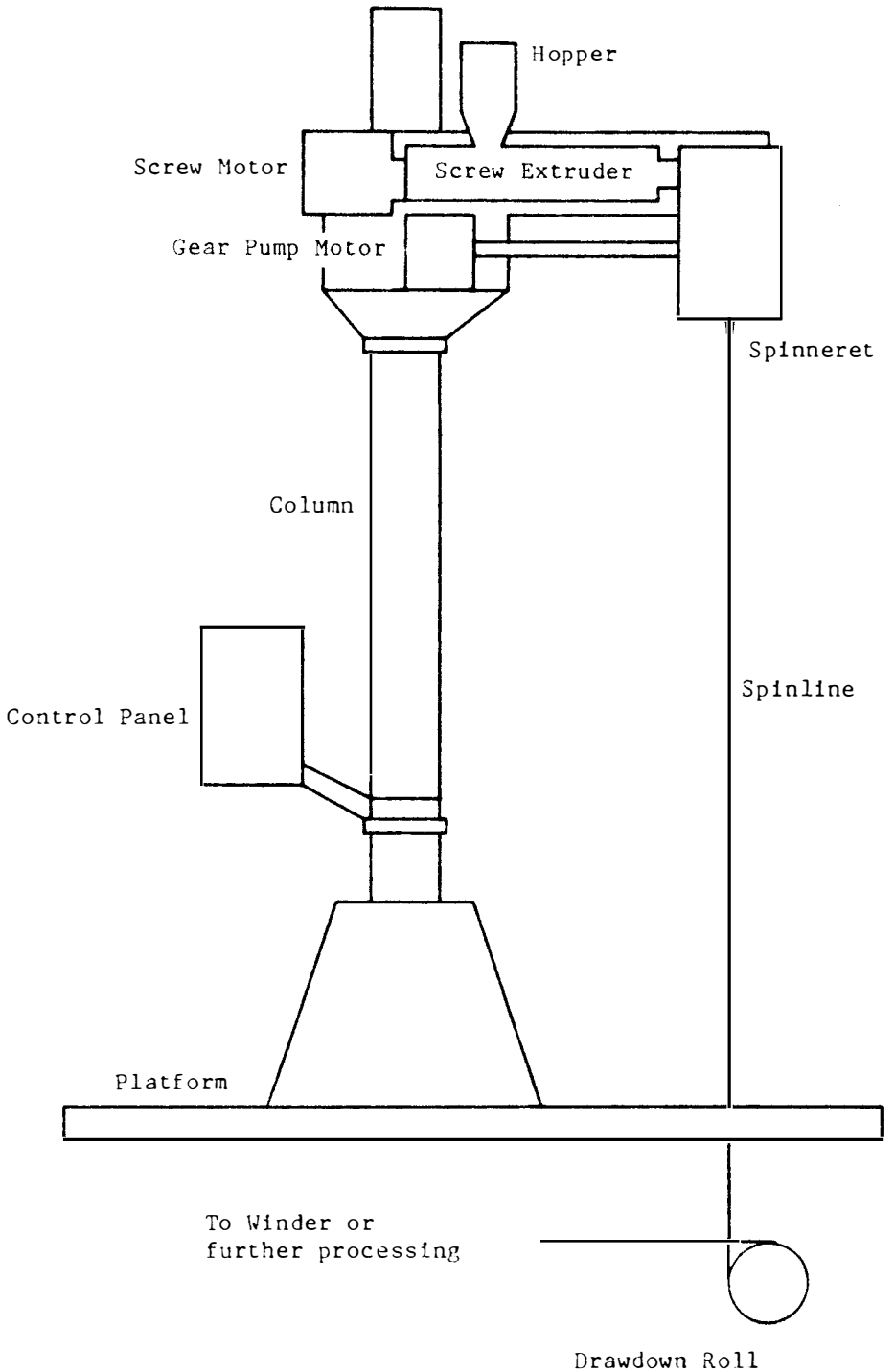


Figure 5.1 Schematic of the experimental apparatus.

The spinneret was designed and manufactured by the Monsanto Fibers and Intermediates Company especially for use in this Fourne extruder with nylon-66. Several grades of extremely pure sand were supplied by Monsanto. Several variations of sand layering procedures were tried and the layering scheme that was finally decided upon consisted of one-half inch layer of grade A sand beneath another one-half inch layer of 800-100 grade sand. This provided the necessary filtration and removal of gel formation without an excessive pressure drop across the spinneret. A variety of spinneret were also available and these are summarized in Table 5.1. The spinneret is shown schematically in Figure 5.2.

Table 5.1 Specification of Monsanto Dies

| Number of holes | Diameter (meters $x10^6$) | Length (meters $x10^6$) |
|---|---|---|
| 1 | 635 | 3810 |
| 4 | 635 | 3810 |
| 12 | 228 | 685 |
| 21 | 228 | 685 |
| 28 | 228 | 685 |

Because of the design, the spinneret extended below the spinning head, variations in the die temperature were observed. This situation was remedied by the construction and installation of an aluminum extension which surrounded the portion of the spinneret which had been exposed.

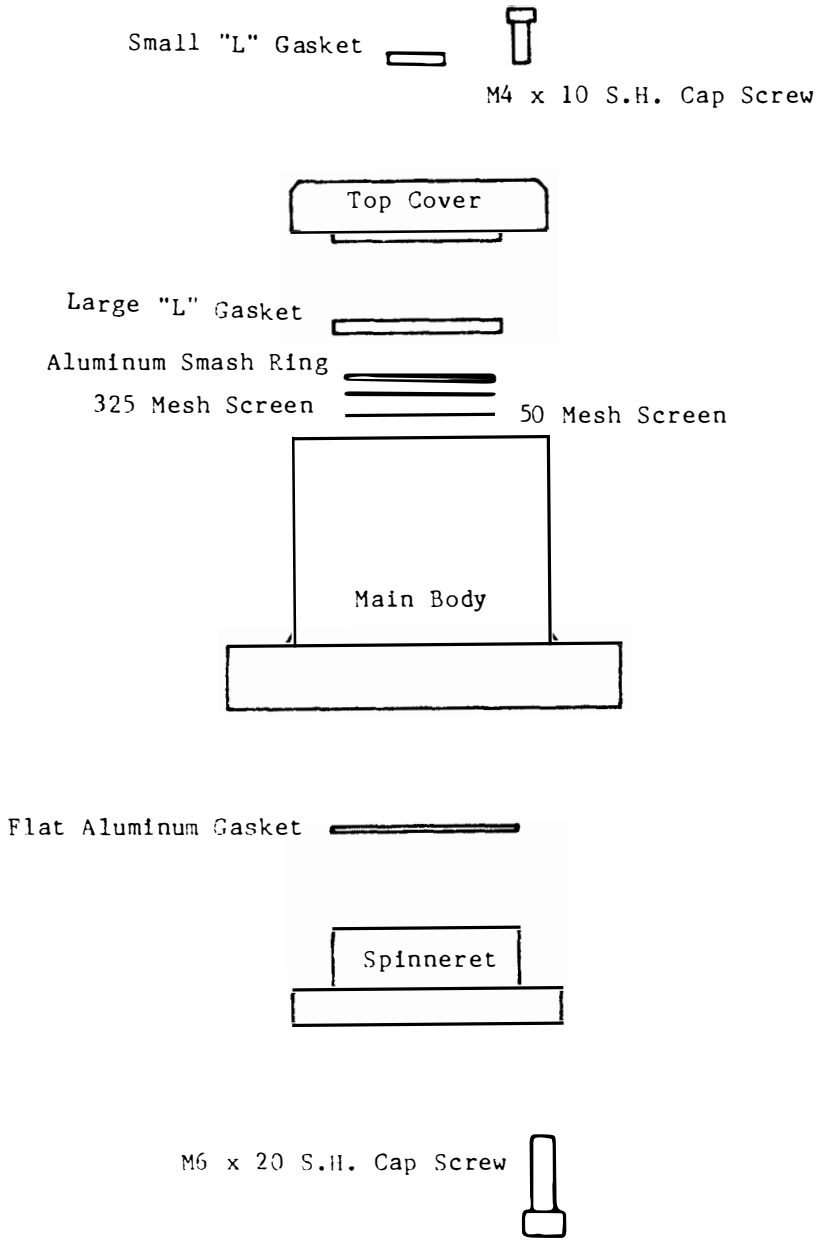


Figure 5.2 Schematic diagram of the Monsanto spinneret.

A band heater and Athena temperature controller were used to maintain the die at the desired extrusion temperature.

Four take-up devices were used in this study. Two Leesona winders (Models 559 and 959), a high speed godet supplied by Monsanto and an air jet drawdown device which was on loan from Rhone-Poulenc Fibres were available. The two winders were capable of take-up speeds up to 2000 meters per minute, the range of the godet was 2500-5500 meters per minute and the air jet was capable of reaching speeds up to 8000 meters per minute depending on the polymer viscosity. The extruder and spinning head were mounted on a movable carriage which allowed for variation in spinline length without repositioning of the take-up devices.

Experimental Procedure

Several initial runs were performed to determine the optimum set of operating parameters (i.e. heater controller, screw speed and gear pump speed set points, etc.) which produced a stable spinline.

The nylon-66 pellets were dried in a vacuum oven at 115 °C for twenty-four hours and stored in Teflon®-sealed glass jars purged with prepurified nitrogen prior to all spinning operations.

A typical run began with the loading of the dried nylon-66 pellets into the nitrogen purged hopper. The appropriate operating parameters were chosen and the heaters and cooling water turned on. Sufficient time (usually one to two hours) was allowed to let the equipment reach operating temperature and to insure that any material left over from previous runs in the extruder and spinning head was

completely melted. An appropriate spin pump speed was selected to produce the desired mass throughput. The relationship between the rotational speed and the mass throughput was determined by experience. Next the extruder speed was chosen in such a manner that the pressure between the extruder and the gear pump was maintained in the range 1000-2000 psi. Here again the selection process was a matter of experience. Once the spinline was established the equipment was allowed to run for several hours to insure that steady state was reached.

Each of the take-up devices operated along slightly different principles. The two winders were capable of providing a constant speed drawdown and winding the fiber onto a bobbin at constant tension. The godet provided a constant speed drawdown but the fiber was removed from the winding drum with a sucker gun and dumped into a collection box. The air jet relied upon high velocity air to provide the drawdown force, thus it was not possible to directly control the take-up velocity. The take-up velocity was computed subsequently from the continuity equation.

As soon as was practical the samples of nylon-66 fibers collected were removed to the conditioning room in the Department of Textiles, Merchandising and Design. This room maintained a constant temperature of 70 °F and a relative humidity of 65%. The samples were allowed to equilibrate with that environment before any subsequent experiments were performed.

## Diameter and Birefringence Measurement

The diameter and birefringence of the nylon-66 fibers were determined using an Olympus polarizing microscope (Model 206080) equipped with a bifilar eyepiece, a pair of Leitz 10 and 30 order tilting plane compensators (Models 553095 and 553096, respectively) and an Olympus 4 order Berek compensator (Model CTP1-200105).

The bifilar eyepiece was calibrated with a standard scale at the same magnification that was to be used in the collection of the diameter data. Samples of the fiber were mounted on glass slides with double stick tape and placed in the microscopes translator. Precautions were taken to avoid stretching the fiber during the mounting procedure. The translator was used to bring the fiber into the microscopes field of view. The position of the eyepiece cross-hairs at the left and right edges of the fiber were recorded.

In the case of the online measurements the microscope was mounted transversely to the spinline and a special guide was constructed to keep the threadline in the field of view while the measurements were being taken.

Once the diameter readings were taken the polars on the microscope were crossed and the compensator was inserted into the microscope. At the zero reading on the compensator a black band was observed across the field of view, when a birefringent fiber was maneuvered into view the black band was shifted and the optical crystal of the compensator was tilted until the black band was brought back to the "zero" reference position. Since the crystal could tilt in either direction two readings were possible, one on the red, or

forward, scale and one on the black, or backward, scale depending on which way the crystal was tilting. Both readings were necessary to perform the optical retardation computation.

At least ten sets of measurements on the final fibers were taken at each different spinning condition and the results averaged. In the case of the online measurements a set of diameter readings and compensator readings were taken as close to the take-up device as possible and then at ten centimeter intervals toward the spinneret. This was continued until the point was reached where the fiber temperature was such that it would begin to stick to the guide and the spinline would break.

## Temperature Measurement

The temperature along the spinline was determined during the spinning operation through the use of a Barnes Infrared microscope (Model RM2B) which was borrowed from the Celanese Corporation. A schematic of this apparatus is shown in Figure 5.3. A black body radiator was constructed so that the temperature of the fiber could be determined without the need of extensive calibration procedures. The radiator consisted of a small electrically controlled heater placed in intimate contact with a copper block. The copper block was coated with high temperature optically black paint. This radiator then provided a means of exhibiting a constant background radiation at any temperature in the range 30-300 °C.

The experimental procedure was to select a temperature for the radiator, this would cause a deflection on the intensity scale of the

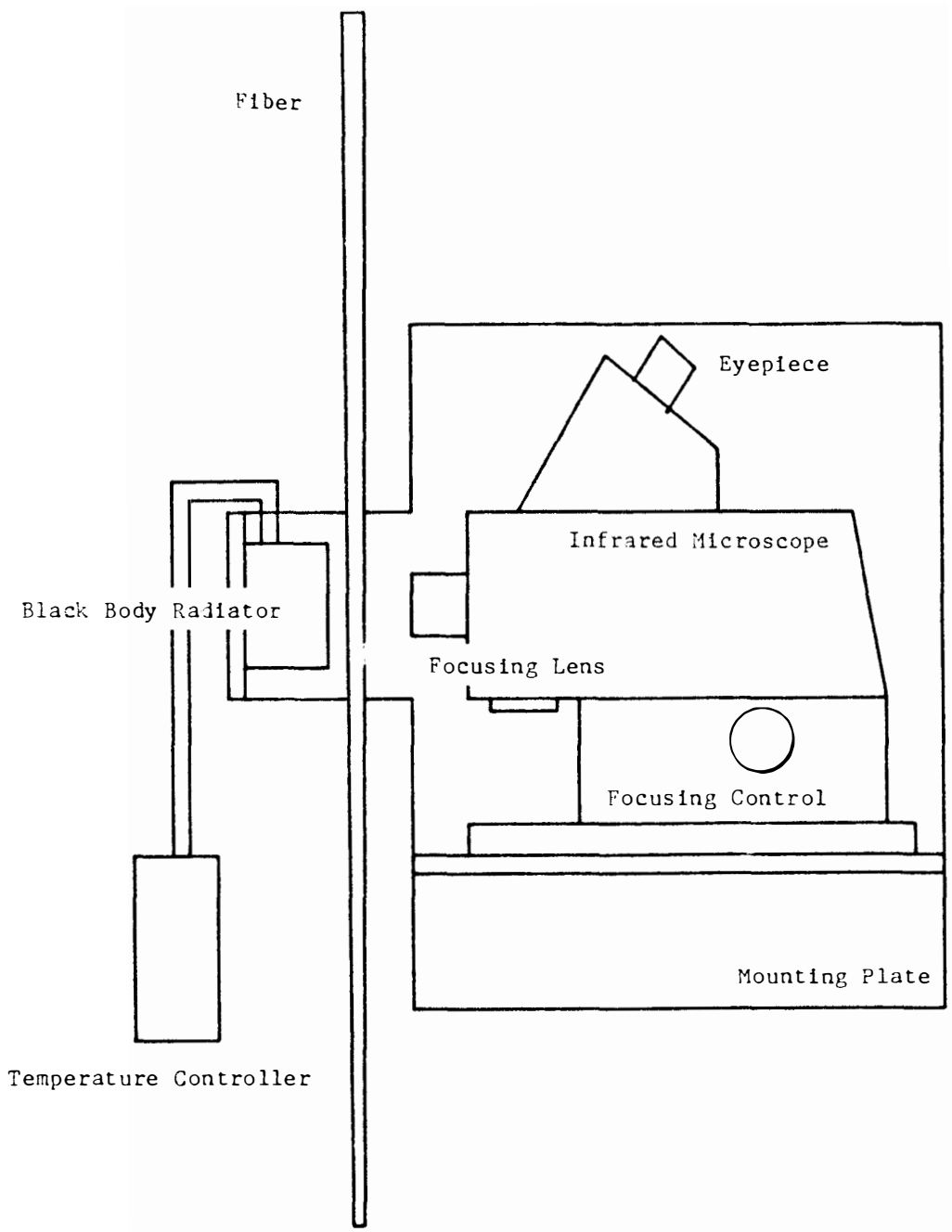


Figure 5.3 Schematic of the temperature measuring apparatus.

microscope. The microscope was then maneuvered into a position where the running spinline was in the focal spot of the microscope. If the fiber temperature was higher than the radiator a positive deflection from the background value would be noted on the intensity scale. If the fiber temperature was lower than the radiator a negative deflection would be seen. When the fiber and the radiator were at the same temperature no movement on the meter was to be seen. Experimentally the entire microscope and radiator apparatus was mounted on an adjustable carriage. When a deflection was observed the entire apparatus was moved up or down, depending on the sign of the deflection, until there was no observable deflection. The distance from the spinneret was measured with a meter stick and this was recorded along with the temperature of the radiator.

The procedure used in this study was to select an initial temperature near the extrusion temperature and locate this temperature on the spinline. Then the temperature of the radiator was reduced by 10 °C and ten minutes was allocated so that the radiator would have enough time to reach steady state at the new temperature and then the position of this temperature was determined using the procedure outlined previously. This was repeated down the length of the spinline.

## Spinline Force Measurement

The force in the spinline was determined using a Rothchild Electric Tensiometer (Model R 1092) and a Rothchild four gram measuring head (Model A69148). This instrument was calibrated according to the manufacturers instructions using a dead weight technique so that

the force measurement would be referenced to zero fiber velocity. The force was measured by carefully inserting the measuring head into the spinline at a point just above the take-up device. The force was then directly recorded off the previously calibrated scale.

## Characterization of Nylon-66 Fibers

### Dilute Solution Viscosity

Intrinsic viscosities were obtained for the original nylon-66 pellets, those which had been dried in a vacuum oven at 115 °C for twenty four hours and for fiber samples spun under a variety of conditions. These measurements were performed to ascertain whether any physical or chemical degradation had occurred during the drying and/or processing of the nylon-66.

Taylor (173) reported a series of dilute solution viscosity experiments on various polymers and determined for nylon-66 in 90% formic acid at 25 °C a set of Mark-Houwink coefficients ($k = 1.1 \times 10^{-3}$, $a = 0.72$) which produced the number averaged molecular weight from the Mark-Houwink equation.

The intrinsic viscosity of the nylon-66 used in this study was determined using a Ubbelohde capillary viscometer (#106, size 75) in a temperature controlled water bath at 25 ± 0.3 °C. An accurately weighed amount of nylon-66 sample was added to 90% formic acid (reagent grade) in a volumetric flask to prepare the standard solution. Since the nylon-66 contained $TiO_2$ as a filler material it was necessary to filter the standard solution.

Viscometer #106 was chosen so that a sufficiently long flow time was achieved to insure that kinetic energy effects could be safely neglected. The flow times were measured five times at each concentration and at ten concentrations of each sample to insure accuracy and reproducibility. The results are summarized in Table 5.2.

Table 5.2 Intrinsic viscosity of Monsanto nylon-66

| Run Number | Take-up Velocity (meters/min) | Intrinsic Viscosity (dl/gm) | K' | K" | $M_n$ (gm/mole) |
|---|---|---|---|---|---|
| R00042 | 2500 | 1.19 | 0.167 | -0.286 | 16,400 |
| R00043 | 3000 | 1.22 | 0.078 | -0.258 | 16,900 |
| R00044 | 3500 | 1.12 | 0.323 | -0.218 | 15,000 |
| R00045 | 4000 | 1.18 | 0.345 | -0.258 | 16,200 |
| R00046 | 4500 | 1.16 | 0.161 | -0.274 | 15,800 |
| R00047 | 5000 | 1.14 | 0.126 | -0.260 | 15,400 |
| R00048 | 5500 | 1.22 | 0.058 | -0.364 | 16,900 |
| Pellet | -- | 0.96 | 0.069 | -0.334 | 12,100 |
| Pellet | Dried | 0.96 | 0.115 | -0.270 | 12,100 |

The drying procedure had no effect on the intrinsic viscosity, but there was a significant increase in all of the as-spun fiber samples. The increase in intrinsic viscosity was attributed to the fact that when nylon-66 is heated in the presence of nitrogen, or other antioxidents, it undergoes a chemical reaction at the amine end and forms branched structures; whereas, heating in air caused oxidation at the acid end leading to a decrease in the intrinsic viscosity. In this study the nylon-66 pellets had been stored in prepurified nitrogen after drying and during all spinning operations.

## Capillary Rheometry

An Instron floor model capillary rheometer (Model TT-D) was used to determine the shear viscosity of the nylon-66 used in this study. A one thousand pound load cell (model A368) was used in all experiments. A series of four capillary dies of L/D ratios 10, 20, 30 and 40 were used. The diameter of the dies was 0.058 inches. Crosshead speeds of 0.2, 0.5, 1.0, 2.0, 5.0 and 10.0 inches per minute were used. The temperature was maintained at 280 °C during all experiments. Prepurified nitrogen was used to prevent degradation of the nylon-66 during testing. The data were analyzed using the Bagley plot for exit effects and the results are summarized in Table 5.3.

Table 5.3 Shear viscosity of Monsanto nylon-66

| Material | Shear Rate ($sec^{-1}$) | Shear Stress (pascal) | Shear Viscosity (pascal-sec) |
|---|---|---|---|
| Filler free | 46 | 3300 | 72 |
| | 93 | 5800 | 63 |
| | 186 | 12000 | 68 |
| | 465 | 31000 | 68 |
| | 930 | 62000 | 66 |
| $TiO_2$ filled | 19 | 1200 | 65 |
| | 47 | 3700 | 78 |
| | 95 | 8200 | 87 |
| | 190 | 14000 | 78 |
| | 475 | 41000 | 86 |
| | 950 | 76000 | 80 |

## Wide Angle X-ray Scattering

A General Electric-Rigaku RV3U rotating anode x-ray generator was used to obtain wide angle x-ray scattering (WAXS) patterns of the as-spun fibers. The unit was operated at 40 kilovolts and 40 millampheres using pinhole collimation. The WAXS patterns were recorded on Kodak Blue Brand x-ray film using a sample to film distance of 3 centimeters. The exposure times ranged from one to two hours. After exposure the films were developed in Kodak Industrex developer for five minutes, fixed in Kodak Rapidfix for five minutes and then given a ten minute water wash.

## Crystalline Orientation Functions

The crystalline orientation functions of the as-spun fibers were obtained from data collected by a Rigaku Geigerflex diffractometer interfaced with a Digital Equipment Corporation PDP 11/34 computer. The computer controlled all data collection and sample manipulation procedures.

The intensity of the diffracted beam was measured at $2\Theta$ values of 20.75° (corresponding to the (100) plane) and 22.15° (corresponding to the (110) plane). Prior to each run a $2\Theta$ scan was performed to locate each of the peaks exactly. Once the $2\Theta$ value was set, intensities were measured at $\beta$ values (the azimuthal angle) ranging from 0° to 90° in one degree steps. Background intensities were also collected at $2\Theta$ values of 15° and 32° . The data were processed via a program written by Galen Richeson to compute the $\langle \mathrm{Cos}^2 \phi_{hkl,z} \rangle$ for the chosen $2\Theta$ value.

## Small Angle X-ray Scattering

Small angle x-ray scattering (SAXS) patterns of the as-spun fibers were obtained using a Keissig camera and Kodak Blue Brand film. A Phillips x-ray generator (Model 12045B) was used at 35 kilovolts and 20 milliampheres. The sample to film distance was forty centimeters and exposure times ranged from forty-eight to seventy-two hours. The exposed film was processed in the same manner as that described for the WAXS patterns. The SAXS film patterns were digitized using a technique developed for small angle light scattering by Larry Effler.

## Density

The densities of the original nylon-66 pellets and the as-spun fibers were determined in a toluene-carbon tetrachloride density gradient column at 23 °C. The column ranged from 1.110 to 1.200 $gm/cm^3$ and was prepared and calibrated in accordance with ASTM standard D 1505 - 68. The fiber samples were placed in a toluene-carbon tetrachloride solution and spun down in a Sorvall SS-3 centrifuge at 5000 rpm for ten minutes to remove any trapped gases and to insure wetting of the fiber surface. The position of the sample in the column was measured twenty-four hours after it was introduced into the column so that it had reached its equilibrium position. The density of the samnple was then computed from a calibration chart which had earlier been constructed.

## Differential Scanning Calorimetry

A Perkin-Elmer Series 7 Thermal Analysis Differential Scanning Calorimeter was used to obtain thermal traces of the as-spun fibers.

Small samples (from two to ten milligrams) of fiber were cut and sealed in aluminum sample pans supplied by Perkin-Elmer. The samples were weighed on a Mettler analytical balance (Model 760) to the tenth of a milligram. All experiments were conducted from 0 °C to 300 °C at a heating rate of 20 °C per minute. Four replicates were performed for each spinning speed and the final result was an average of these.

Mechanical Properties

The mechanical properties (modulus, tenacity and elongation to break) were determined from data acquired by an Instron Universal Testing Instrument (Model 1122) in the tensile mode. A two thousand gram load cell (Model 2511-102) was utilized in all experiments. The testing conditions were a crosshead speed of 100 millimeters per minute, chart speed of 500 millimeters per minute and a chart full scale of 100 grams. All testing was carried out at room temperature. The testing procedure was as follows; the grips were set three centimeters apart and a single fiber was placed securely in the grips. The chart and crosshead were started and the force, as measured by the load cell, was recorded as a function of time. For each spinning speed at least ten experiments were performed so that a statistical average could be obtained for each property. The diameter of each fiber was determined prior to each test using the Olympus microscope previously described (see Diameter and Birefringence Measurement, page 74).

# CHAPTER 6

# DATA ANALYSIS

## Diameter and Birefringence

The overall birefringence and diameter profiles along the spinline were determined from data acquired by the Olympus microscope and Leitz and Olympus compensators. The diameter was computed by subtracting the eyepiece scale readings and multiplying the result by a scale factor which had been previously determined by calibration with an optical standard (1 division = $8.7 \times 10^{-5}$ meters). The optical retardation was determined by adding the red and black scale readings of the compensator and performing a table interpolation using values supplied with the compensator. The interpolated value was multiplied by a constant associated with the particular compensator that was used (6.07 for the Leitz, 2.065 for the Olympus) and this produced the optical retardation in meters. The birefringence was then the optical retardation divided by the diameter.

## Crystalline Index

The crystalline index of the as-spun nylon-66 fibers was determined from data acquired from the density gradient column and the differential scanning calorimeter.

### Density

The density of the as-spun fibers was determined from the calibration plot constructed using floats of known density. The

crystalline index was calculated by assuming that the material consisted of two distinct phases, crystalline ($\rho_c$ = 1.226 gm/cm$^3$) and amorphous ($\rho_a$ = 1.069 gm/cm$^3$) and their volumes were additive. These assumptions led to the following relationship

$$\Theta = 7.809 - 8.348/\rho \qquad (6\text{-}1)$$

where $\rho$ was the density of the fiber.

Differential Scanning Calorimetry

The energy evolved during the melting of any material in the DSC can be determined by measuring the area under the peak on the thermal trace obtained. The amount of energy divided by the sample weight gives the latent heat of fusion for that particular sample. The crystalline index was computed by dividing this value by the heat of fusion for a 100% crystalline material. In this case, the value used for nylon-66 was 45 cal/gm. The area beneath the melting peak was calculated using the software provided by Perkin Elmer. The operator selected the upper and lower temperature limits for the integration which was then performed numerically yielding the heat of fusion for that sample.

## Small Angle X-ray Scattering

The SAXS patterns were digitized using a technique developed by Larry Effler in his analysis of small angle light scattering patterns. The film was back lit using a Gartner polarizing light source and an MTI model 66 digital camera was used to convert the image into a digitized grid. This data was processed by the Video Van Gogh SSP software

from Tecmar and the Plotcall software from Golden Software. The film to camera distance was recorded and the long period (LP) was calculated from

$$LP = \frac{1.542}{2\mathrm{Sin}(\tan^{-1}[x/40]/2)} \tag{6-2}$$

where x is the distance from the center of the pattern to the point of greatest intensity. Contour plots were constructed from the digitized data using the above mentioned software.

## Crystalline and Amorphous Orientation Functions

The crystalline orientation function was computed from

$$f_c = \frac{3\langle \mathrm{Cos}^2\phi_{c,z}\rangle - 1}{2} \tag{6-3}$$

The value of $\langle \mathrm{Cos}^2\phi_{c,z}\rangle$ was calculated from the values of $\langle \mathrm{Cos}^2\phi_{100,z}\rangle$ and $\langle \mathrm{Cos}^2\phi_{110,z}\rangle$. These values were computed from the data acquired by the Rigaku / PDP 11/34 system. In order to compute $\langle \mathrm{Cos}^2\phi_{c,z}\rangle$ from $\langle \mathrm{Cos}^2\phi_{100,z}\rangle$ and $\langle \mathrm{Cos}^2\phi_{110,z}\rangle$ a Wilchinsky analysis (254,255) was performed for the triclinic unit cell of nylon-66. The normals to the (100), (010) and (110) planes were found to be normal to the (1,3,14) plane whose normal lies parallel to the chain axis. The result of the Wilchinsky analysis was the following set of relationships

$$\langle \mathrm{Cos}^2\phi_{100,z}\rangle = \langle \mathrm{Cos}^2\phi_{u,z}\rangle \tag{6-4}$$

$$\langle \mathrm{Cos}^2\phi_{110,z}\rangle = e_{110}{}^2\langle \mathrm{Cos}^2\phi_{100,z}\rangle + f_{110}{}^2\langle \mathrm{Cos}^2\phi_{v,z}\rangle$$

$$+ 2e_{110}f_{110}\langle \mathrm{Cos}\phi_{u,z}\mathrm{Cos}\phi_{v,z}\rangle \qquad (6\text{-}5)$$

$$\langle \mathrm{Cos}^2\phi_{010,z}\rangle = e_{010}{}^2\langle \mathrm{Cos}^2\phi_{100,z}\rangle + f_{010}{}^2\langle \mathrm{Cos}^2\phi_{v,z}\rangle$$

$$+ 2e_{010}f_{010}\langle \mathrm{Cos}\phi_{u,z}\mathrm{Cos}\phi_{v,z}\rangle \qquad (6\text{-}6)$$

$$\langle \mathrm{Cos}^2\phi_{c,z}\rangle = 1 - \langle \mathrm{Cos}^2\phi_{100,z}\rangle - \langle \mathrm{Cos}^2\phi_{v,z}\rangle \qquad (6\text{-}7)$$

Since only two hk0 type reflections were available it was assumed that $\langle \mathrm{Cos}^2\phi_{010,z}\rangle = \langle \mathrm{Cos}^2\phi_{110,z}\rangle$, this gave

$$\langle \mathrm{Cos}^2\phi_{c,z}\rangle = 1 - \left[\frac{e_{010}f_{010} - e_{110}f_{110}}{e_{010}f_{010}f_{110}{}^2 - e_{110}f_{110}f_{010}{}^2}\right]\langle \mathrm{Cos}^2\phi_{110,z}\rangle$$

$$+\left[\frac{e_{010}f_{010}[f_{110}{}^2-e_{110}{}^2] + e_{110}f_{110}[e_{010}{}^2-f_{010}{}^2]}{e_{010}f_{010}f_{110}{}^2 - e_{110}f_{110}f_{010}{}^2}\right]$$

$$\langle \mathrm{Cos}^2\phi_{100,z}\rangle \qquad (6\text{-}8)$$

The dependence of the directional cosines, $e_{hkl}$ and $f_{hkl}$, on the unit cell parameters is shown in Table 6-1. The angles between the normals were calculated from the formula given by Cullity (256).

Table 6-1. Directional cosines for nylon-66 unit cells.

| Unit Cell | Alpha | Beta | Gamma |
|---|---|---|---|
| $\phi_{100,110}$ | 114.03 | 113.64 | 120.01 |
| $e_{110}$ | -0.407 | -0.401 | -0.500 |
| $f_{110}$ | 0.913 | 0.916 | 0.866 |
| $\phi_{100,010}$ | 64.28 | 35.71 | 60.04 |
| $e_{010}$ | 0.434 | 0.812 | 0.499 |
| $f_{010}$ | 0.901 | 0.584 | 0.866 |

The amorphous orientation function was computed from

$$f_a = \frac{\Delta n - \Theta f_c \Delta_c^0}{(1-\Theta)\ \Delta_a^o} \qquad (6\text{-}9)$$

assuming the additivity of the crystalline and amorphous phases to the birefringence and that form birefringence could be neglected.

## Mechanical Properties

The Instron tensile tester produced a plot of force as a function of time for each sample. The elongation at break was calculated by measuring the distance between the start of the test and the point at which the fiber broke with a steel ruler. This distance was divided by the chart speed, multiplied by the crosshead speed and divided by the initial length of the test fiber to produce the elongation at break. The tenacity was calculated by determining the force at the

breaking point from the chart and dividing this by the fibers initial cross-sectional area. The initial modulus was calculated by constructing a tangent line to the linear portion of the force versus time chart prior to the point where the fiber had begun to yield. The modulus was the slope of this line after conversion of the force to stress and time to strain.

# CHAPTER 7

# RESULTS AND DISCUSSION

## Predictions of the Model for Nylon-66

The mathematical model developed for the high speed melt spinning of crystallizable polymers was applied to nylon-66 under processing conditions corresponding to those used in the experimental online measurements. These processing conditions are summarized in Table 7.1.

Table 7.1 Summary of experimental processing conditions

| | | |
|---|---|---|
| Extrusion temperature | - | 275 °C |
| Spinline length | - | 2.5 meters |
| Mass throughput | - | $4.2 \times 10^{-5}$ kg/sec |
| Die diameter | - | 635 micrometers |
| Take-up velocities | - | 2800 - 6600 m/min |

In all cases except where noted all the assumptions and parameter values are those described in Chapter 4. Figure 7.1 shows the predicted velocity profiles for the six take-up velocities. Initially there is a gradual increase in the velocity at each speed. At speeds below 5400 meters per minute there is a smooth increase in the

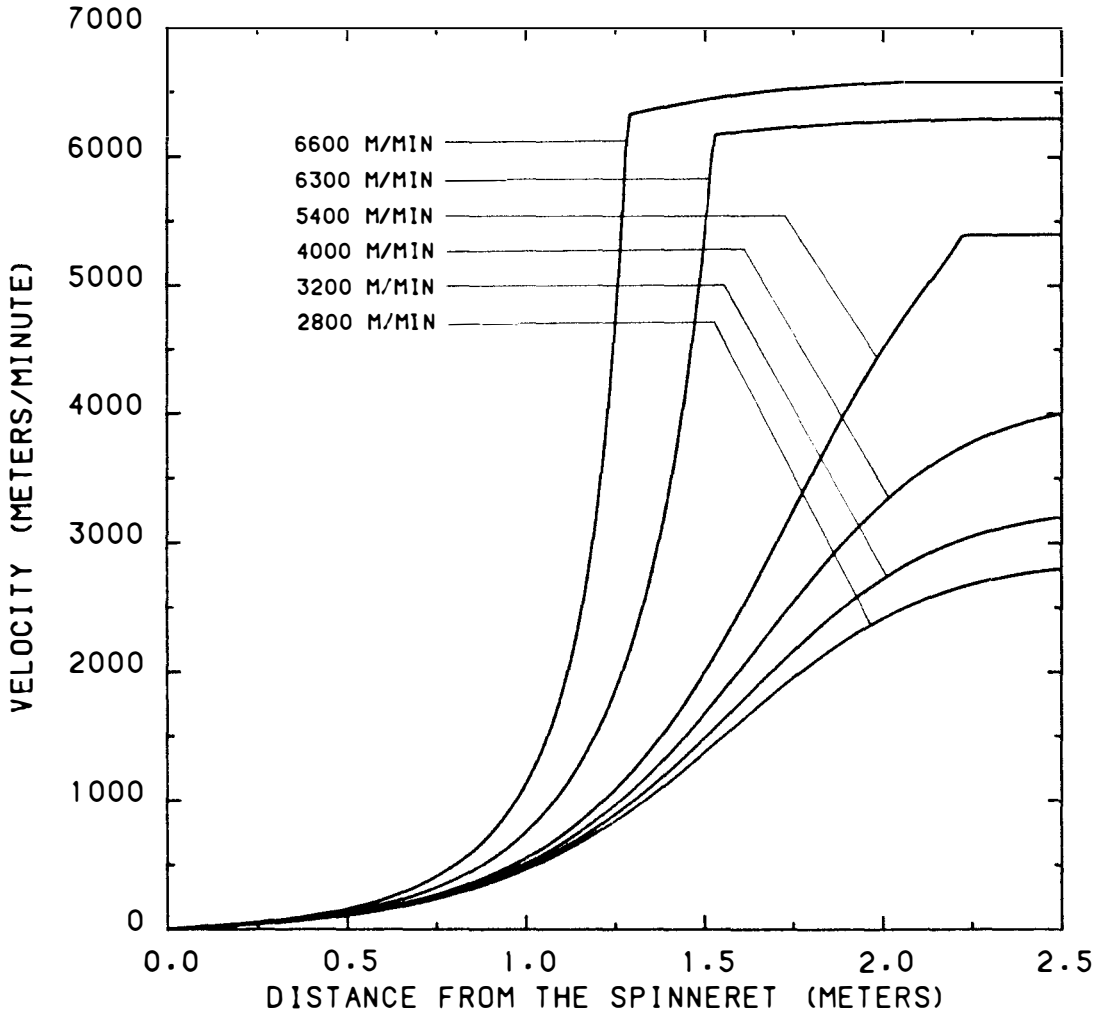


Figure 7.1 Predicted velocity profiles for nylon-66 with a mass throughput of 2.5 gm/min and n = 3.

velocity until the terminal velocity is reached at the take-up device. Above 5400 meters per minute the velocity increases smoothly to an abrupt plateau, where the velocity increases insignificantly thereafter. The distance from the spinneret at which this transition occurs moves closer to the spinneret with increasing take-up speed. This behavioral transition is due to the strain hardening effect of crystallization taking place within the spinline at the higher speeds.

Figure 7.2 presents the corresponding diameter profiles. As in the case of the velocity profiles at speeds below 5400 meters per minute the diameter draws down smoothly to its final value at the take-up device which would be expected from continuity. Above 5400 meters per minute the diameter decreases smoothly to a specific value well before the take-up device and remains essentially unchanged from that point on to the take-up device. This is also a consequence of the crystallization which is taking place within the spinline. The position where the diameter reaches its final value is also the point where the velocity achieves the plateau region.

The predicted birefringence profiles are shown in Figure 7.3. At low speeds there is a gradual increase in the birefringence, but the final values are rather low compared to the intrinsic birefringences of nylon-66. At higher speeds the birefringence starts out slowly but then rises abruptly at positions corresponding to the onset of crystallization to a value which is very near the final predicted birefringence.

Figure 7.4 plots the crystalline index profiles at each take-up speed. At low speeds there is no appreciable crystallization taking

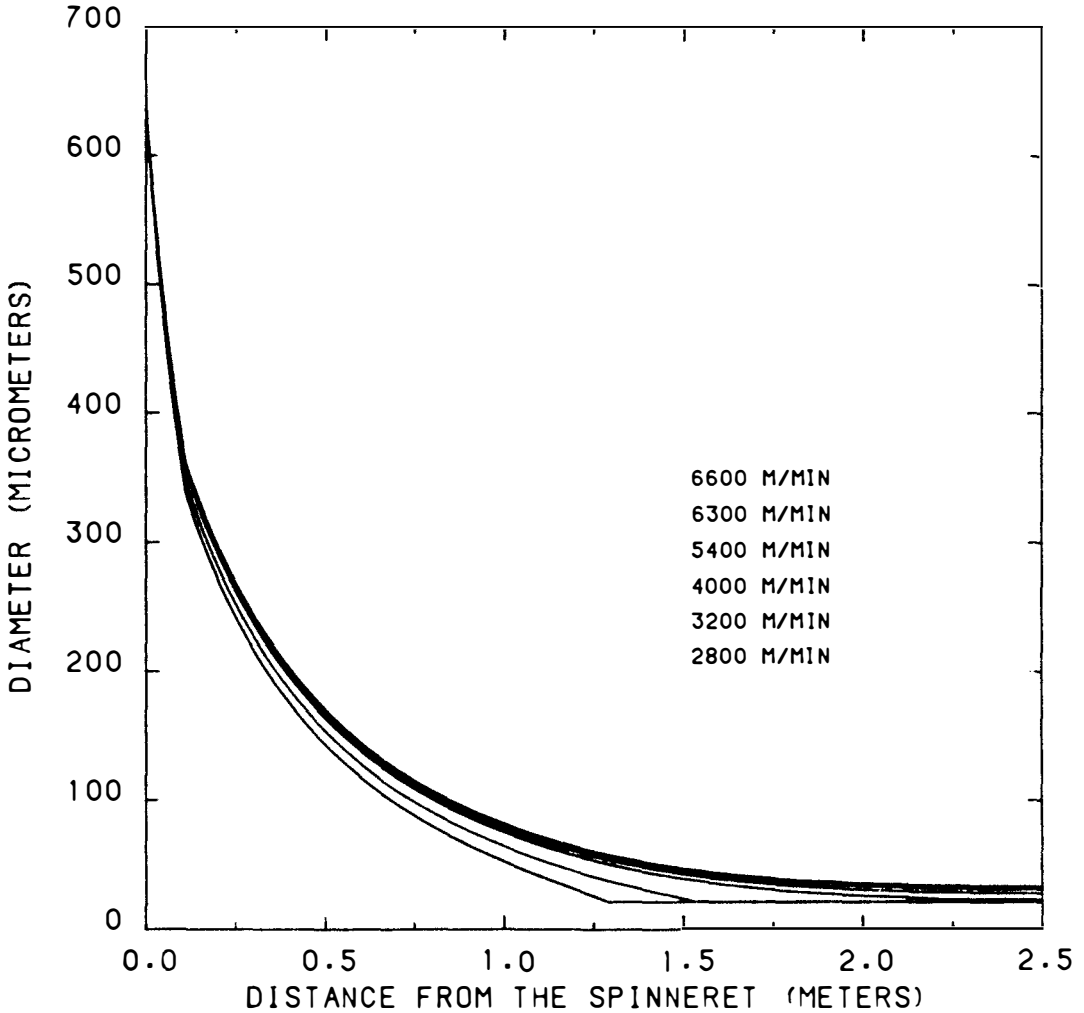


Figure 7.2 Predicted diameter profiles for nylon-66 with a mass throughput of 2.5 gm/min and n = 3.

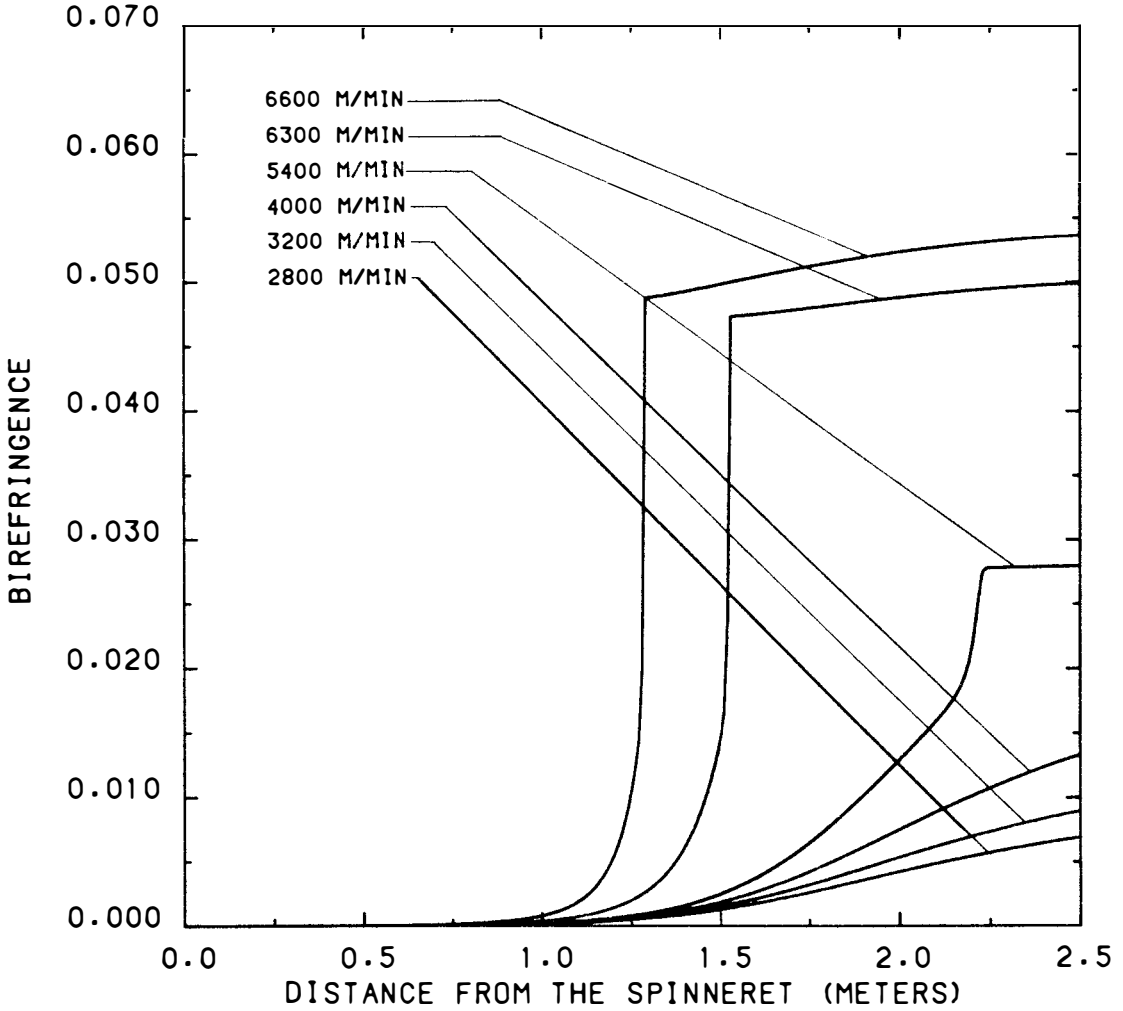


Figure 7.3 Predicted birefringence profiles for nylon-66 with a mass throughput of 2.5 gm/min and n = 3.

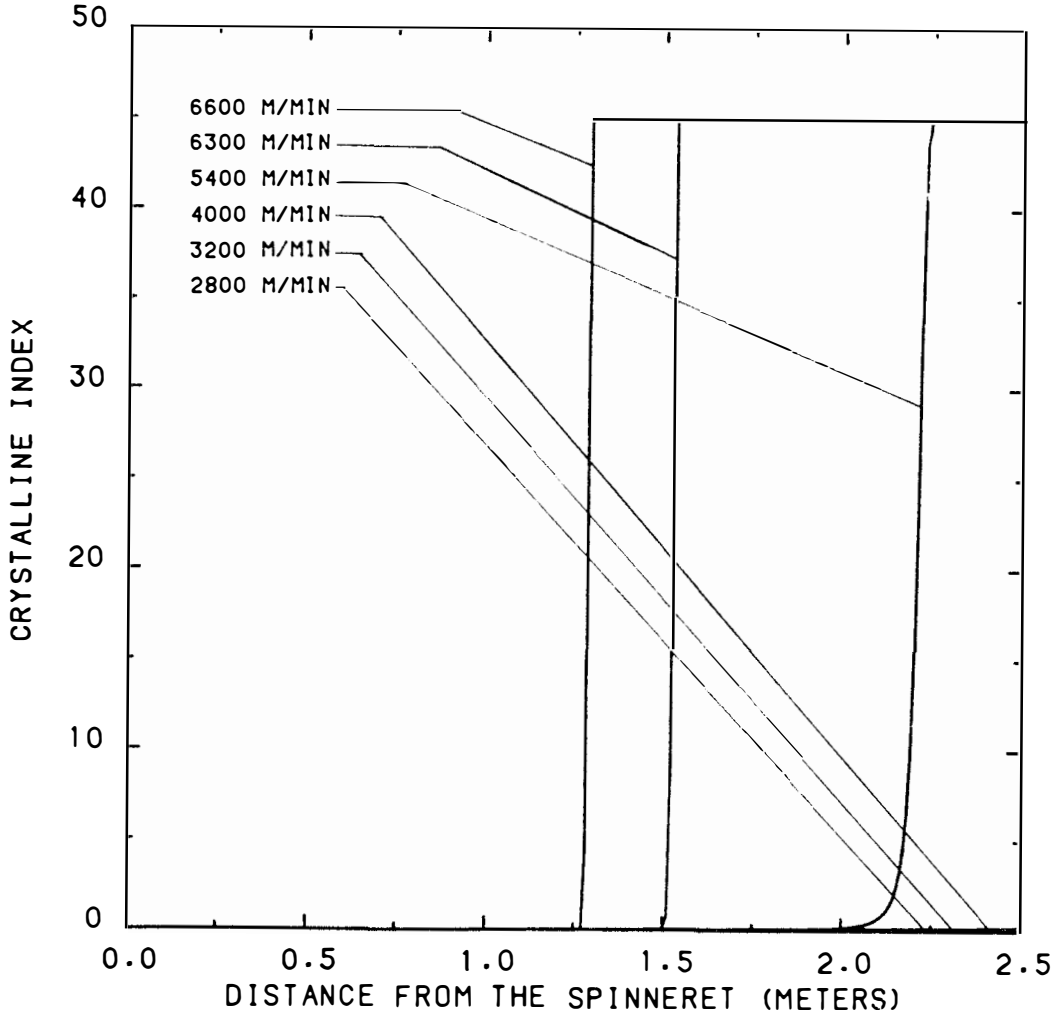


Figure 7.4 Predicted crystalline index profiles for nylon-66 with a mass throughput of 2.5 gm/min and n = 3.

place in the spinline. This is consistent with the gradual increase and low final values for the birefringence at low spinning speeds. At higher speeds there is a rapid (almost step) increase in the index corresponding to the onset of orientation induced crystallization which is taking place at positions closer to the spinneret with increasing take-up speed.

Figure 7.5 shows the predicted temperature profiles. These profiles indicate almost no variation with regard to spinning speed. There is a small temperature plateau at 5400 meters per minute corresponding to the onset of crystallization and a much smaller plateau at 6300 meters per minute. This is a result of the position in the spinline at which crystallization is taking place. At higher speeds the crystallization process is proceeding at higher temperatures because the kinetics are more rapid there due to molecular orientation. The higher temperatures and kinetic rates combine to allow the energy released to be transferred to the surroundings much more efficiently, negating the appearance of a protracted temperature plateau.

The predicted buildup of the stress in the spinline is presented in Figure 7.6. At the lower speeds the stress within the spinline increases smoothly to its final value at the take-up device. At 5400 meters per minute the stress increases smoothly to a plateau which corresponds to the point where crystallization has begun. At 6300 and 6600 meters per minute the stress increases sigmoidally up to the plateau. At all three speeds the crystallization process is initiated when the stress reaches a value of around $2 \times 10^7$ pascals. The crystallization process is greatly enhanced by orientation of the

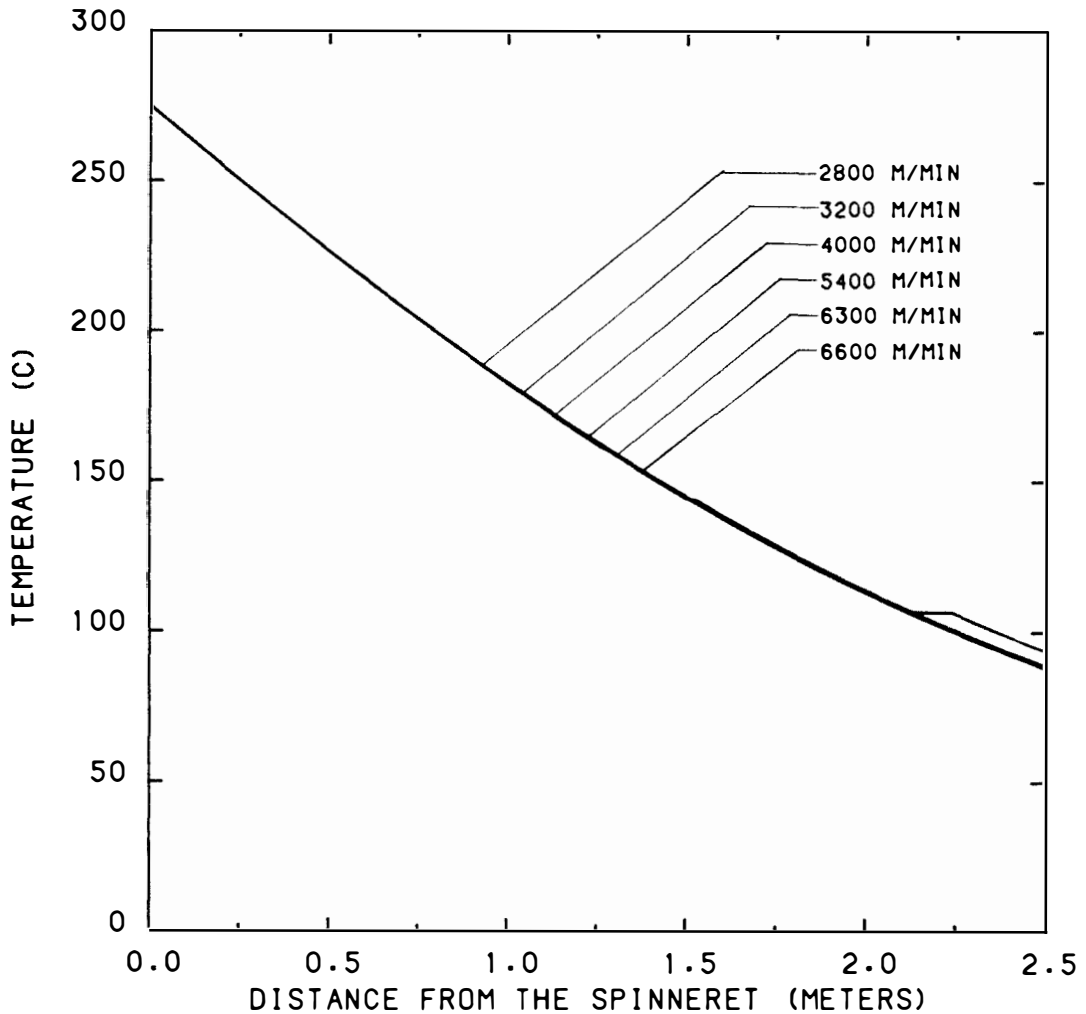


Figure 7.5 Predicted temperature profiles for nylon-66 with a mass throughput of 2.5 gm/min and n = 3.

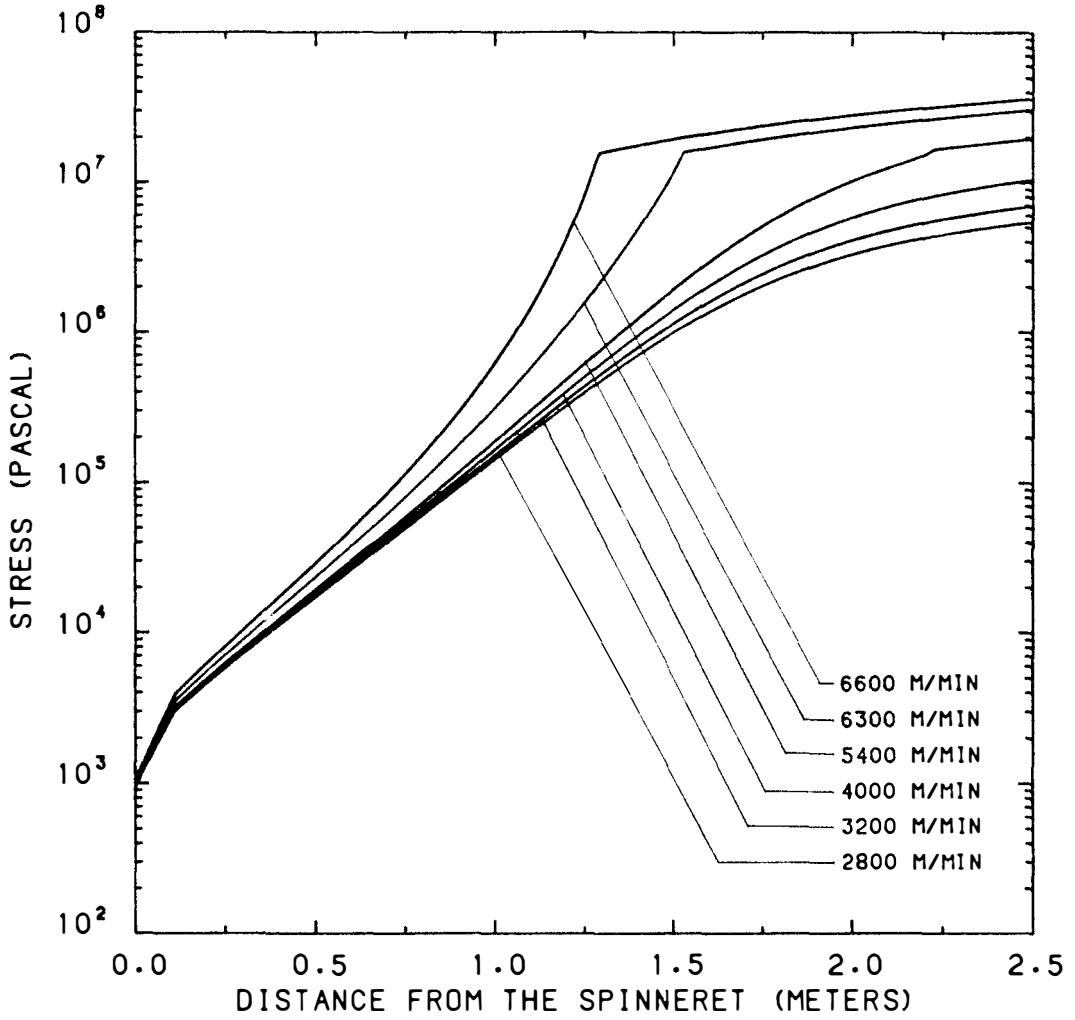


Figure 7.6 Predicted stress profiles for nylon-66 with a mass throughput of 2.5 gm/min and n = 3.

molecules prior to the process taking place. The driving force for molecular orientation within the spinline is the stress. The model predicts that when a sufficient level of stress (orientation) has been achieved the crystallization process becomes orientation driven rather than temperature driven. This is also demonstrated in Figure 7.7 where the amorphous orientation factor is small at the low speeds but increases abruptly at the higher speeds to the limit necessary to instigate the crystallization process.

Figures 7.8 - 7.13 show the distribution of forces within the spinline as a function of distance from the spinneret. At the lower speeds (Figures 7.8 - 7.10) the increase in rheological force is due almost entirely to the acceleration of the fiber until the length of the spinline becomes such that the exposed area of the fiber is great enough so that the drag force becomes significant. In terms of the traditional analyses applied to melt spinning, this regime is a step above the assumption of a constant rheological force. Here the velocities are such that inertia and drag become significant only after the fiber has achieved a velocity of around 1000 meters per minute. Below this speed the rheological force remains essentially constant.

Figure 7.11 indicates the force distribution at 5400 meters per minute. The acceleration and drag forces combine to increase the rheological force to a level which provides sufficient molecular orientation for a rapid increase in the crystallization kinetics. The force distributions at 6300 and 6600 meters per minute (Figures 7.12 and 7.13) show that the increase in the the fiber's acceleration alone is sufficient to increase the rheological force to the level necessary to

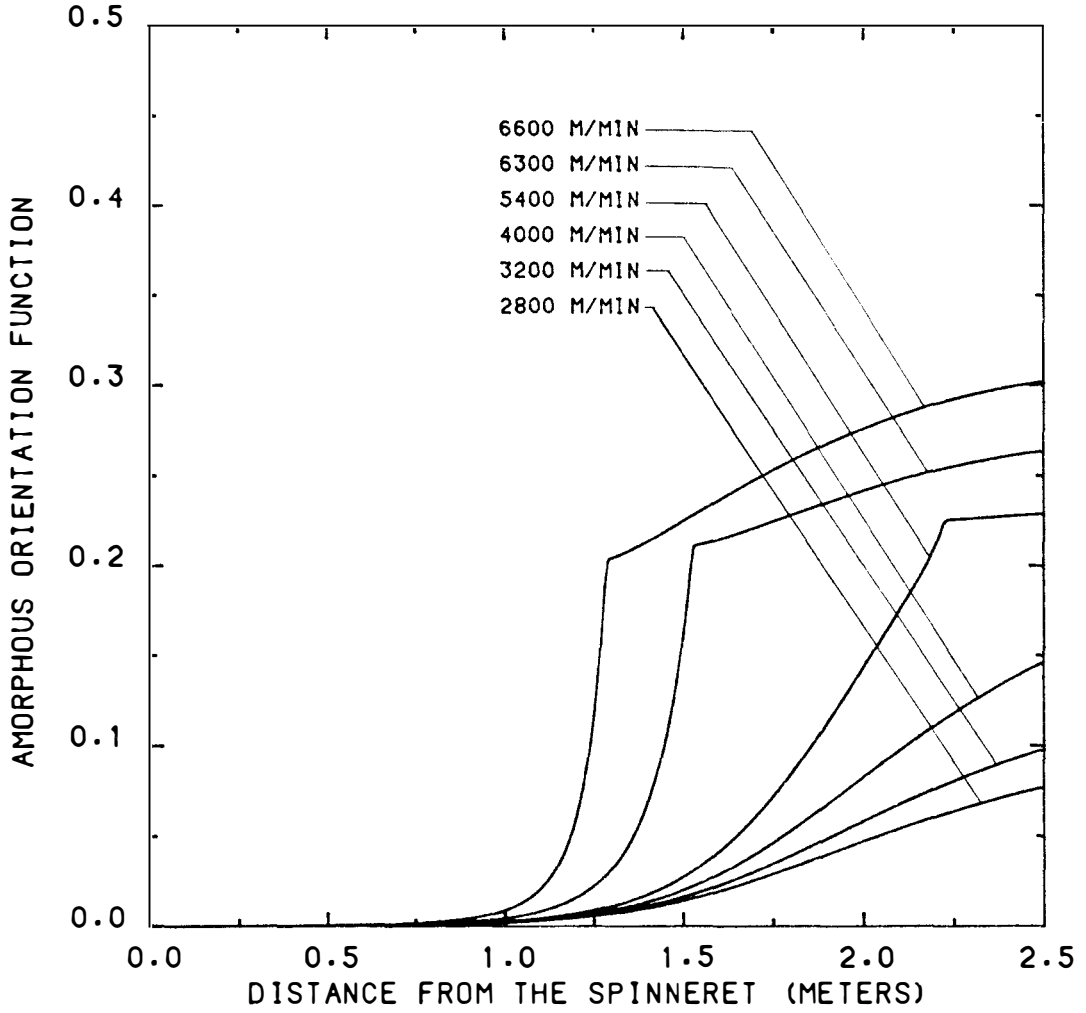


Figure 7.7 Predicted amorphous orientation function profiles for nylon-66 with a mass throughput of 2.5 gm/min and n = 3.

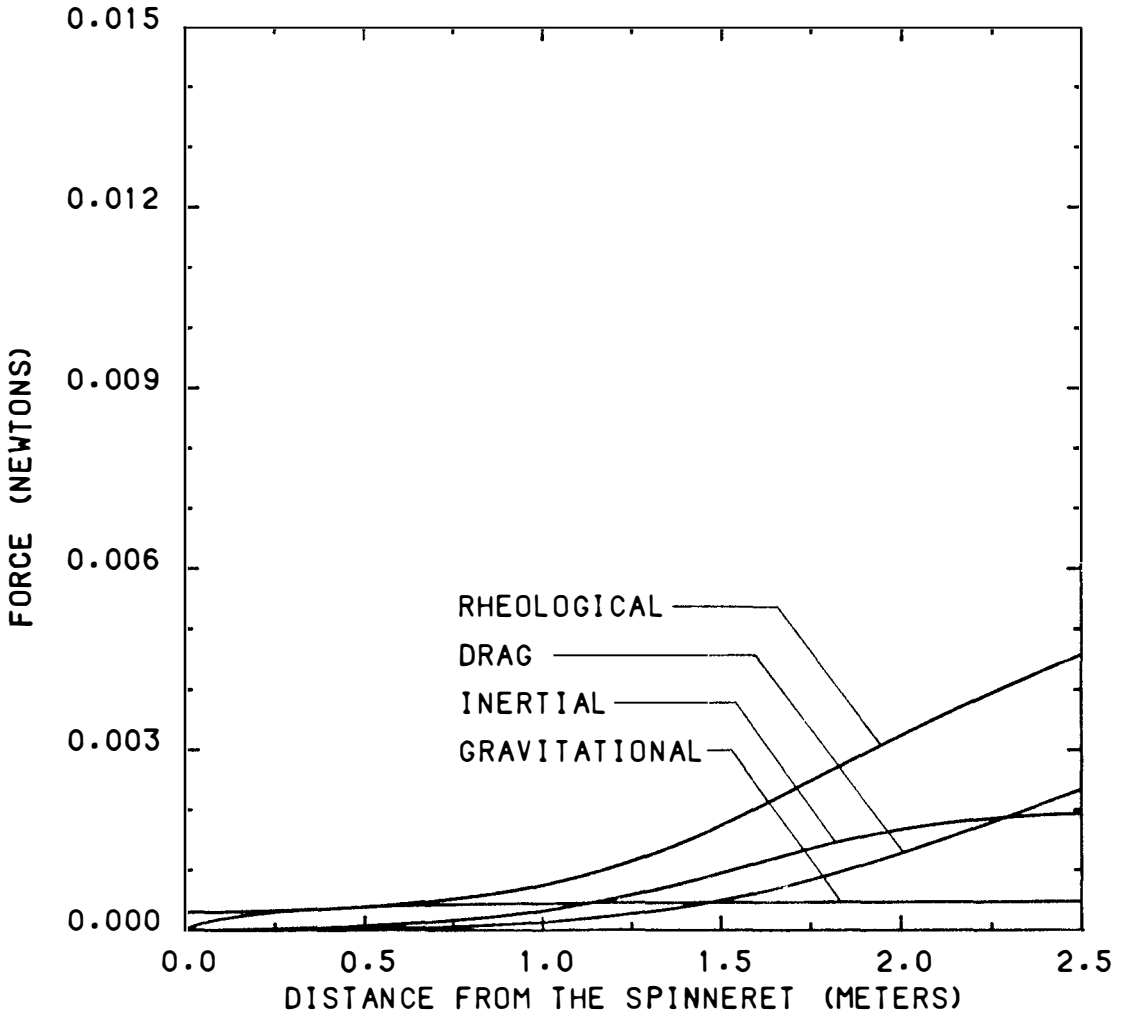


Figure 7.8 Predicted rheological, drag, inertia and gravitational force profiles for nylon-66 at a spinning speed of 2800 meters/minute.

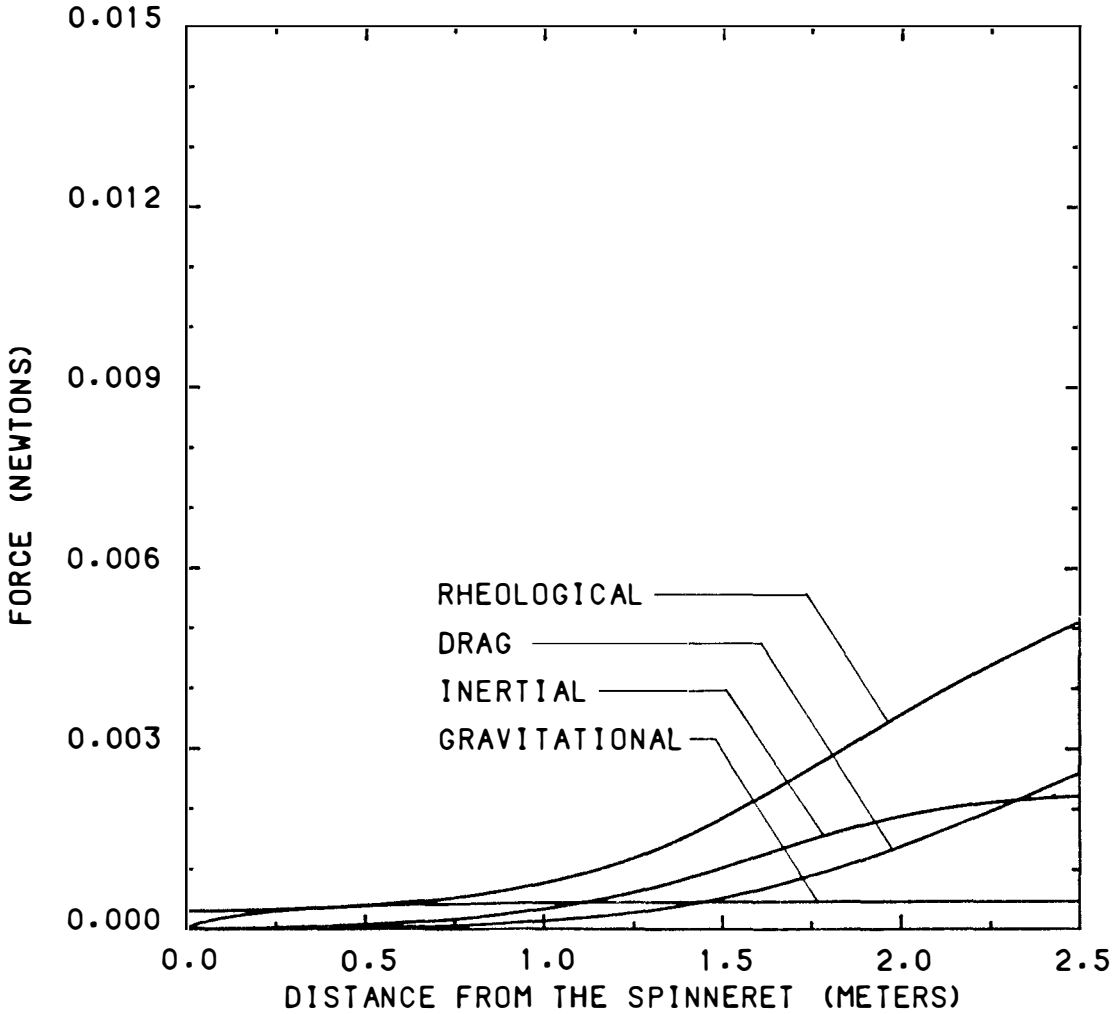


Figure 7.9 Predicted rheological, drag, inertial and gravitational force profiles for nylon-66 at a spinning speed of 3200 meters/minute.

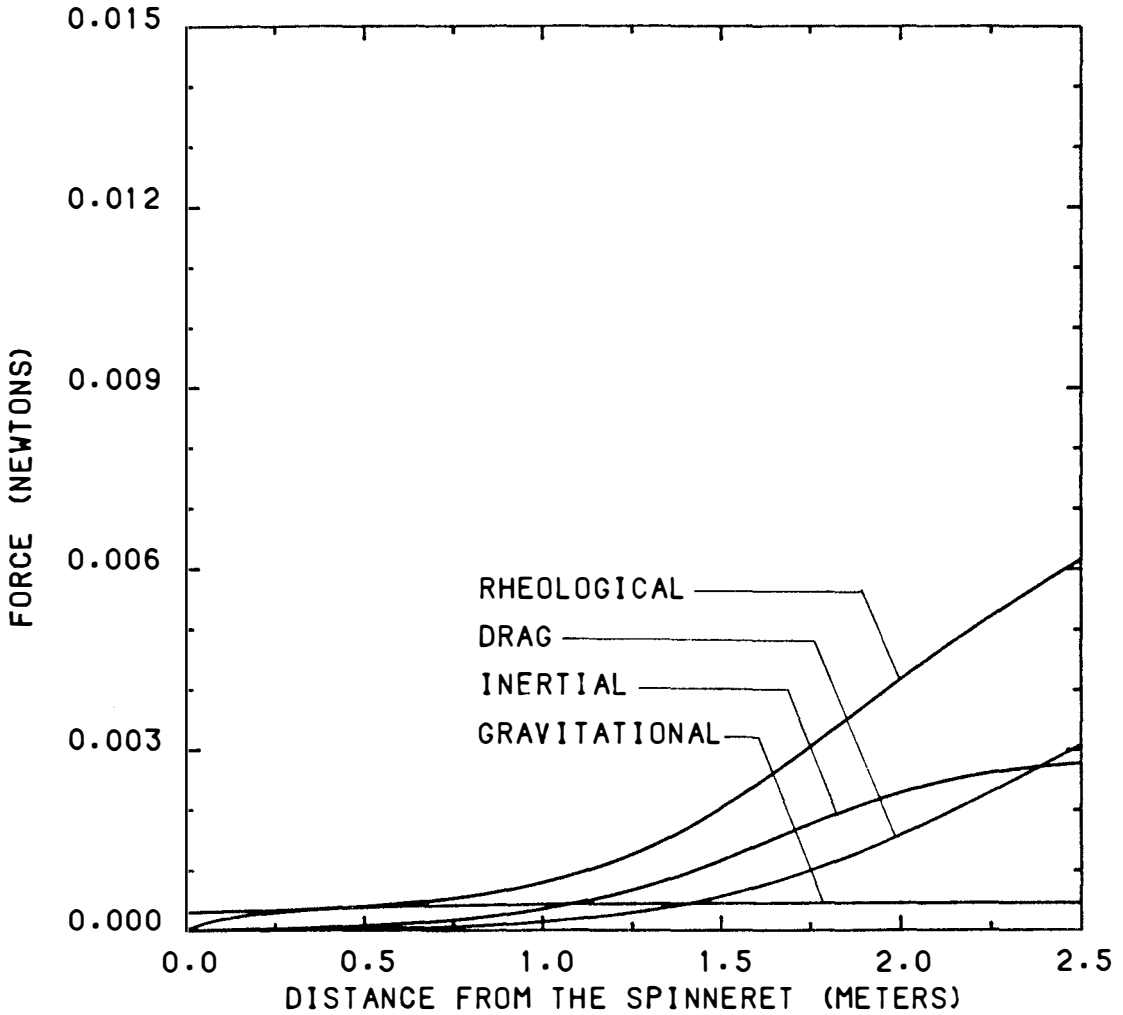


Figure 7.10 Predicted rheological, drag, inertial and gravitational force profiles for nylon-66 at a spinning speed of 4000 meters/minute.

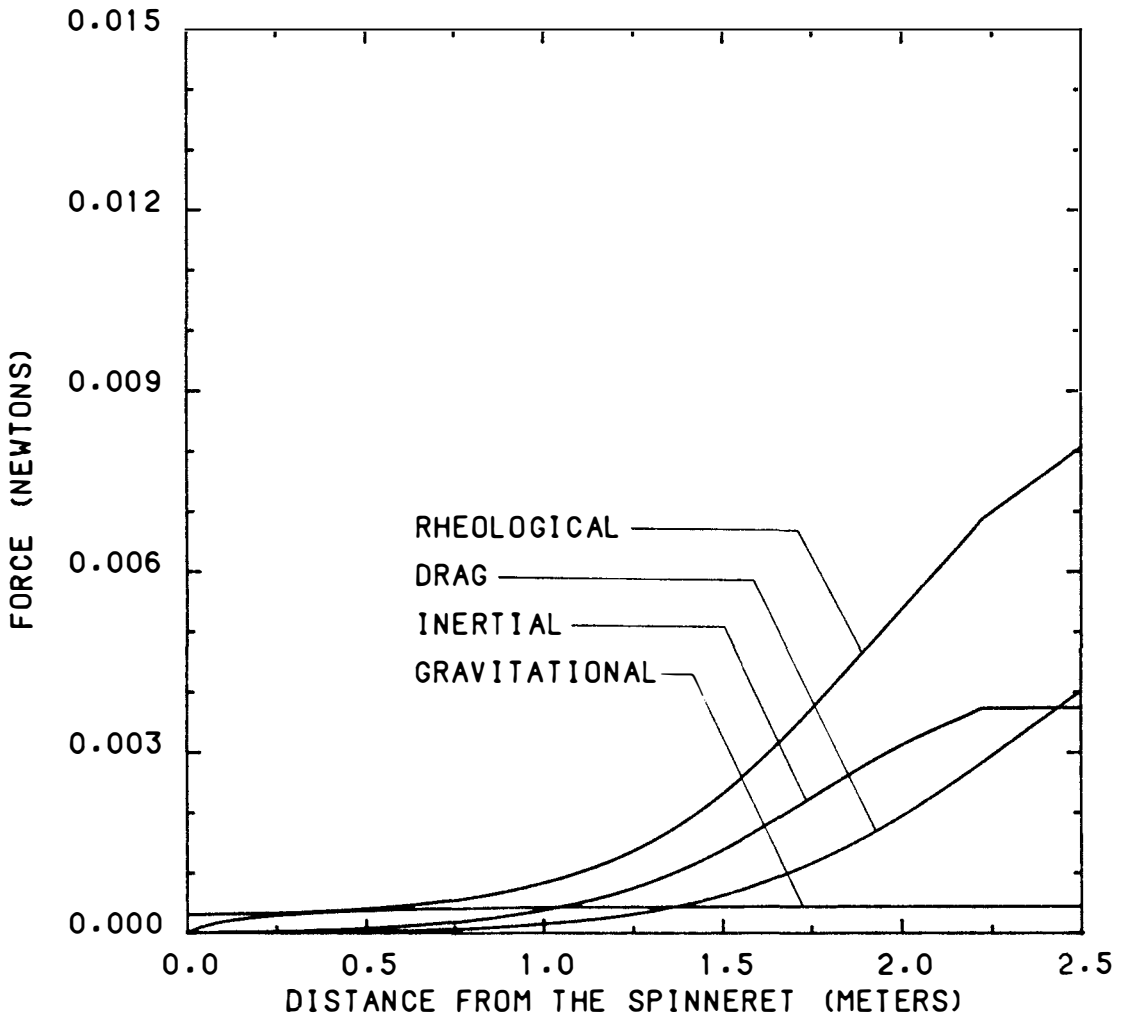


Figure 7.11 Predicted rheological, drag, inertial and gravitational force profiles for nylon-66 at a spinning speed of 5400 meters/minute.

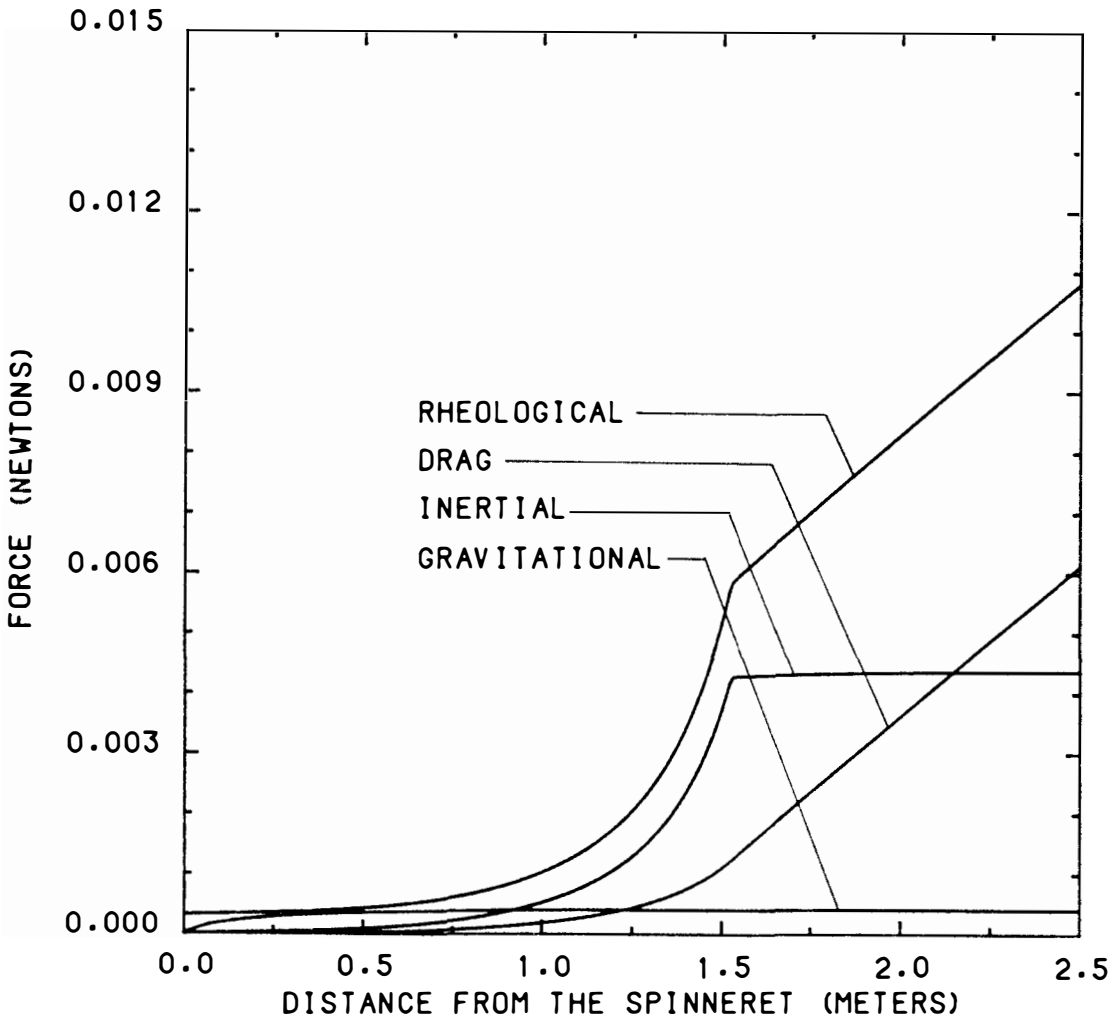


Figure 7.12 Predicted rheological, drag, inertial and gravitational force profiles for nylon-66 at a spinning speed of 6300 meters/minute.

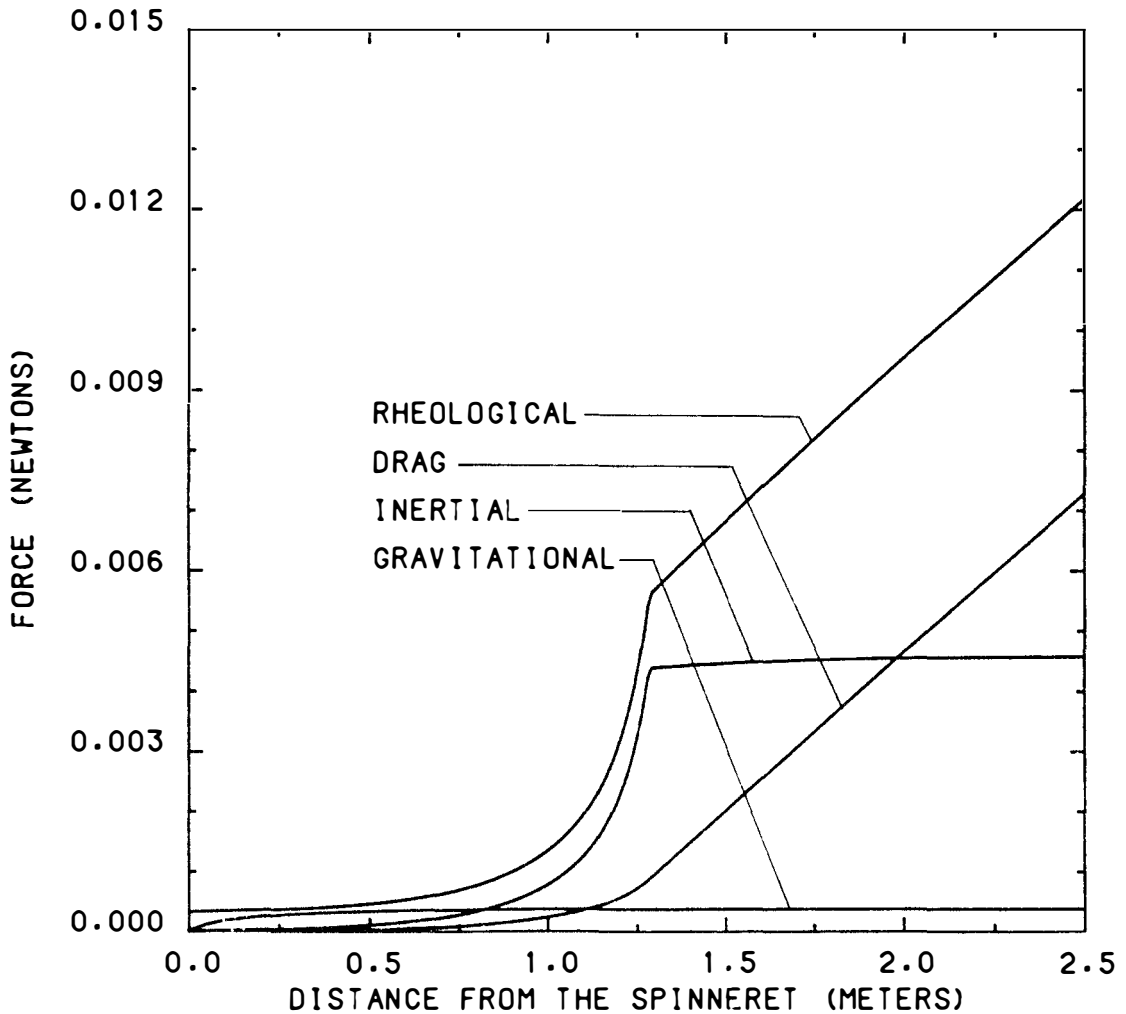


Figure 7.13 Predicted rheological, drag, inertial and gravitational force profiles for nylon-66 at a spinning speed of 6600 meters/minute.

provide the high molecular orientation needed to drive the crystallization kinetics.

The predicted velocity profiles for the same processing conditions but using a value of one for the Avrami index are shown in Figure 7.14. Comparing Figure 7.14 with 7.1 (n = 3) shows no significant differences in the character of the profiles. Figure 7.15 is a plot of the temperature profiles using n = 1 in the model. Comparing this with Figure 7.5 (n = 3) shows essentially the same behavior. The temperature plateaus at 5400 and 6300 meters per minute appear at almost the same temperature but are slightly more protracted than those predicted for n = 3. There is also a very small plateau in the temperature profile for 6600 meters per minute. This is a result of the decrease in kinetic rate corresponding to changing n from 3 to 1. Figure 7.16 shows the crystalline index profiles predicted from the model with n = 1. The profiles predicted at the higher speeds are essentially the same as those predicted with n = 3. At the lower speeds the model predicts crystallization will occur but only to a small extent.

## Online Experimental Results for Nylon-66

The experimental diameter profiles obtained for take-up velocities from 2800 to 6600 meters per minute is presented in Figure 7.17. In the range of distances shown they indicate that at the lower speeds the diameter draws down to the final value at the take-up device but at higher speeds the draw down occurs much more rapidly to what appears to be the final value well before the take-up device.

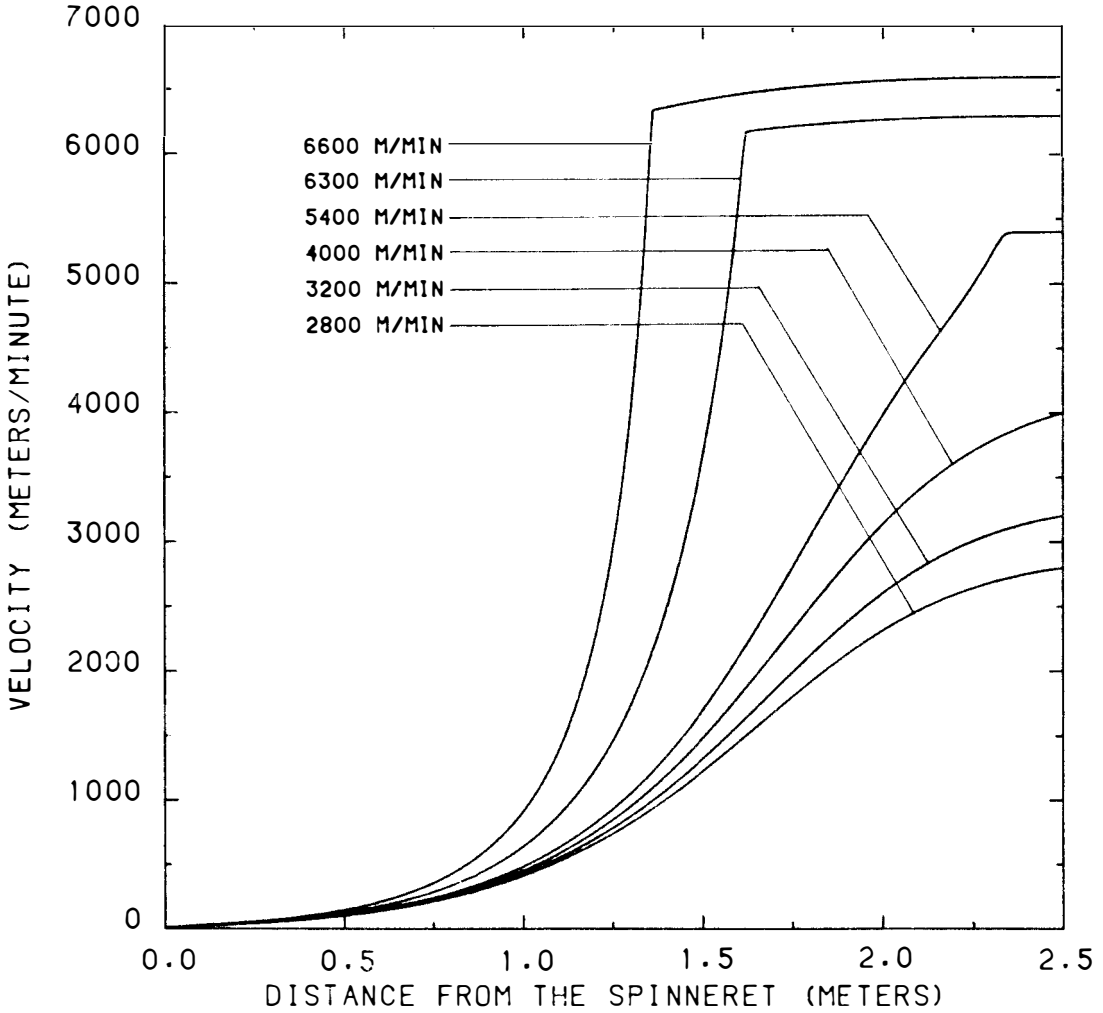


Figure 7.14 Predicted velocity profiles for nylon-66 with a mass throughput of 2.5 gm/min and n = 1.

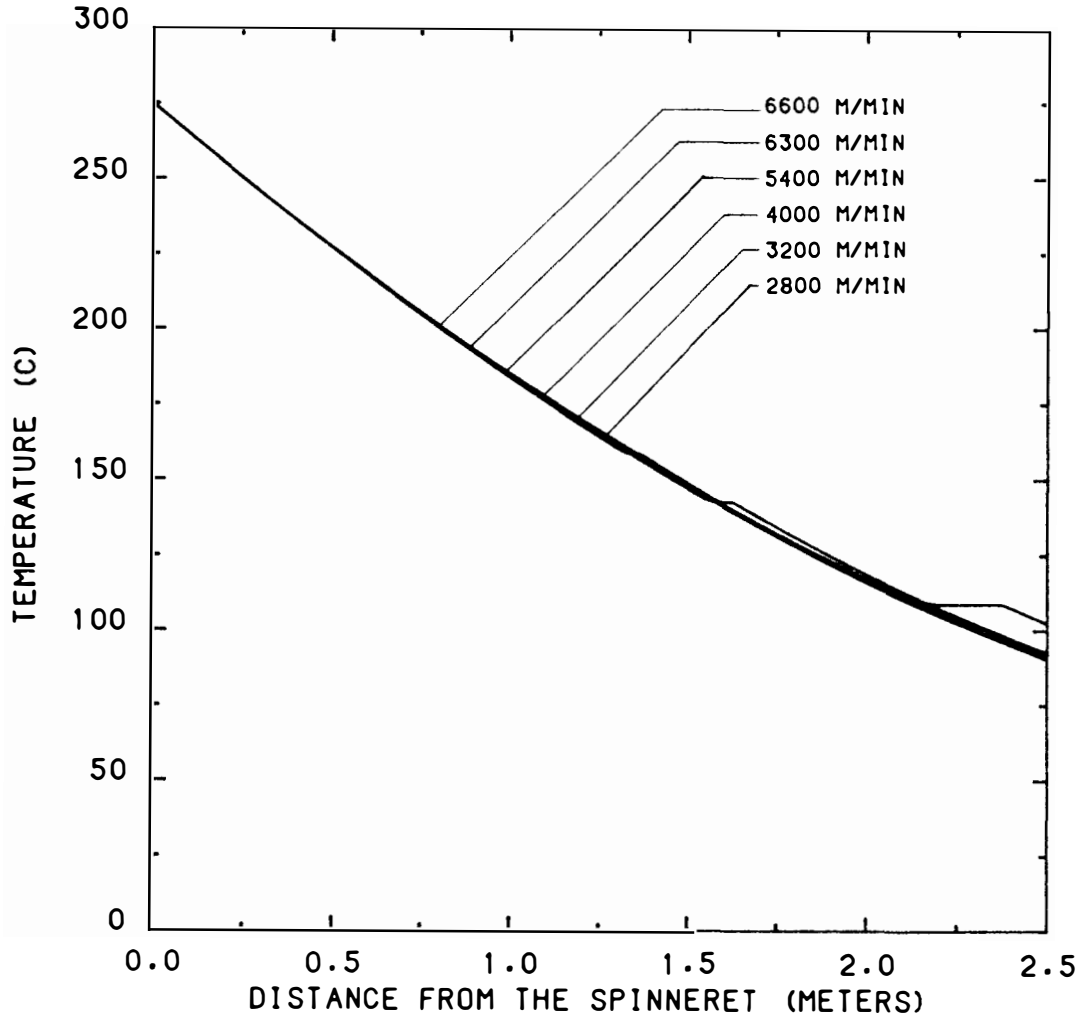


Figure 7.15 Predicted temperature profiles for nylon-66 with a mass throughput of 2.5 gm/min and n = 1.

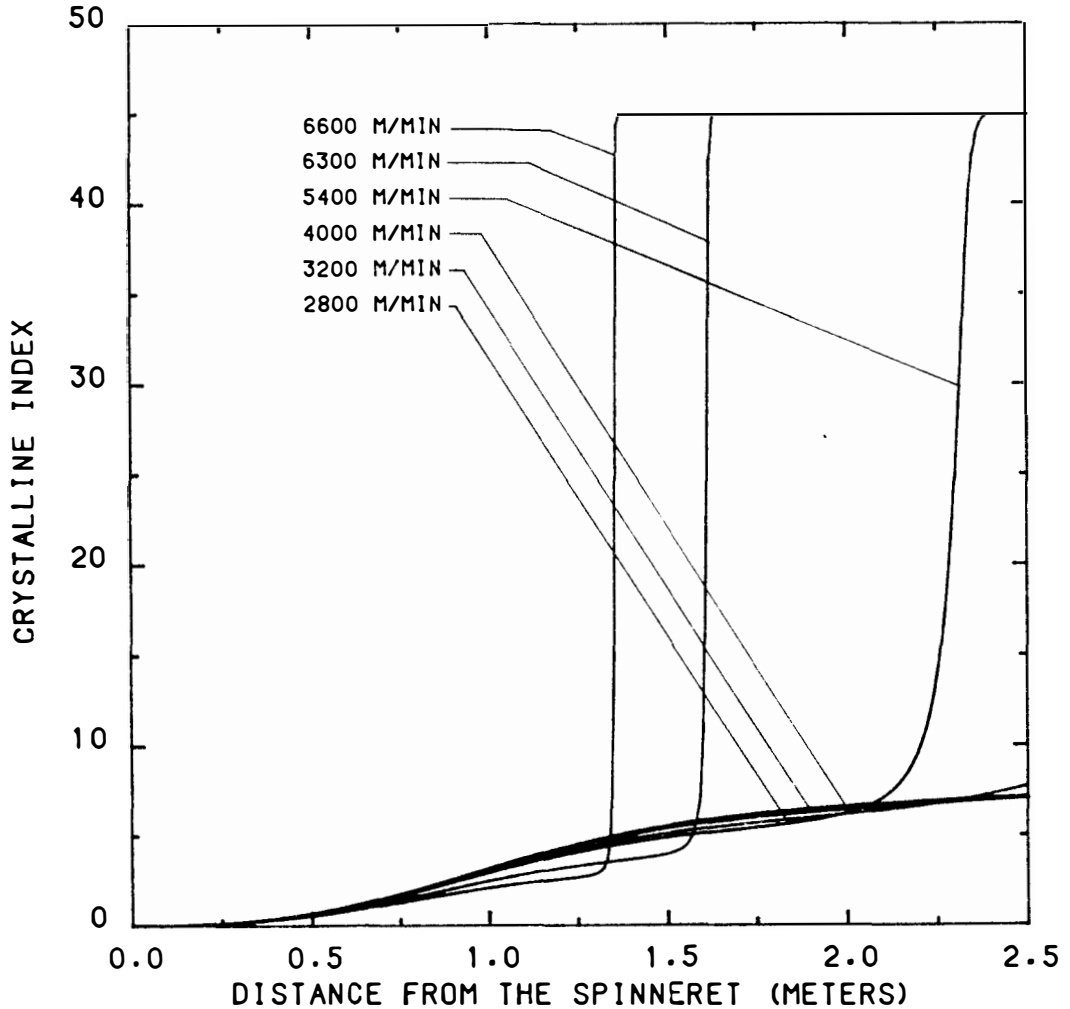


Figure 7.16 Predicted crystalline index profiles for nylon-66 with a mass throughput of 2.5 gm/min and n = 1.

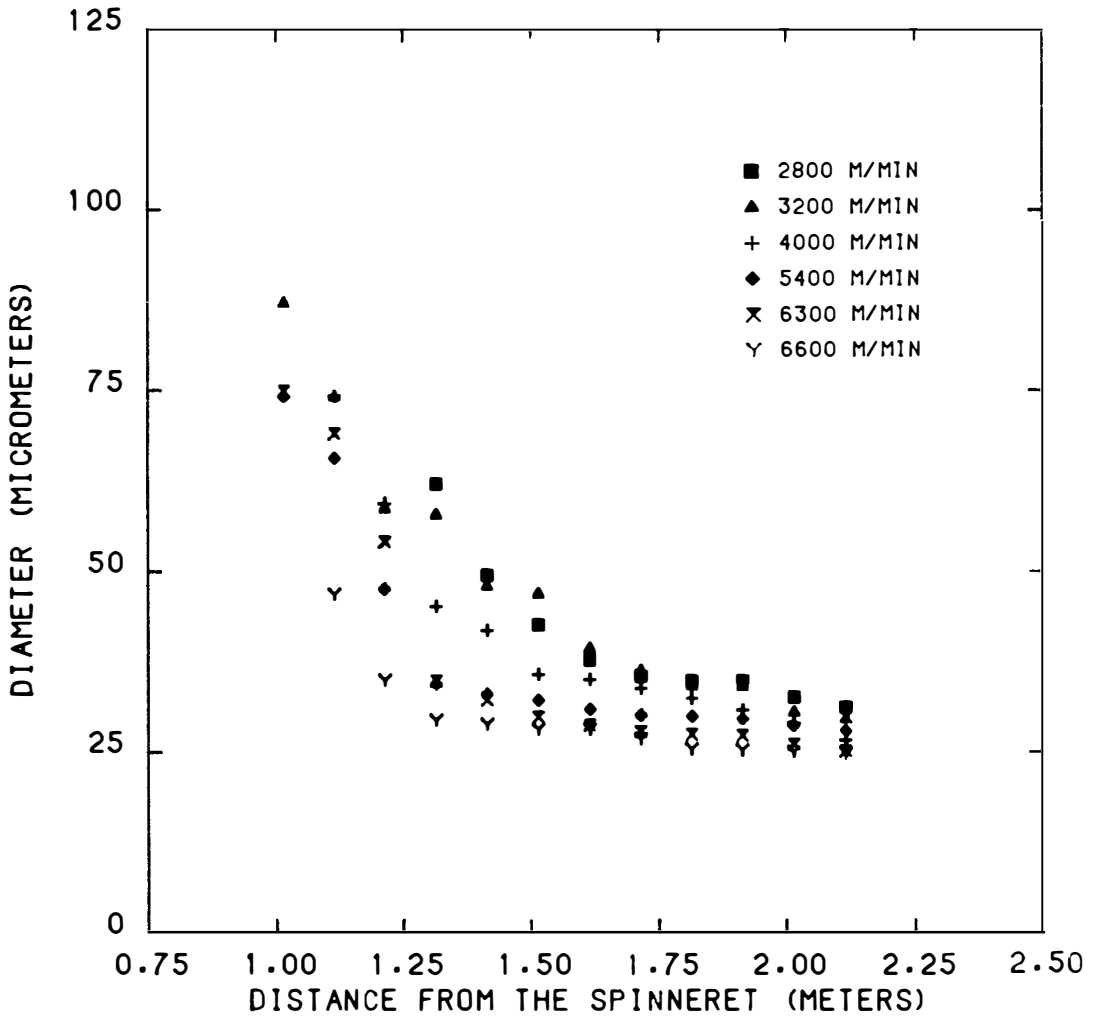


Figure 7.17 Experimental diameter profiles for nylon-66 with a mass throughput of 2.5 gm/min.

The experimental birefringence profiles for the same range of speeds as for the diameter profiles are plotted in Figure 7.18. At low speeds there is a steady increase from the die exit to the take-up. The profiles at the higher speeds indicate a sharp rise in the birefringence up to a plateau region and remains there until the take-up device is reached.

Figures 7.19 - 7.23 are experimental temperature profiles obtained for a variety of processing conditions. Figures 7.19 - 7.22 illustrate the effect of the mass throughput on the temperature profiles. Decreasing the mass throughput increases the rate of heat transfer due to an increase in the surface area to volume ratio.

Figures 7.22 and 7.23 compare the effect of imposing a transverse air flow on the spinline near the spinneret. It should be noted that in each case there was little effect on the profile due to the spinning speed as is the case for the profiles predicted by the model. The experimental results do not seem to indicate the temperature plateaus that are predicted by the model. This may be the result of the plateau occurring out of the measurement range (i.e. near the drawdown device) as would be the case for 5400 meters per minute. Also most of the temperature profiles were obtained at relatively high mass throughputs. This has the effect of lowering the stress in the spinline, thus reducing the effective increase in kinetic rate due to the molecular orientation. It also reduces the heat transfer rate and the fiber remains above the temperature where the kinetic rate is high. These factors combine to postpone the crystallization process, hence the plateaus are not experimentally observed.

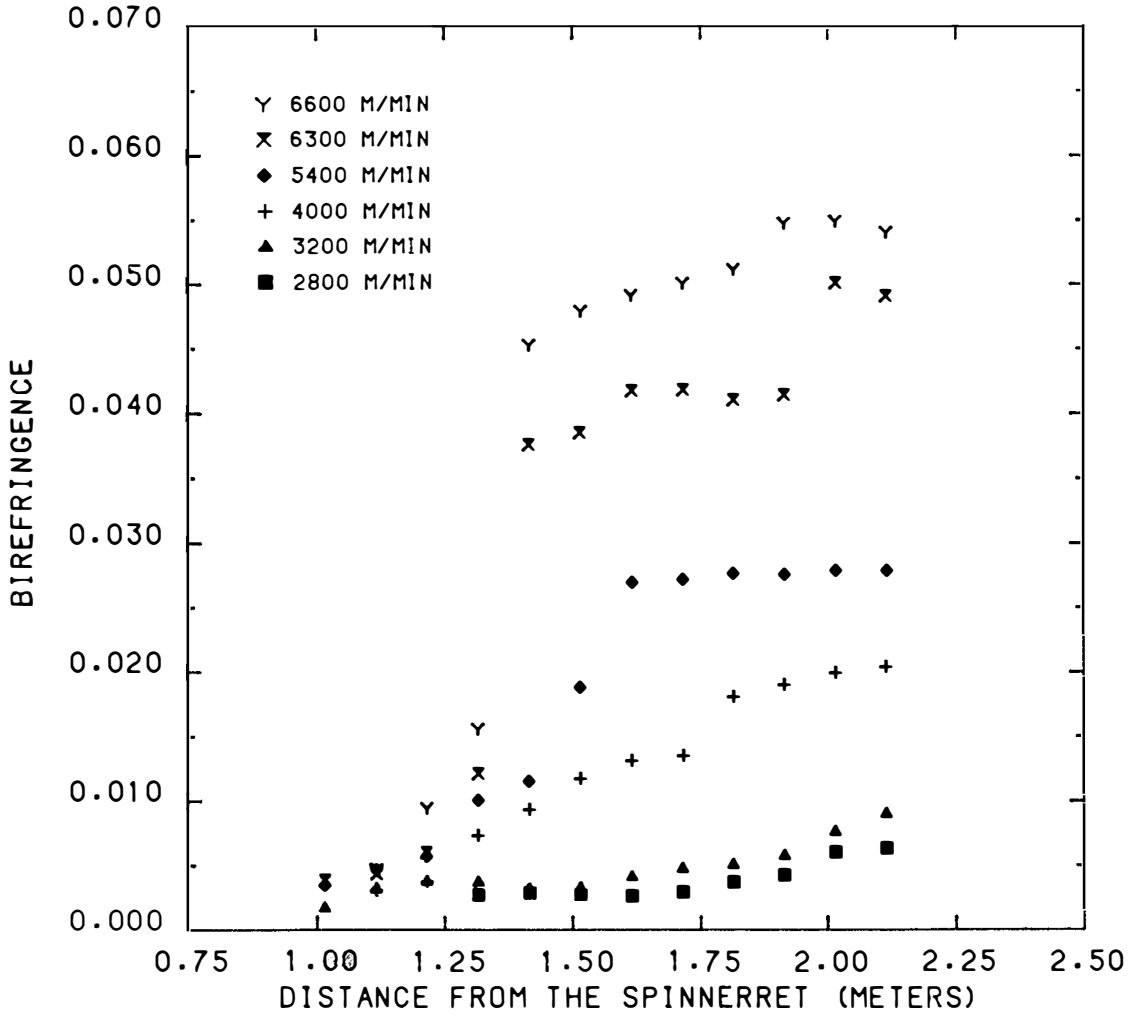


Figure 7.18 Experimental birefringence profiles for nylon-66 with a mass throughput of 2.5 gm/min.

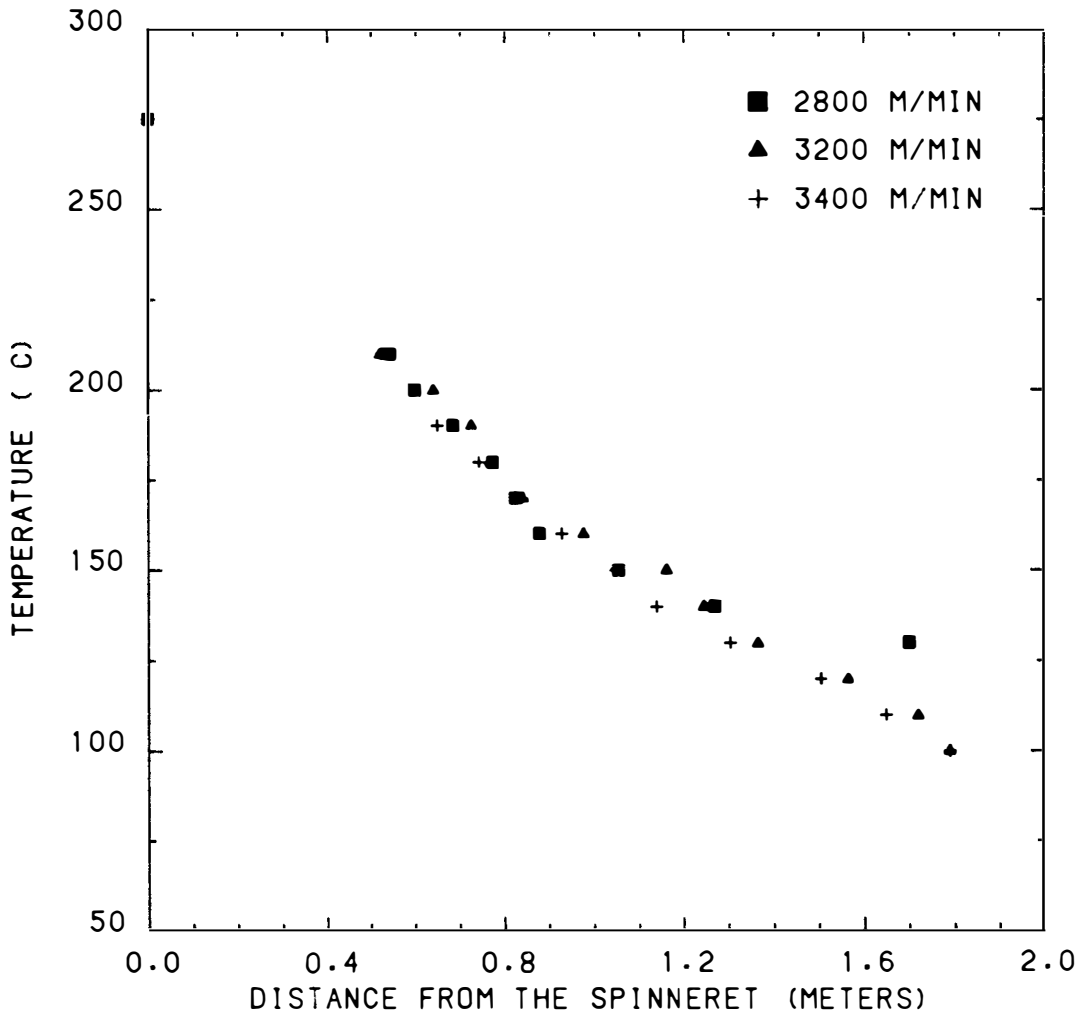


Figure 7.19 Experimental temperature profiles for nylon-66 with a mass throughput of 2.5 gm/min.

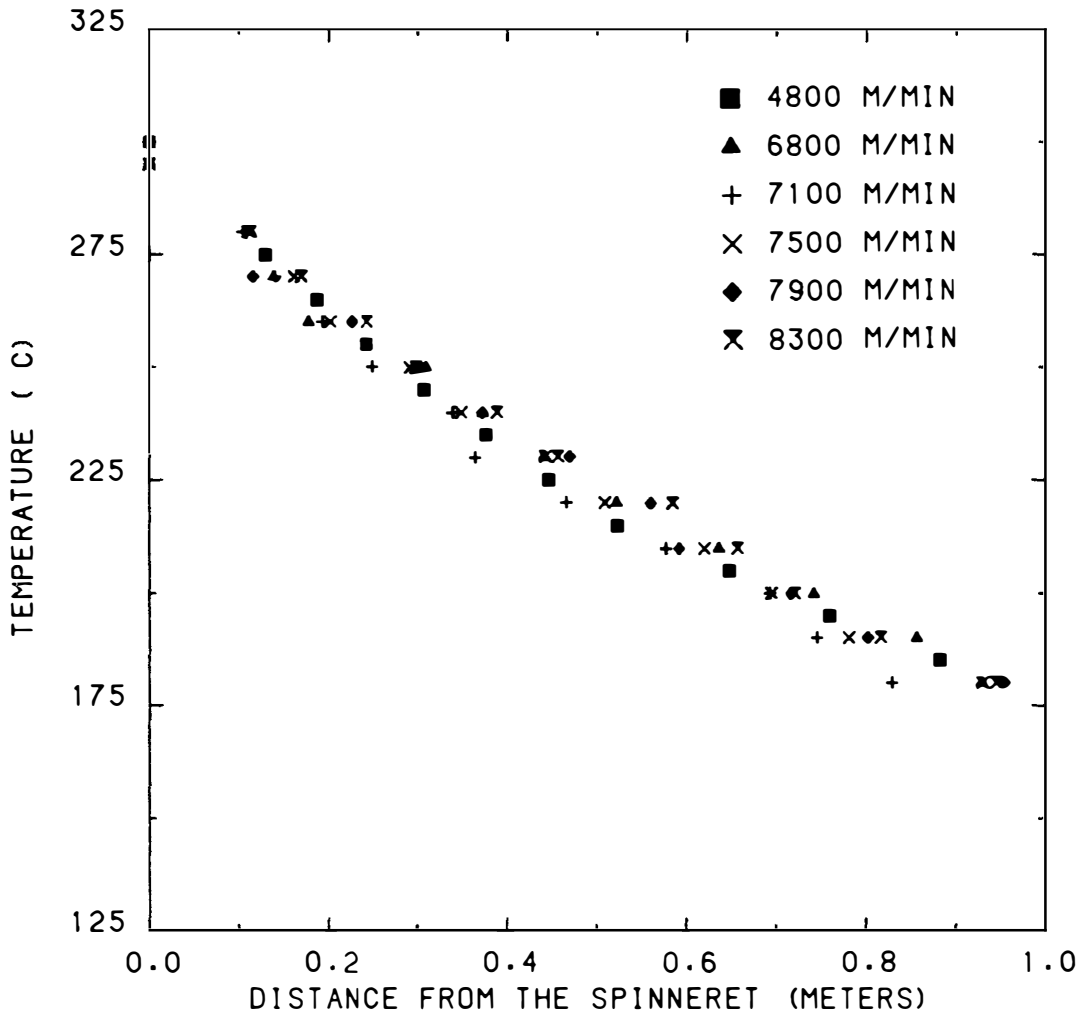


Figure 7.20 Experimental temperature profiles for nylon-66 with a mass throughput of 2.8 gm/min.

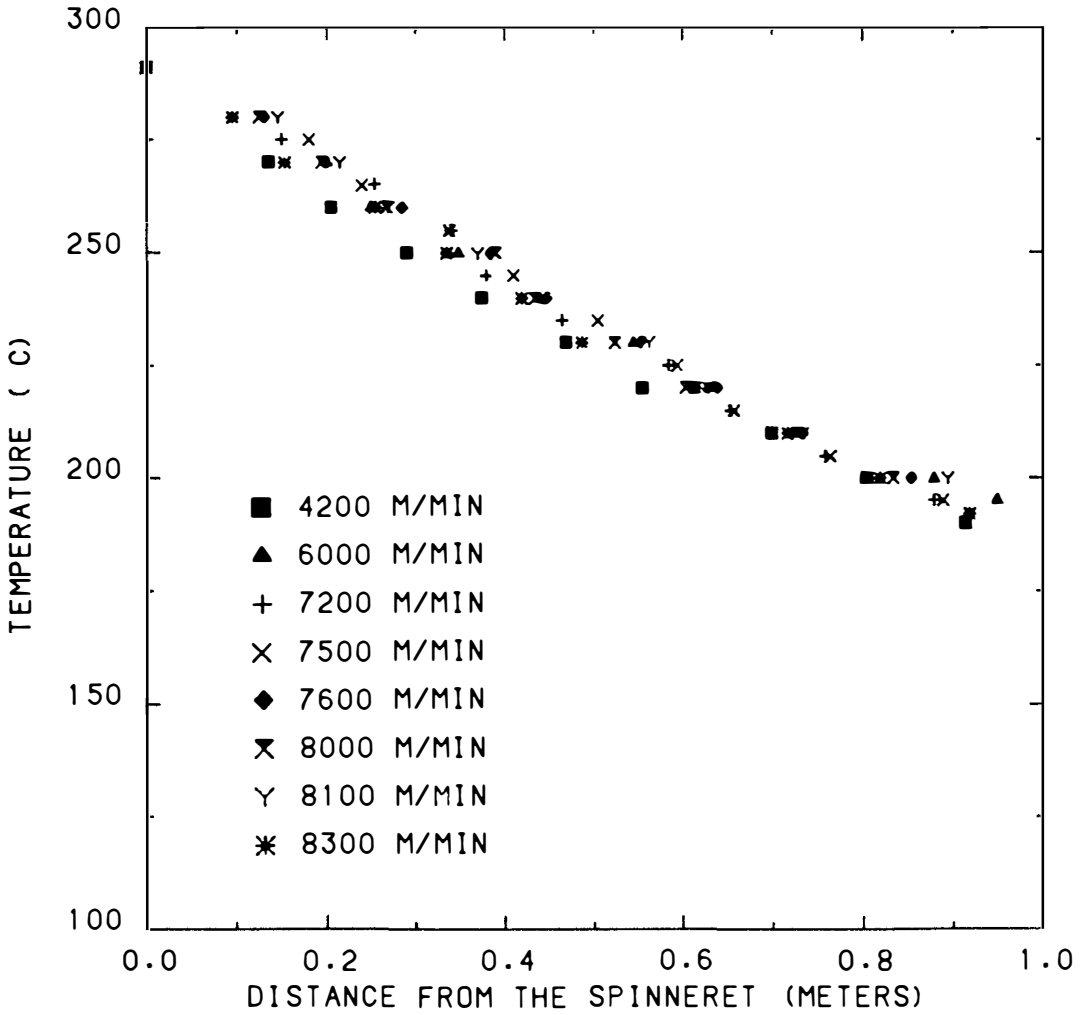


Figure 7.21 Experimental temperature profiles for nylon-66 with a mass throughput of 4 gm/min.

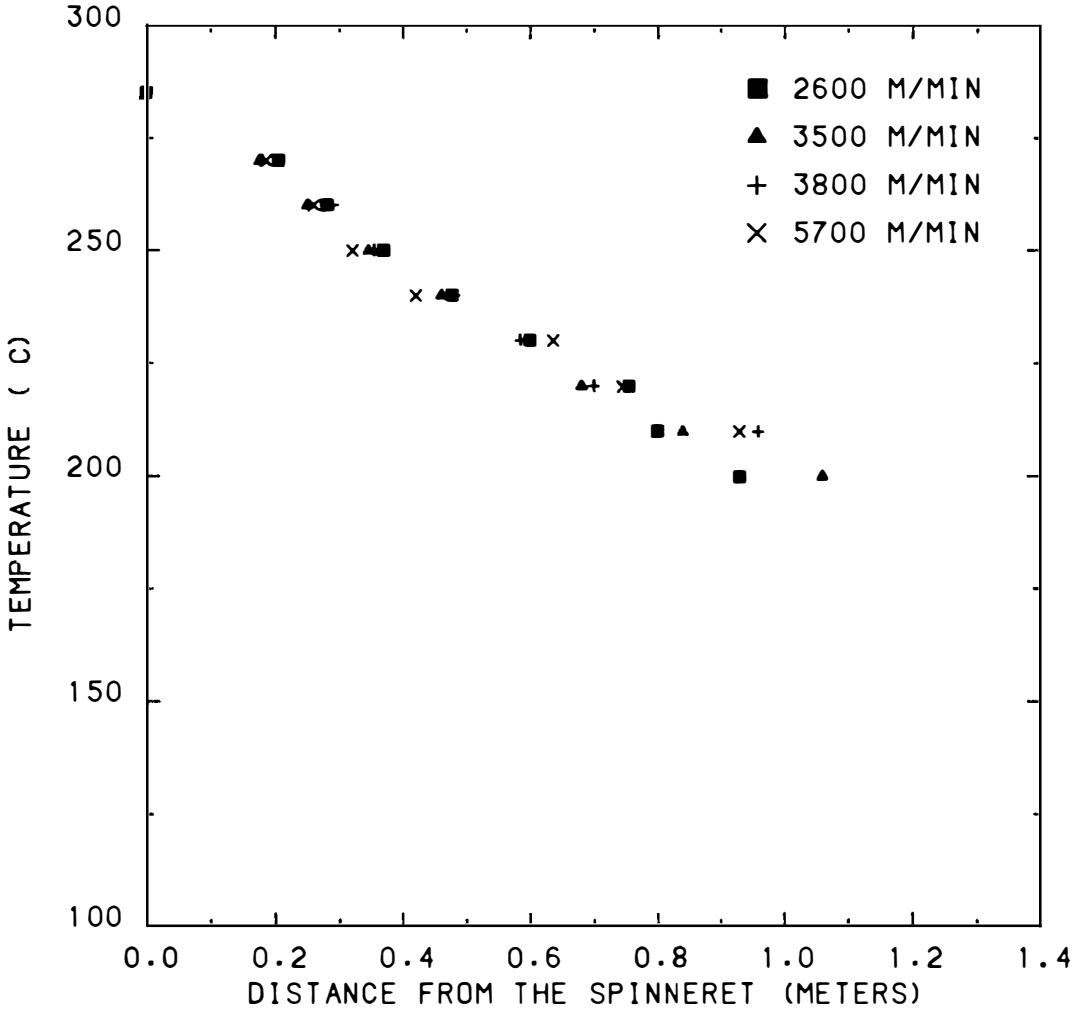


Figure 7.22 Experimental temperature profiles for nylon-66 with a mass throughput of 5.2 gm/min.

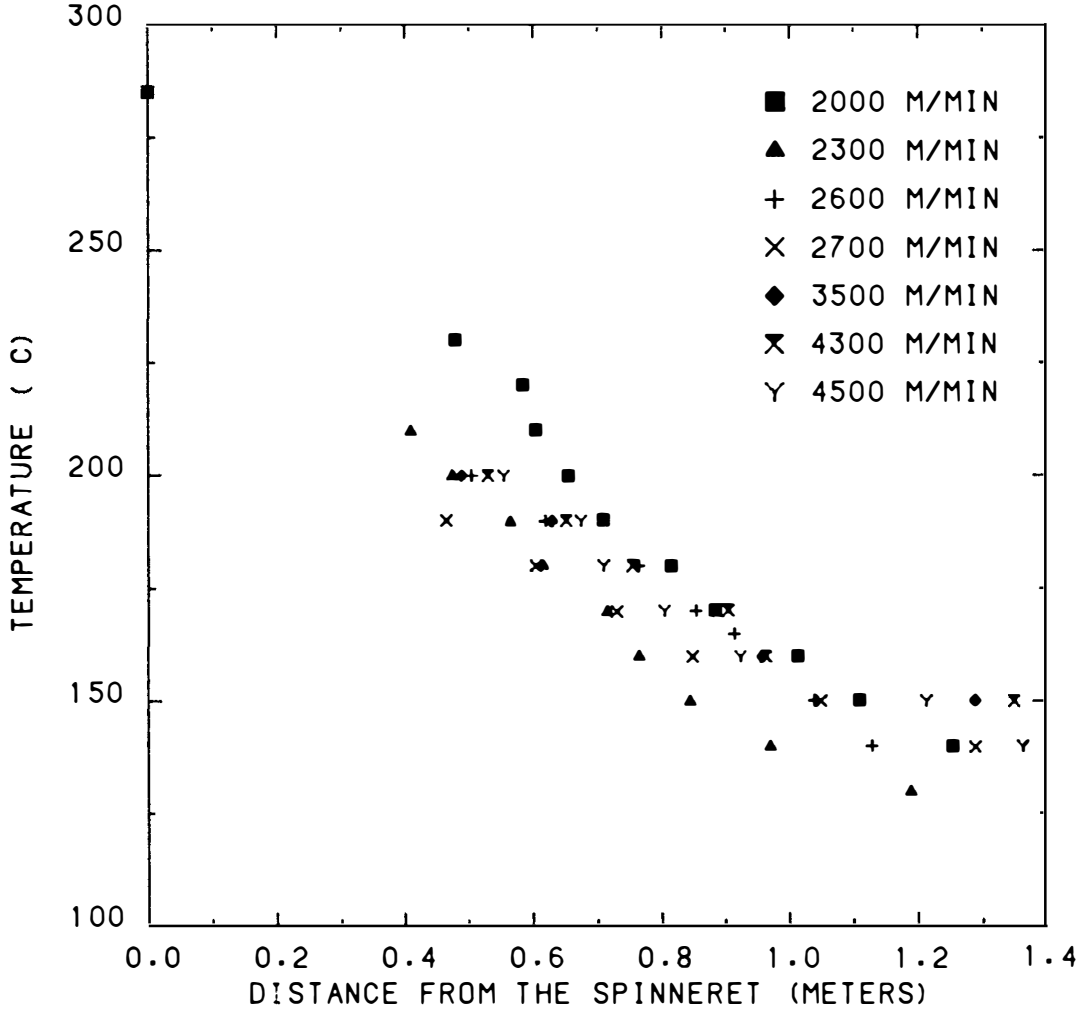


Figure 7.23 Experimental temperature profiles for nylon-66 with a mass throughput of 5.2 gm/min with transverse air flow.

## Comparison of Model Predictions and Online Experimental Profiles for Nylon-66

Figures 7.24 - 7.26 are comparisons between the experimentally obtained diameter profiles and predicted profiles using values of 1, 2 and 3, respectively for the Avrami index. There are no significant differences between the profiles predicted by the three indices. This may be a result of the relatively high crystallization kinetics of nylon-66. The effect of varying the index is most noticeable at the intermediate take-up speeds. This is also apparent in the comparison between the experimental and predicted birefringence profiles (Figures 7.27 - 7.29) for the three Avrami indices. At the lower take-up speeds the crystallization kinetics remain essentially temperature driven, while at the highest speeds the orientation effects overwhelm the temperature influence. At the intermediate speeds they both exert an influence on the kinetic rate.

Figure 7.30 is a comparison of the diameter profiles predicted by the model with n = 1 and substituting 2 for 12 in the equation for the crystallinity effect on the elongational viscosity and the experimentally obtained profiles. The diameter draws down slightly faster than experimentally observed at the highest spinning speeds, this being a consequence of the increased strain hardening effect. Figure 7.31 compares the predicted and experimental birefringence profiles. The abrupt rise in birefringence at the highest speeds appears nearer the spinneret when the exponent is reduced from 12 to 2. This is also a result of the increased strain hardening effect. The increase in elongational viscosity causes higher stresses within the fiber

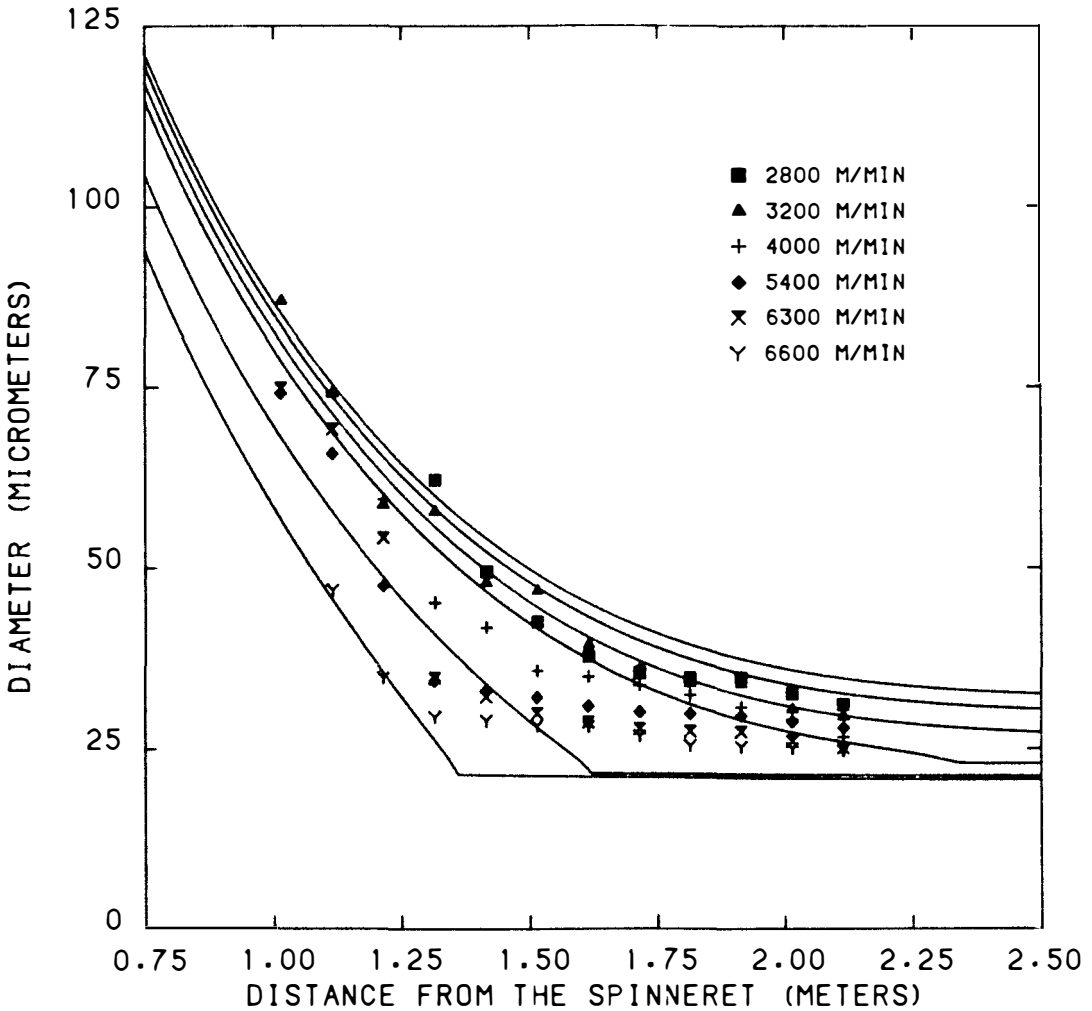


Figure 7.24 Comparison of predicted and experimental diameter profiles for nylon-66 with n = 1.

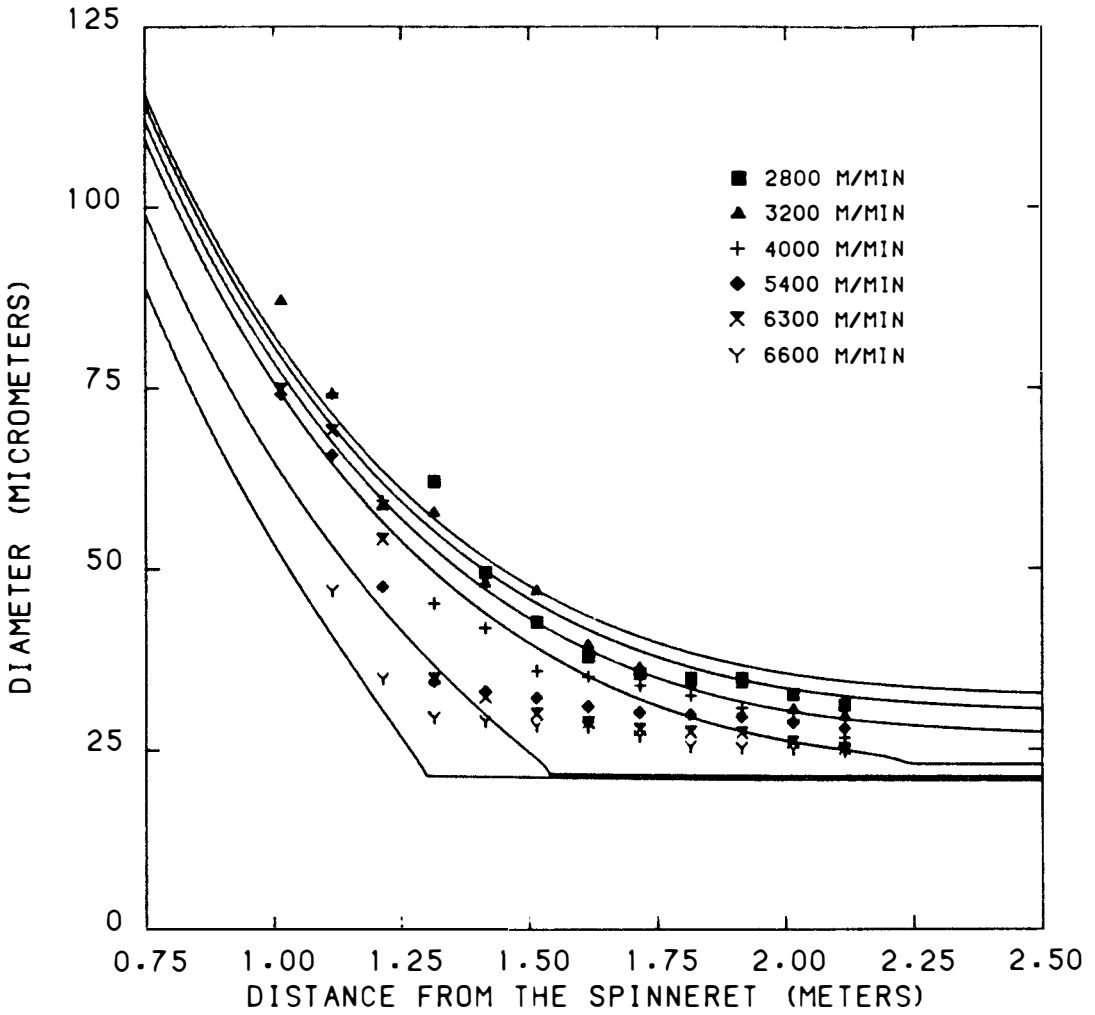


Figure 7.25 Comparison of predicted and experimental diameter profiles for nylon-66 with n = 2.

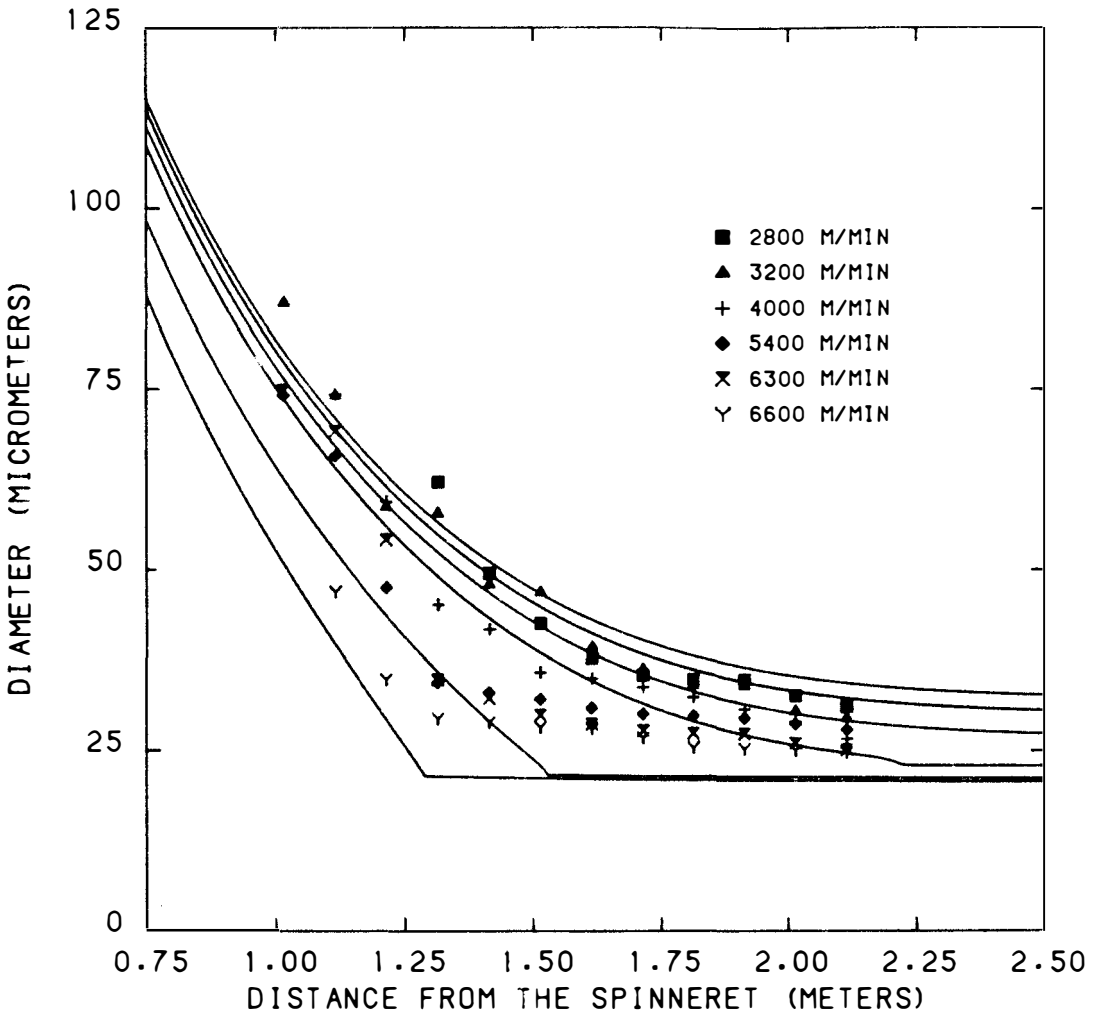


Figure 7.26 Comparison of predicted and experimental diameter profiles for nylon-66 with n = 3.

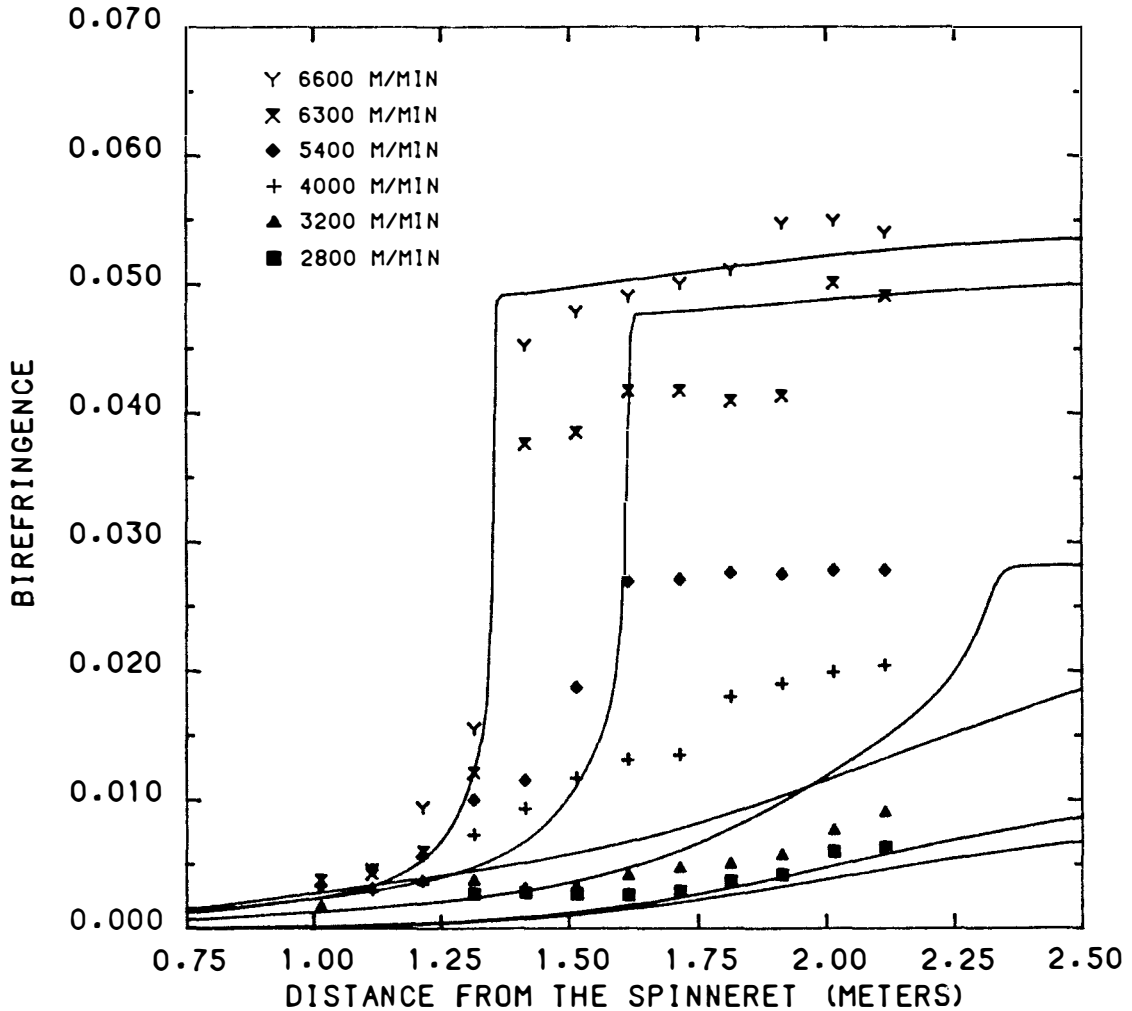


Figure 7.27 Comparison of predicted and experimental birefringence profiles for nylon-66 with n = 1.

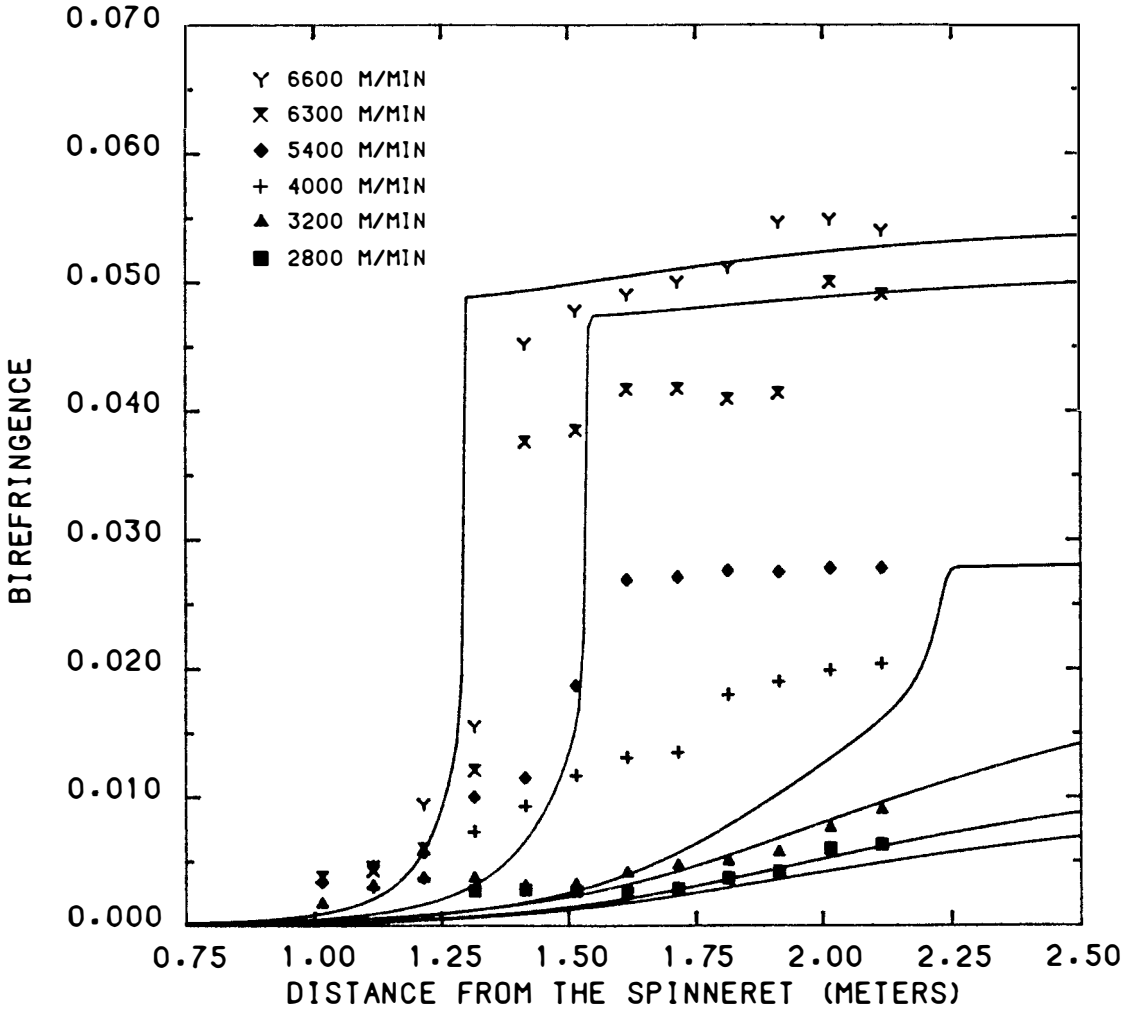


Figure 7.28 Comparison of predicted and experimental birefringence profiles for nylon-66 with n = 2.

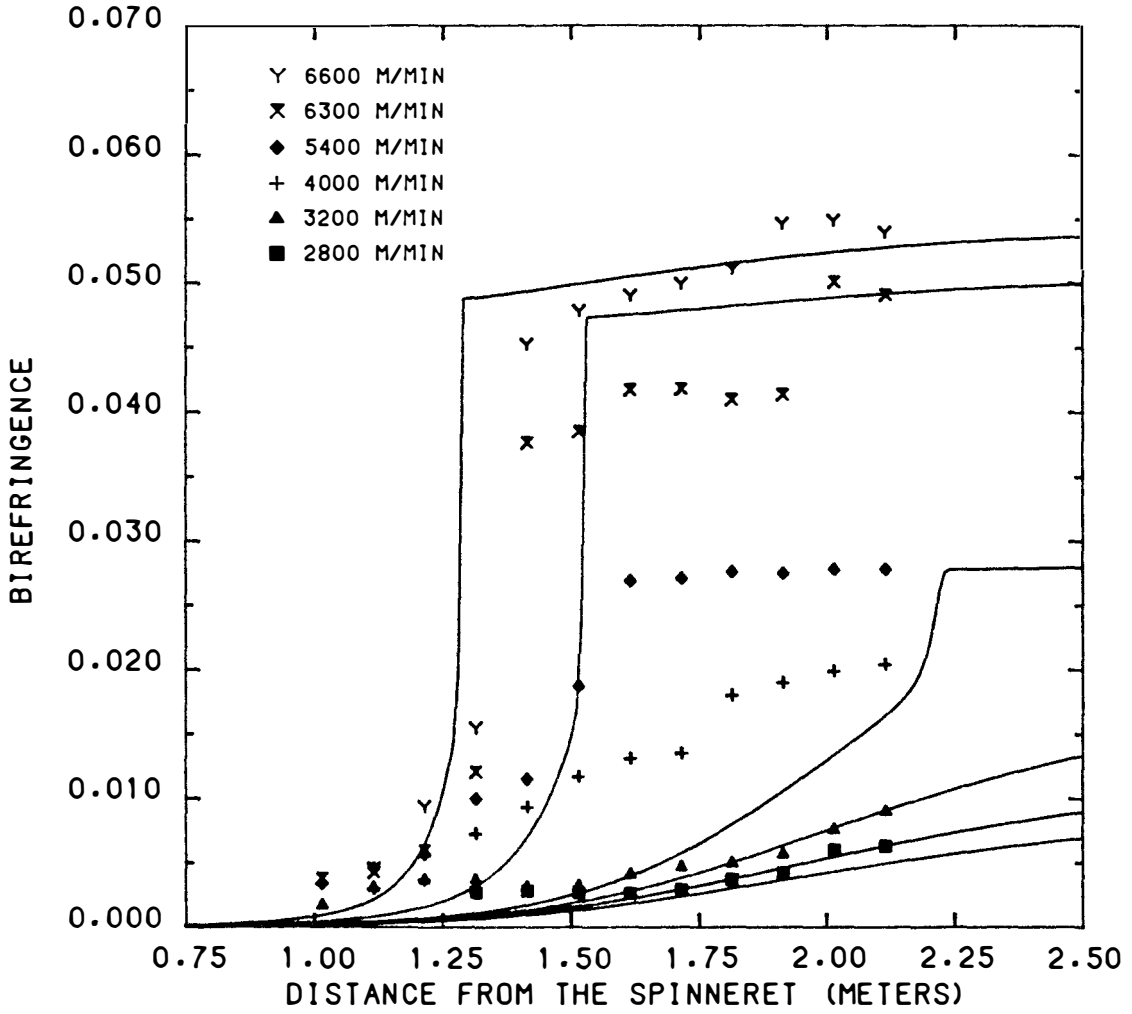


Figure 7.29 Comparison of predicted and experimental birefringence profiles for nylon-66 with n = 3.

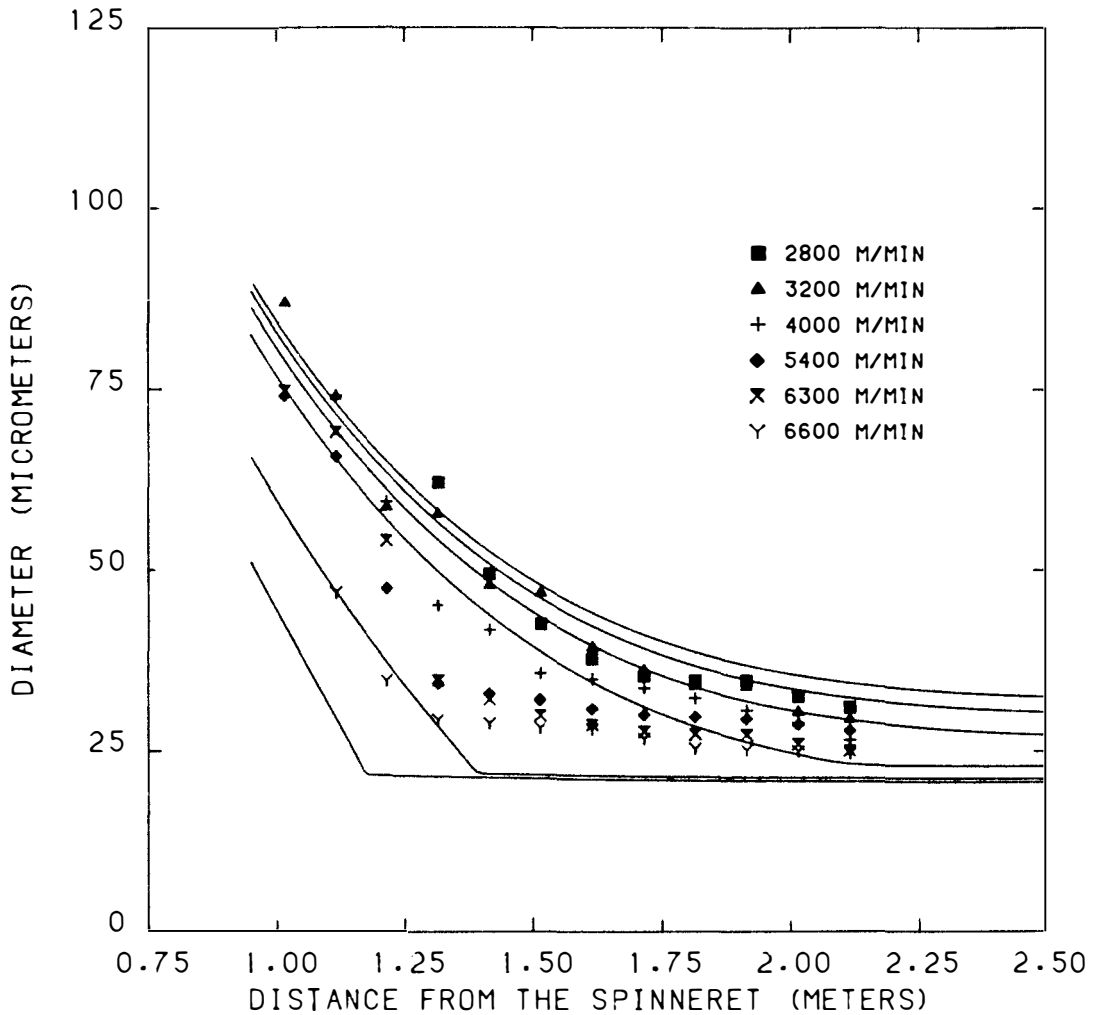


Figure 7.30 Comparison of predicted and experimental diameter profiles for nylon-66 using a value of 2 for the exponent in the relationship for the effect of crystallinity on the elongational viscosity.

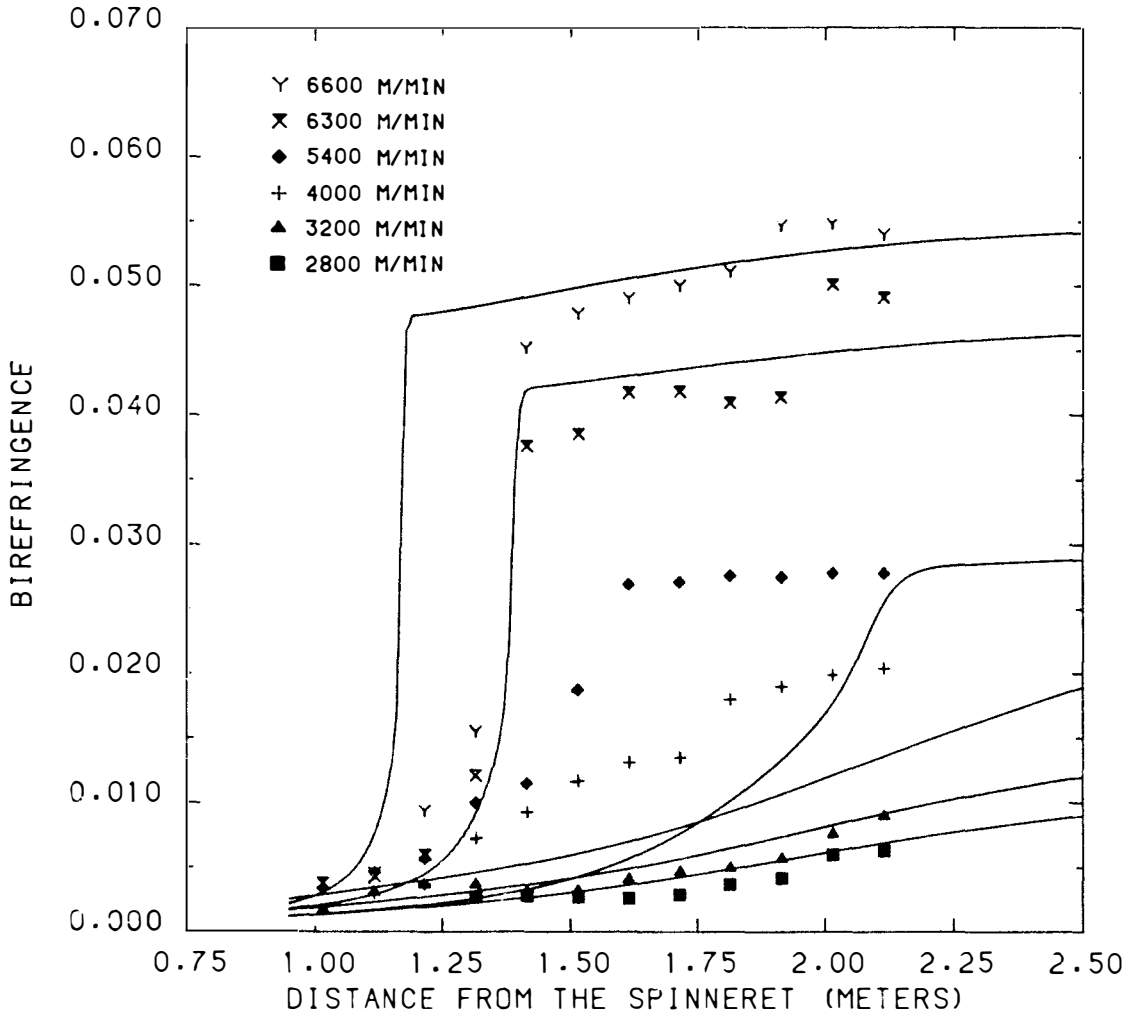


Figure 7.31 Comparison of predicted and experimental birefringence profiles for nylon-66 using a value of 2 for the exponent in the relationship for the effect of crystallinity on the elongational viscosity.

which, at the same spinning speed, results in faster diameter drawdown and higher molecular orientation than predicted in the case where the exponent was 12. It is this higher molecular orientation that triggers the crystallization process at positions nearer the spinneret. The predicted crystalline index profiles (Figure 7.32) demonstrate this result. There was little effect on the predicted temperature profiles (Figure 7.33) since the crystallization rate of nylon-66 is already quite high.

From a comparison of the experimental and predicted profiles it is apparent that there does not exist a one to one correspondence. This is due to a combination of experimental errors incurred during the data collection procedures and constraints imposed on the model during its development. The most severe limit imposed on the model is the neglecting of variations across the fiber radius. This was necessary to convert the formulation from a two dimensional system of partial differential equations to a set of ordinary differential equations which could then be solved numerically. This assumption has a series of implications.

The force balance includes the force caused by the friction between the moving fiber and the stagnant air. The net effect of applying the "one-dimensional" assumption is to transfer that contribution from exerting shear at the fiber surface to increasing the force which is responsible for uniaxial elongation across the radius. This assumption means that the temperature and orientation are uniform across the radius. With the force and temperature uniformly distributed across the radius the deformation across the radius will

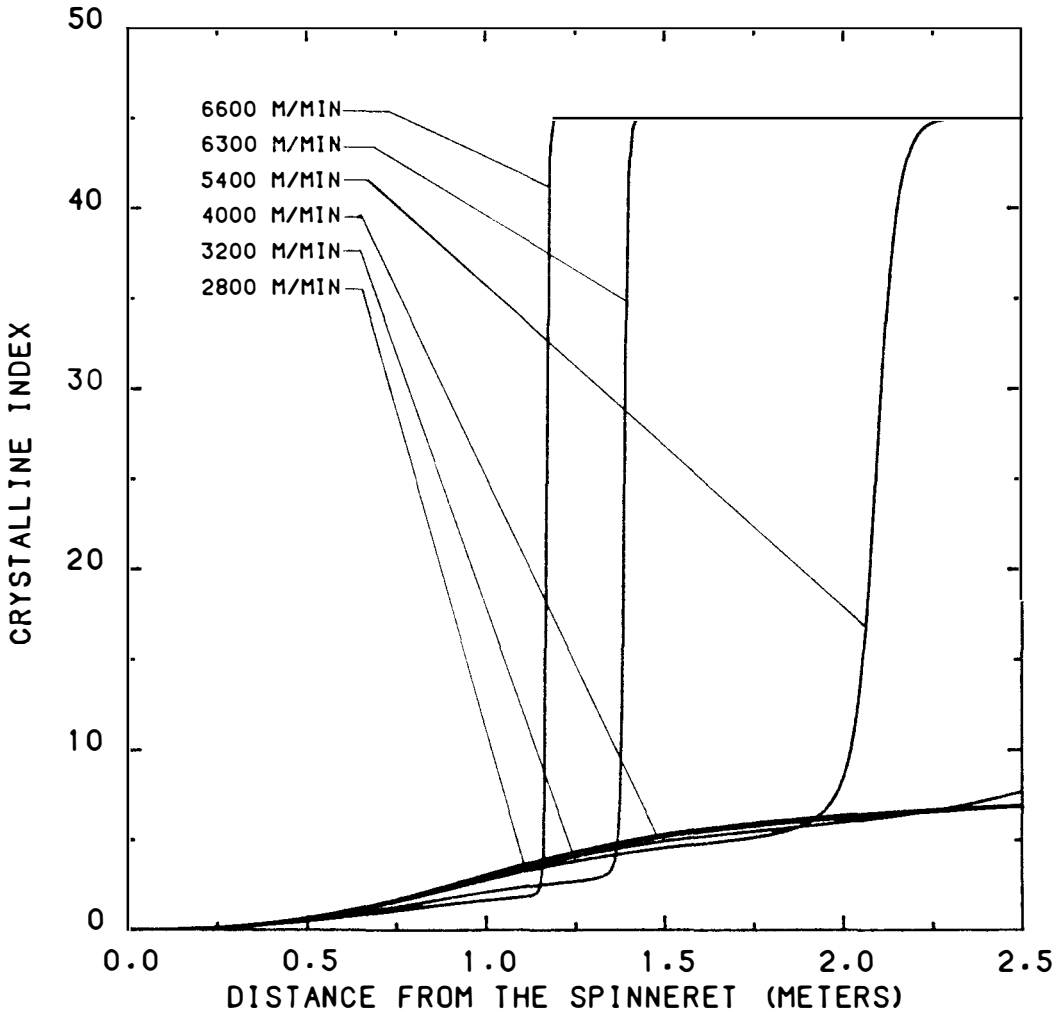


Figure 7.32 Predicted crystalline index profiles for nylon-66 using a value of 2 for the exponent in the relationship for the effect of crystallinity on the elongational viscosity.

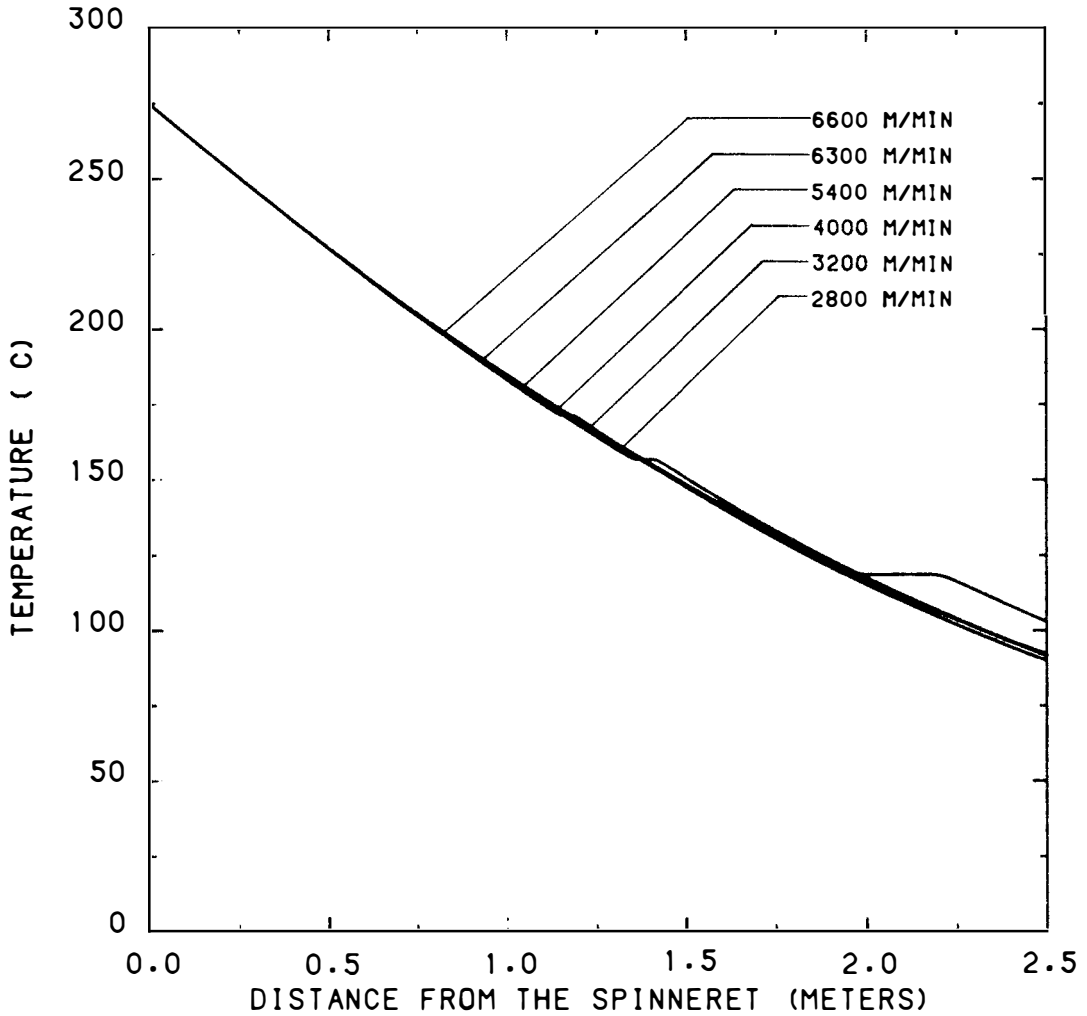


Figure 7.33 Predicted temperature profiles for nylon-66 using a value of 2 for the exponent in the relationship for the effect of crystallinity on the elongational viscosity.

also be uniform. The crystallization process will also occur uniformly across the radius since the temperature and orientation are uniform. In the characterization of several polymers spun at high speeds it has been found that under certain spinning conditions there are large differences in the structure across the radius, leading to a skin - core model (9-11,108-115). This model shows that the skin has a higher orientation and crystallinity than the interior core of the fiber. The present model is unable to deal with these observations.

The molecular orientation of the amorphous material was determined by the birefringence. The relationships which described the birefringence in the model was a combination of the stress optical law and a Maxwell element. This provided a means of computing the change in birefringence along the spinning path. This method along with neglecting radial variations means that the molecular orientation of all the amorphous material at a given distance from the die would be the same. This would occur even when some of the amorphous material would be converted during crystallization. There was no mechanism to account for the depletion of the oriented amorphous material during crystallization along the spinning path. This is also true for the orientation of the growing crystals. A more conceptually satisfying alternative would be to describe the orientation of the amorphous and crystalline materials in terms of distributions that are linked to each other by the crystallization kinetics. Abhiraman (56) has attempted to perform an analysis along these lines but the relationships he derived involve several questionable assumptions and would

need several more to modify them enough so that they could be incorporated into the present framework.

Even with the incorporation of orientation distributions there still remains the question of how to describe the temperature and orientation effects on the crystallization kinetics. The formulation used in this study is a result of empiricism (temperature dependence) and a simplified theoretical development (orientation effects) by Ziabicki. This is due in part to the large difficulties associated with designing an experiment to actually study the kinetics of an oriented material and maintain and completely characterize that orientation during crystallization. Add to that the lack of a fundamental theoretical basis for the nucleation and growth phases of the crystallization process in polymers. Even in terms of the simplified Avrami expression used here, there is the possibility of the changing of mechanisms (as indicated by a varying Avrami index) as the velocity increases.

The final limitation in the model involves the characterization of the material itself. In terms of the overall melt spinning process the processing conditions can be artificially constructed to reproduce the conditions that the theoretical relationships describe. It is not feasible to manufacture a material which will satisfy all the theoretical requirements over the spectrum of processing conditions which it will experience.

A Newtonian constitutive equation was chosen because it is the simplest form and there is enough information available in the literature to be able to incorporate it into the framework. Even in this

simplest case there are some questions regarding the best means of incorporating the temperature, molecular weight and crystallinity effects into an expression for the elongational viscosity. There is no data available on the variation of the elongational viscosity with the elongation rate or molecular weight distribution for the range of temperatures and elongation rates that are commonly found in melt spinning. Since the polymer experiences such a diversity of conditions it is quite difficult to quantitatively describe, using any available constitutive equation, how the polymer will respond to them all. This situation exists for many of the physical properties such as densities, stress optical coefficients, specific heats, etc. of many common materials. Even in the face of all these difficulties, the model does a remarkable job of predicting the behavior of nylon-66 when spun at high and low speeds. The discrepancies appear at those intermediate speeds where one factor does not play a dominant role in determining the overall behavior of the spinline. At the intermediate speeds it seems to be an interaction or synergism of several factors which the model fails to describe adequately. This does not render the model useless however. The model, as developed, could be used as a tool to evaluate alternative expressions for the crystallization kinetics or to evaluate the various kinetic parameters by trial and error comparisons with experimental data. It can also be used to simulate a wide variety of processing conditions along with the addition of cooling or heating chambers positioned at various points along the spinline without carrying out time consuming and expensive experiments.

## Structure and Properties of Conditioned Nylon-66 Fibers

Samples from numerous spinning experiments under a wide variety of spinning conditions were collected and characterized as described in Chapters 5 and 6. These results were compared to those available in the literature to ascertain whether or not the spinning experiments performed in this study produced fibers which exhibited properties typically reported for high speed spun nylon-66.

Figure 7.34 is a plot of the birefringence of the conditioned final fibers as a function of spinning speed for various processing conditions. These are generally in agreement with results reported by Shimizu et al. (1); since all the material and spinning conditions are not known an exact comparison is unavailable. In general, the birefringence increases with spinning speed, decreasing mass throughput and shorter spinlines.

The density of the conditioned fibers increases slightly with spinning speed (Figure 7.35) for a mass throughput of 2.5 grams per minute. Figure 7.36 shows the crystalline index, determined from density and DSC data, as a function of spinning speed. There is a slight increase in crystallinity with spinning speed and the two methods are in good agreement with each other. These data are similar to those reported by Shimizu et al. (1) for conditioned nylon-66 fibers spun at similar speeds. All the determined crystalline indexes are between 40 and 45%, this is probably of result of post spinning crystallization in the case of the lower speed fibers. These results also reinforce the assumption of a maximum obtainable crystallinity of 45% in the model.

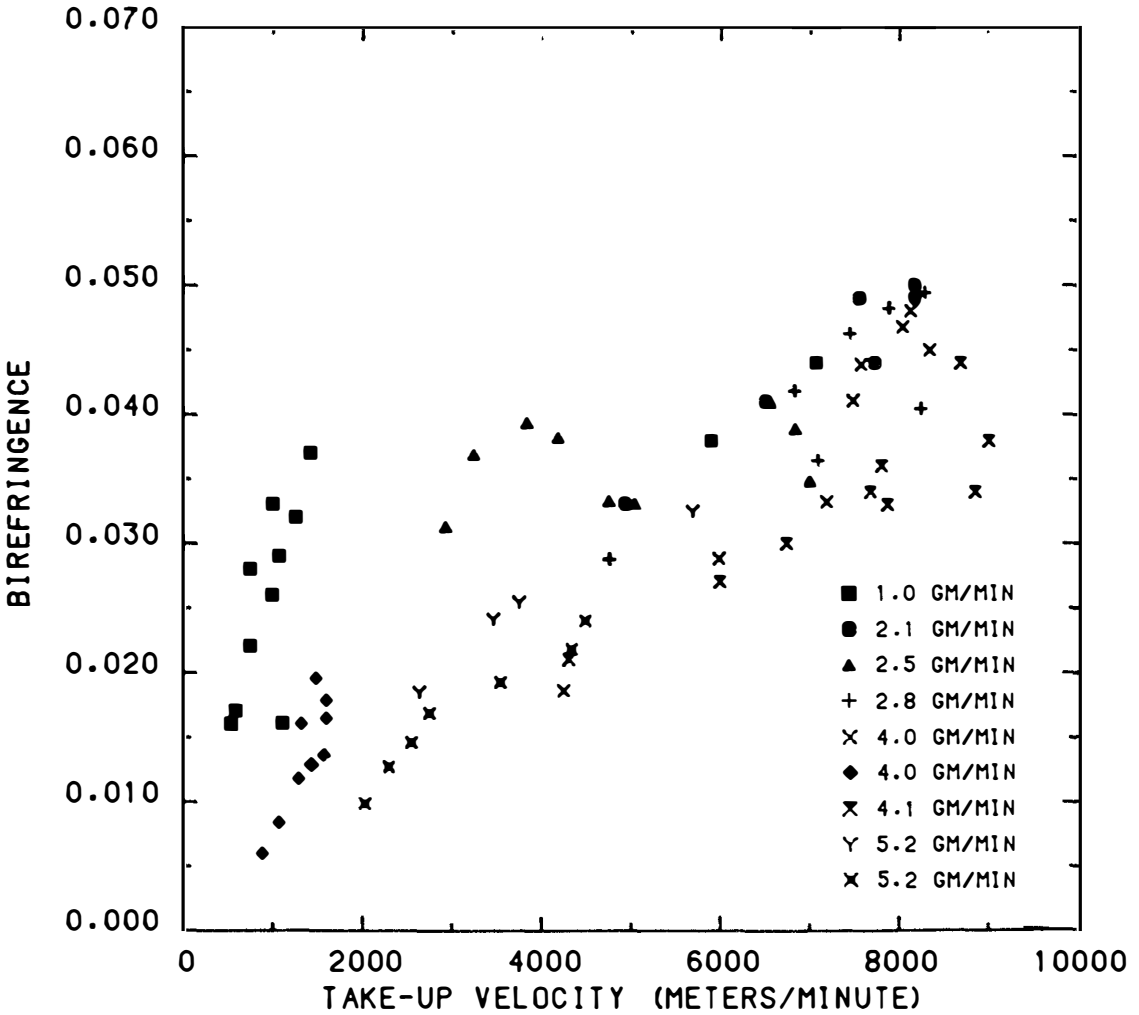


Figure 7.34 Final fiber birefringence as a function of spinning speed for nylon-66.

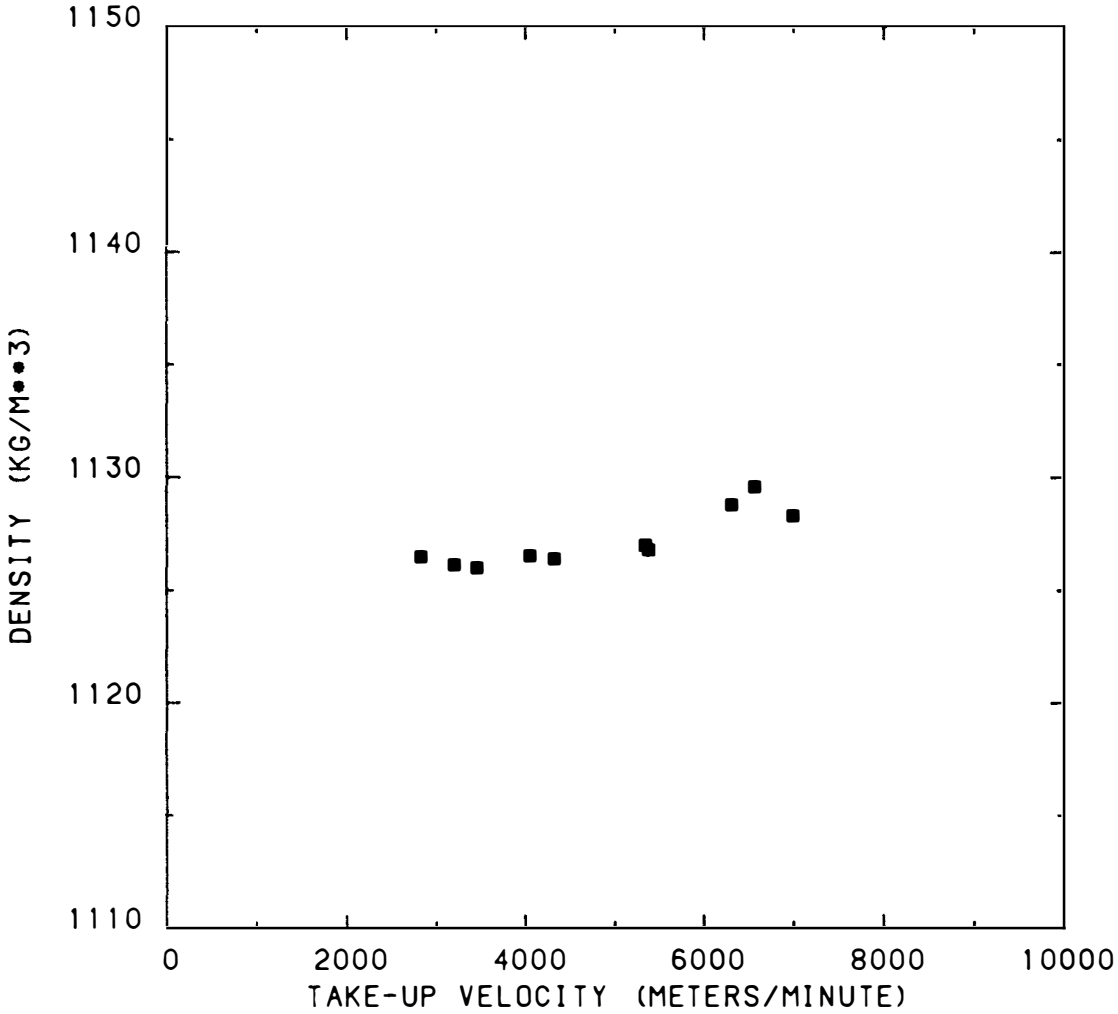


Figure 7.35 Final fiber density as a function of spinning speed for nylon-66 at a mass throughput of 2.5 gm/min.

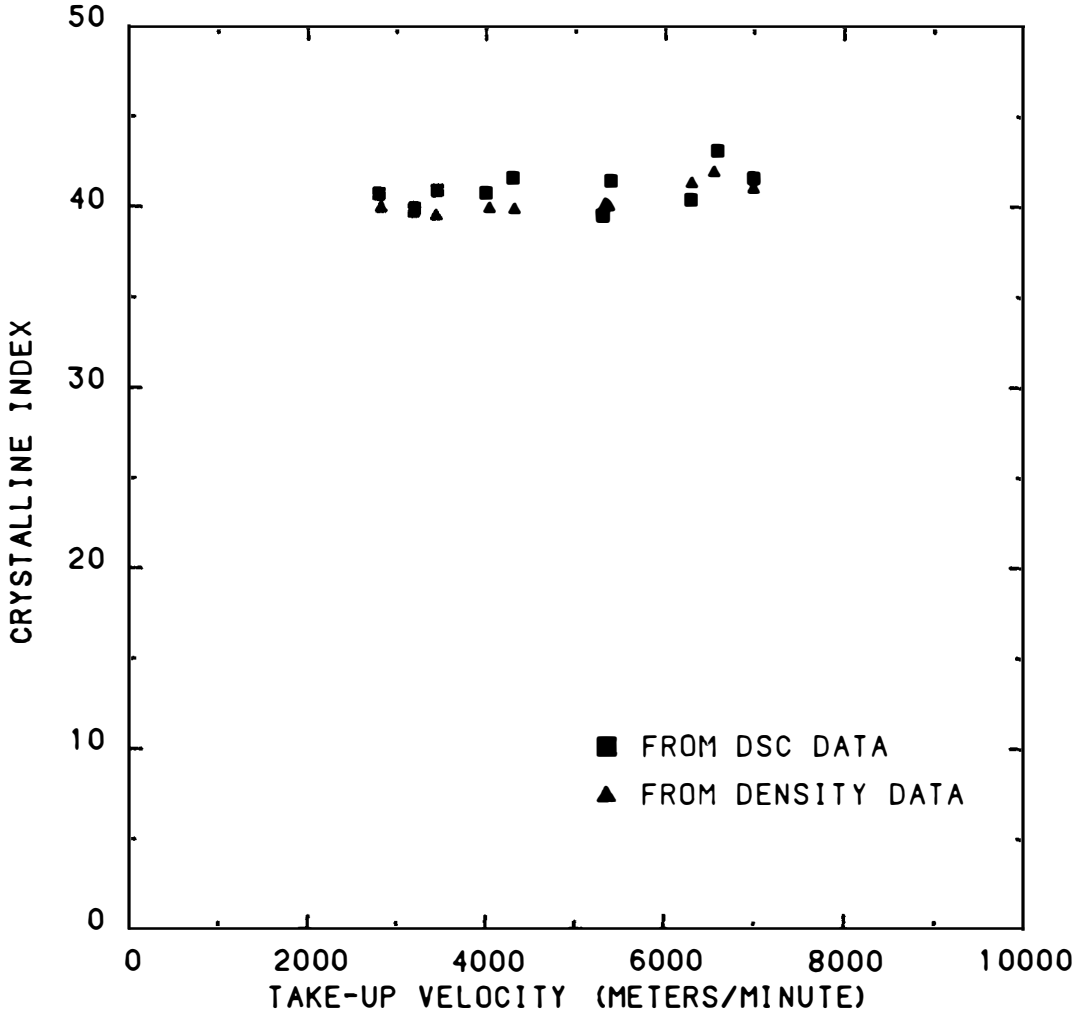


Figure 7.36 Final fiber crystalline index as a function of spinning speed for nylon-66 at a mass throughput of 2.5 gm/min.

The crystal perfection index (Figure 7.37) remained low (30 - 40%) and showed no clear trend. Shimizu et al. (1) presented data which indicated that the crystal perfection index remained around 50% for fibers spun below 4000 meters per minute and rose to approximately 80% for fibers spun at 8000 meters per minute. The lower values obtained in this work may arise from the rather low molecular weight nylon-66 that was being spun. The crystalline and amorphous orientation functions are shown in Figure 7.38 as a function of spinning speed. The crystalline orientation remained high (0.7 - 0.8) at each speed and showed only minor variation with the three different unit cells used in the Wilchinsky analysis. Based on an analysis of the x-ray diffraction scans it is believed that the majority of the crystals present were of the alpha variety. The amorphous orientation function remained low (0.2) at all speeds. These results are slightly lower than those reported by Shimizu, around 0.9 for the crystalline and 0.3 for the amorphous orientation function, and again this may be a result of the low molecular weight nylon-66 or of the background correction.

The long period of the conditioned fibers was determined from SAXS are presented in Figure 7.39 as a function of spinning speed. A comparison with Shimizu's data (1) indicates an increase in long period for fibers spun above 4000 meters per minute. As was the case for the orientation functions the long periods are slightly smaller than Shimizu's but exhibited the same trends. The increase in long period with spinning speed may be taken as indirect evidence that the

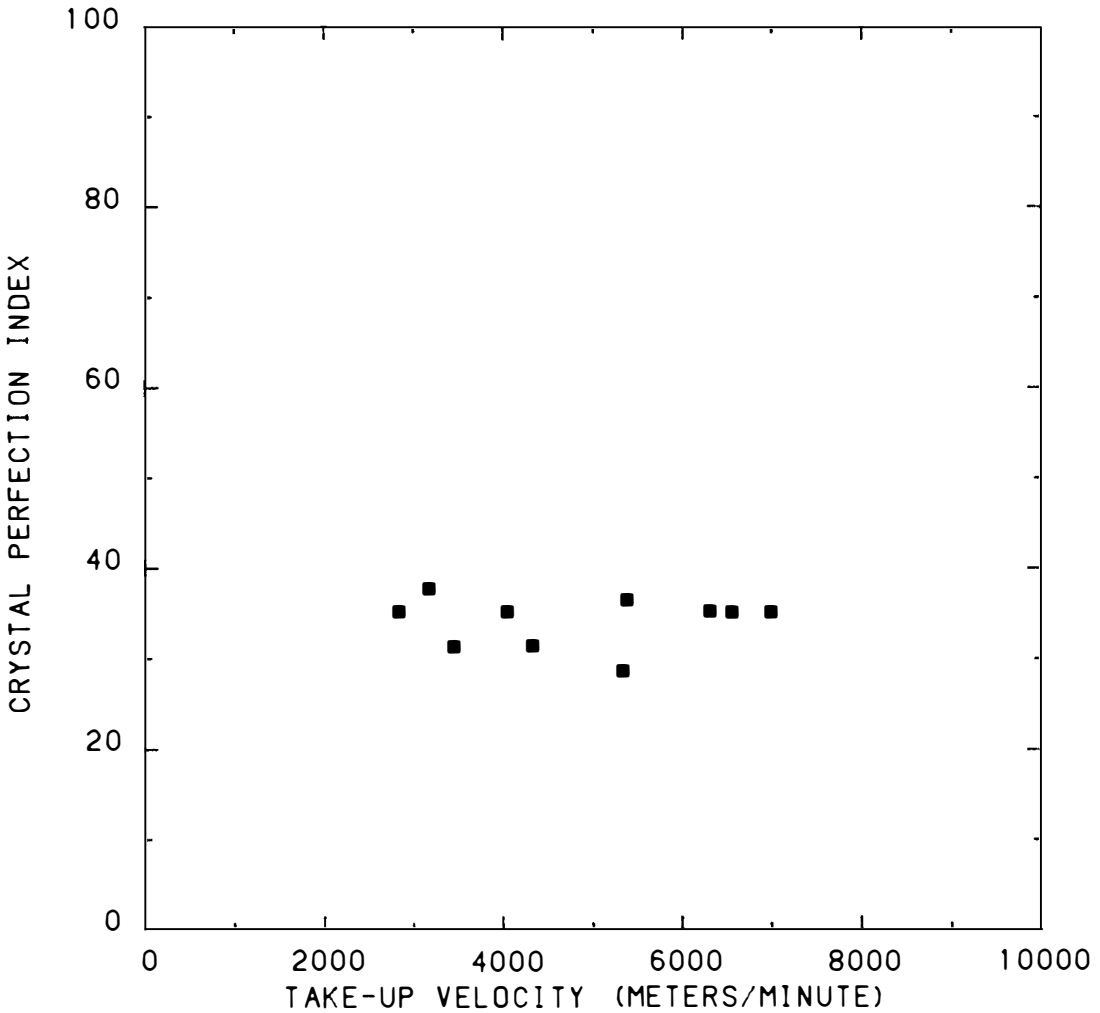


Figure 7.37 Crystal perfection index in the final fiber as a function of spinning speed for nylon-66 at a mass throughput of 2.5 gm/min.

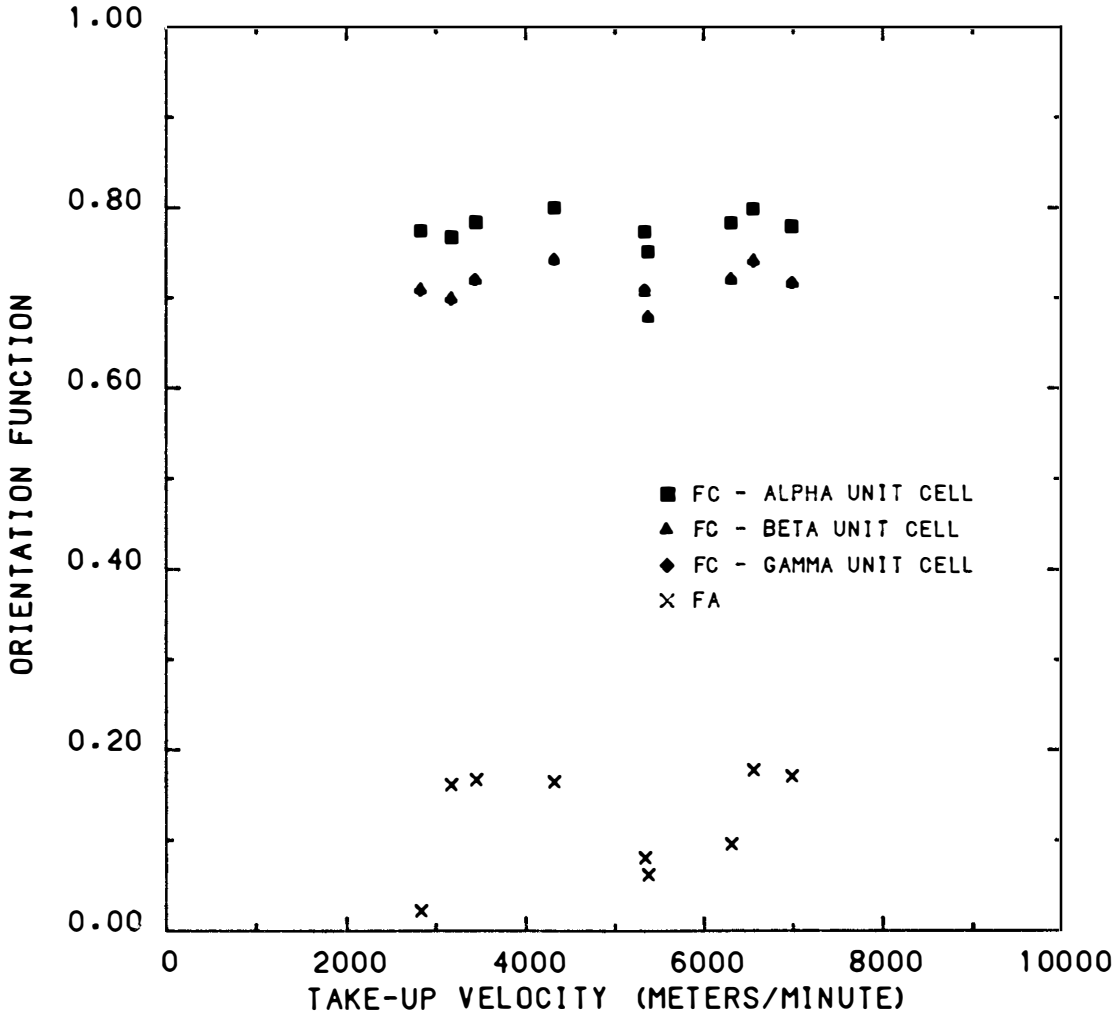


Figure 7.38 Crystalline and amorphous orientation functions in the final fiber as a function of spinning speed for nylon-66 at a mass throughput of 2.5 gm/min.

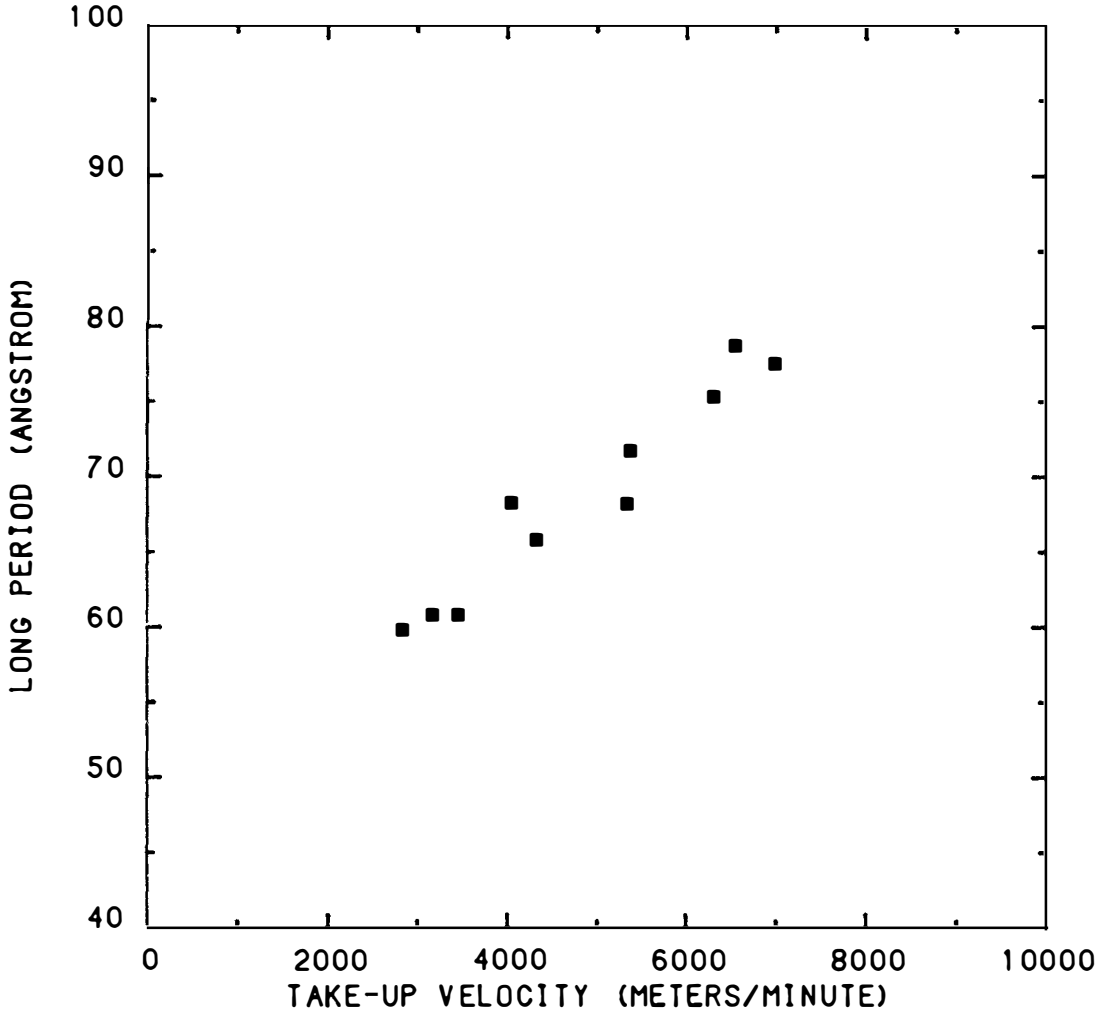


Figure 7.39 Long period in the final fiber as a function of spinning speed for nylon-66 at a mass throughput of 2.5 gm/min.

temperature of crystallization increases with take-up velocity. This result is consistent with the predictions of the model.

The modulus (Figure 7.40), tenacity (Figure 7.41) and elongation to break (Figure 7.42) all exhibited similar numerical values and trends to those reported by Shimizu et al. (1). The modulus and tenacity are slightly lower while the elongation to break was slightly higher, most probably due to the low molecular weight nylon-66 being spun.

## Application of the Model to the Melt Spinning of Polypropylene

The melt spinning model was also applied to polypropylene spun at the conditions given in Table 7.2 by Lu and Spruiell (12). The only changes in the model are those that dealt with the processing parameters and the physical properties of the polymer which are given in Chapter 4.

Figure 7.43 is a comparison of the experimental and predicted diameter profiles for a polypropylene of 178,000 weight average molecular weight. As in the case of nylon-66 the diameters draw down to a value close to the final diameter before the take-up device and this point moves closer to the spinneret with increasing take-up velocity. Figure 7.44 contrasts the predicted and experimental birefringence profiles. The increase in the predicted birefringence is sharper than the experimentally observed rise. This may be a result of the "smearing" of the crystallization process across the radius of the fiber.

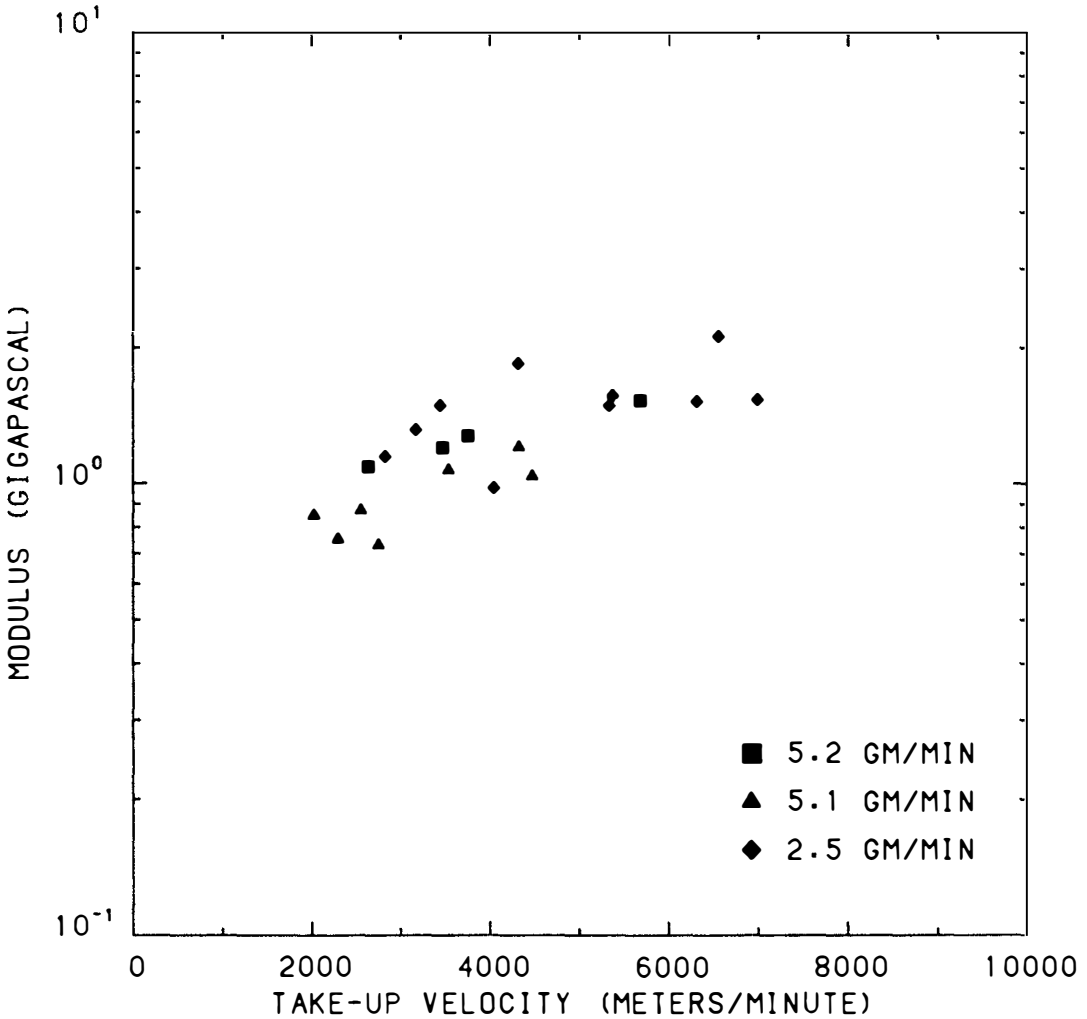


Figure 7.40 Final fiber modulus as a function of spinning speed for nylon-66.

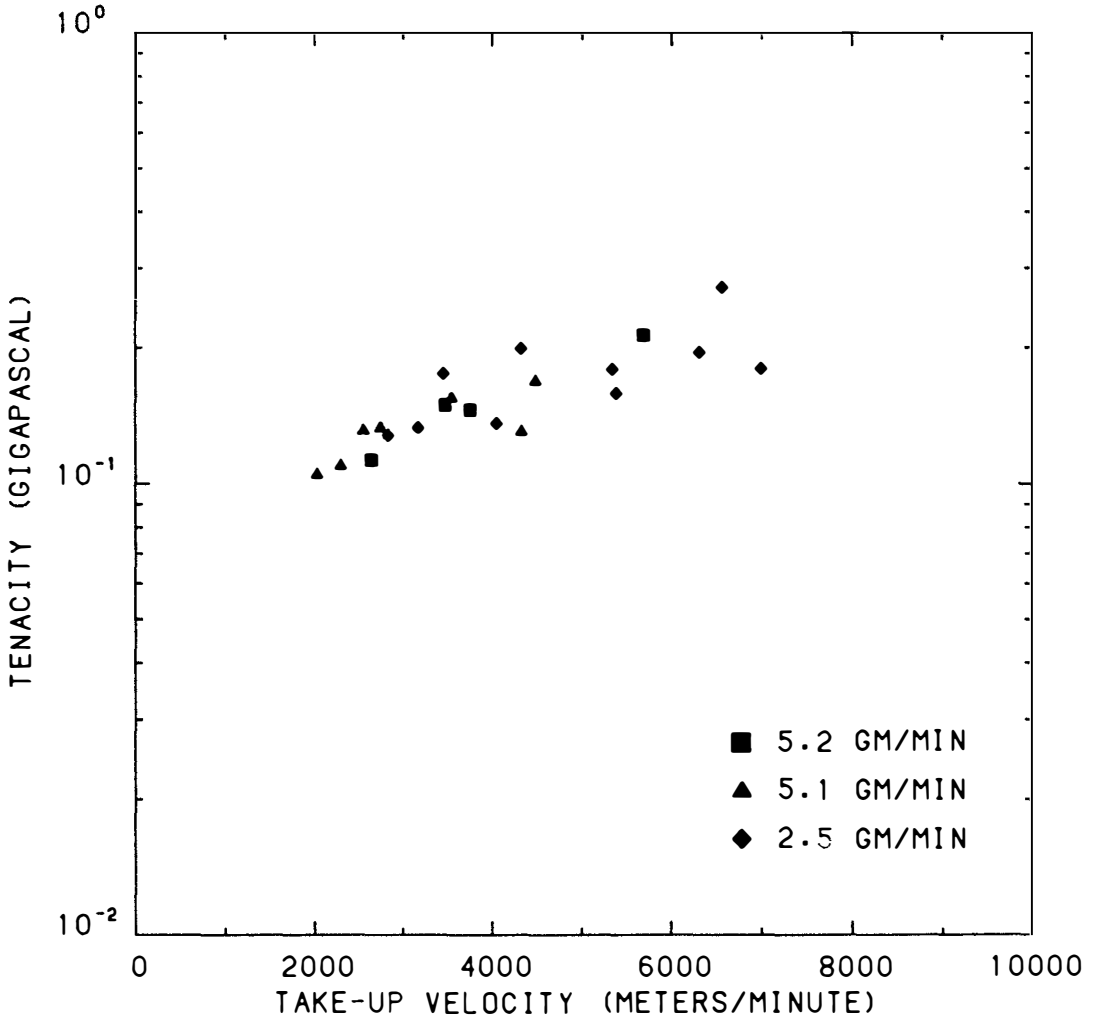


Figure 7.41 Final fiber tenacity as a function of spinning speed for nylon-66.

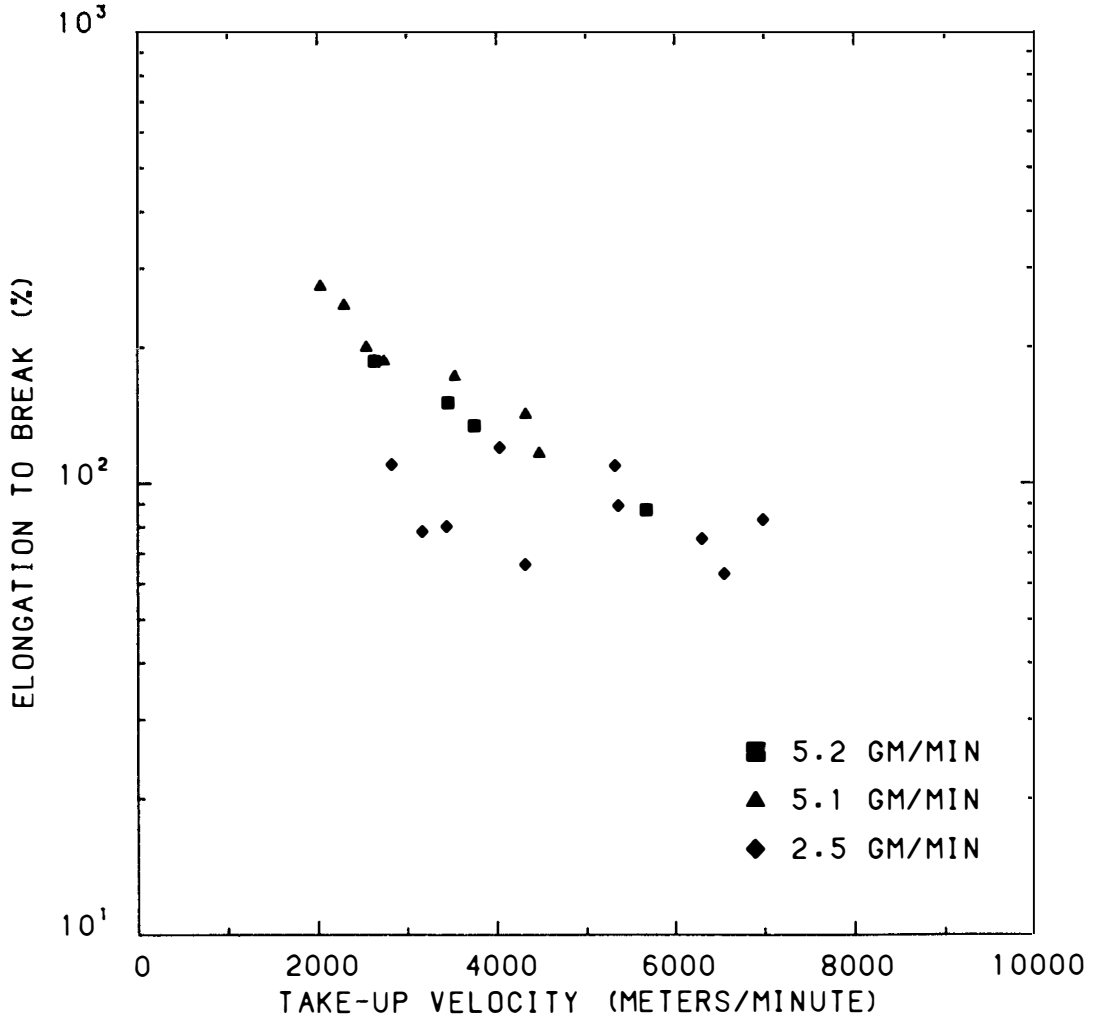


Figure 7.42 Final fiber elongation to break as a function of spinning speed for nylon-66.

Table 7.2 Polypropylene spinning conditions (12).

| | | |
|---|---|---|
| Extrusion temperature | - | 230 °C |
| Spinline length | - | 2.30 meters |
| Mass throughput | - | $2.8 \times 10^{-5}$ kg/sec |
| Die diameter | - | 736 micrometers |
| Take-up velocities | - | 1360 - 5700 m/min |

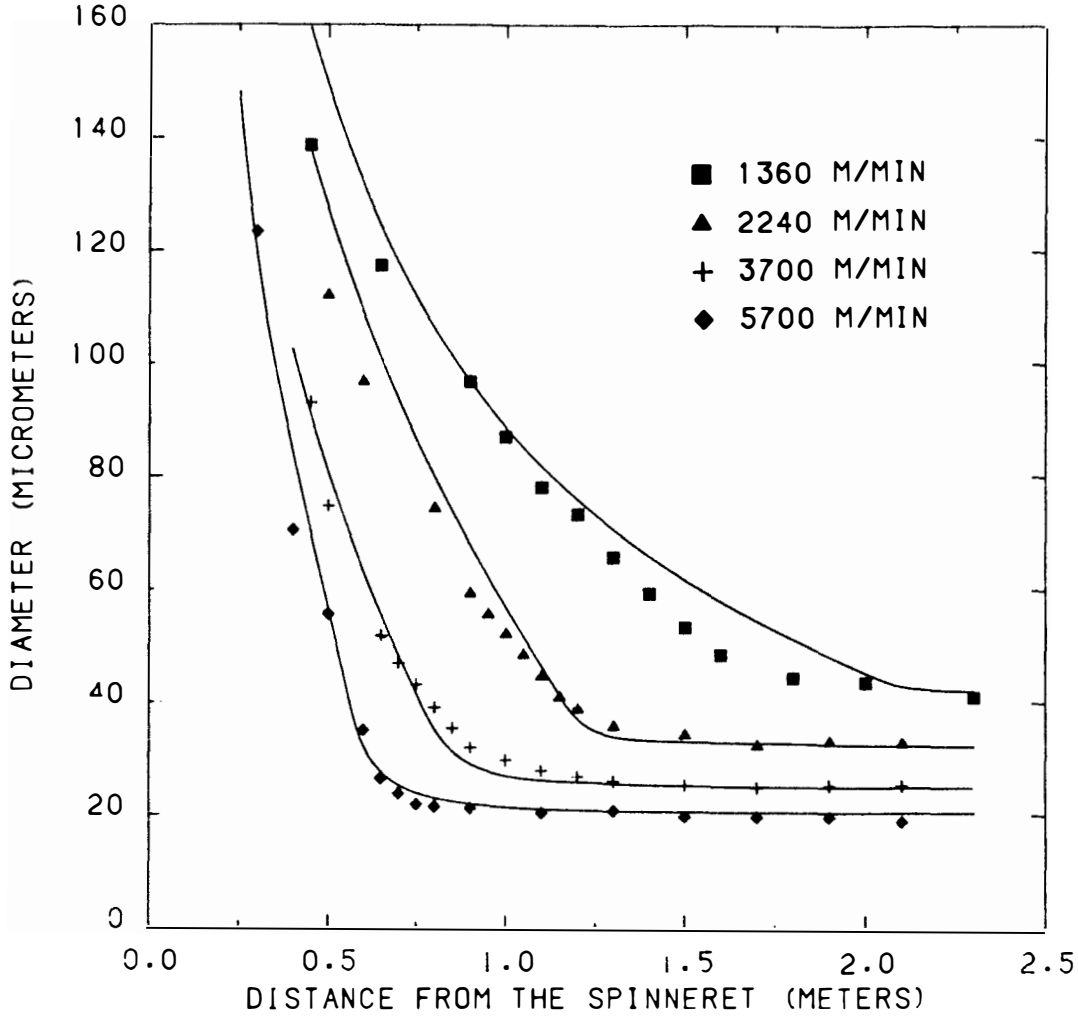


Figure 7.43 Comparison of predicted and experimental diameter profiles for a 178,000 Mw polypropylene with a mass throughput of 1.68 gm/min.

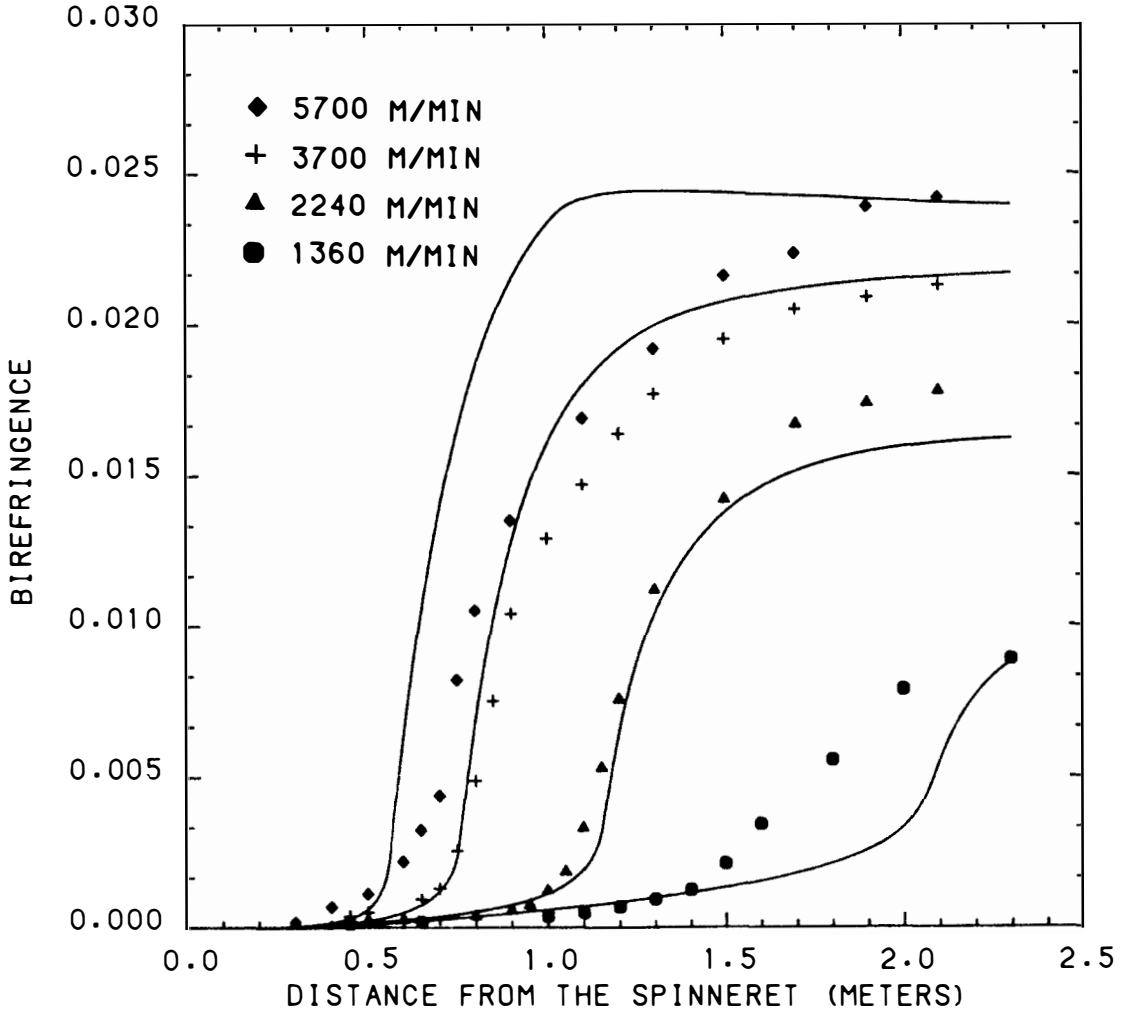


Figure 7.44 Comparison of predicted and experimental birefringence profiles for a 178,000 Mw polypropylene with a mass throughput of 1.68 gm/min.

In the model the crystallization process takes place uniformly within a volume element whereas the analysis of many fibers spun at high speeds indicates significant radial variations. This effect will become more apparent with increasing speed since the the heat transfer ability of the fiber will increase causing larger temperature gradients within the fiber.

The predicted and experimental temperature profiles are compared in Figure 7.45. In all cases the model predicts the appearance of a significant temperature plateau. This plateau appears at higher temperatures and is of a shorter duration with increasing spinning speed. This is a consequence of the higher crystallization rates brought about by the increased molecular orientation. The experimental profiles also indicate these plateaus but they are not as pronounced as those predicted by the model.

Figure 7.46 is a plot of the predicted and experimental temperatures at which the crystallization process is first apparent as a function of spinning speed. The predicted and experimental distances from the spinneret where the crystallization is first apparent at each take-up velocity are compared in Figure 7.47. There is relatively good agreement in both cases. The increase in spinning speed causes the crystallization process to take place at higher temperatures and closer to the spinneret but at the highest speeds there seems to be a decrease in this effect. This results from the decrease in the kinetic rate with increasing temperature. The enhanced molecular orientation is not sufficient to overcome the decrease due to increasing

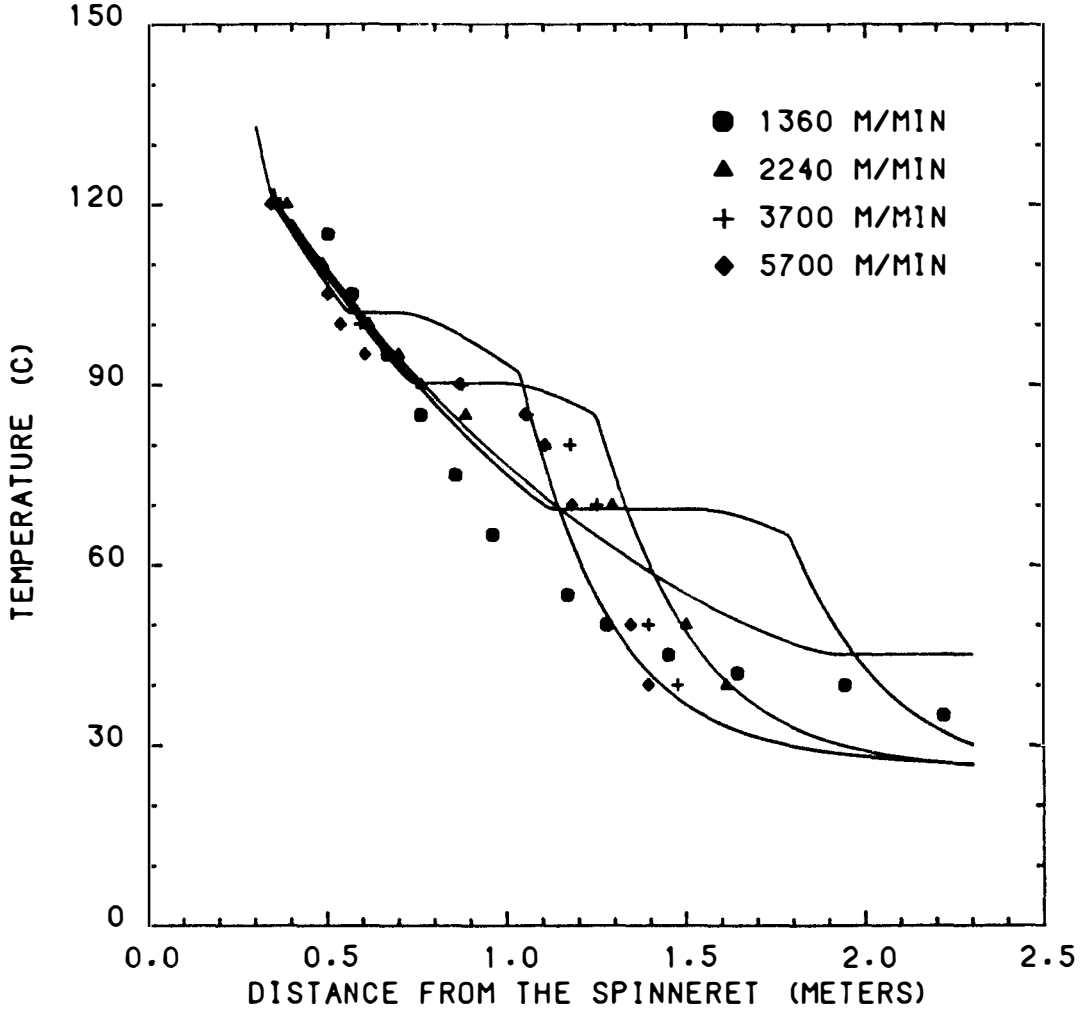


Figure 7.45 Comparison of predicted and experimental temperature profiles for a 178,000 Mw polypropylene with a mass throughput of 1.68 gm/min.

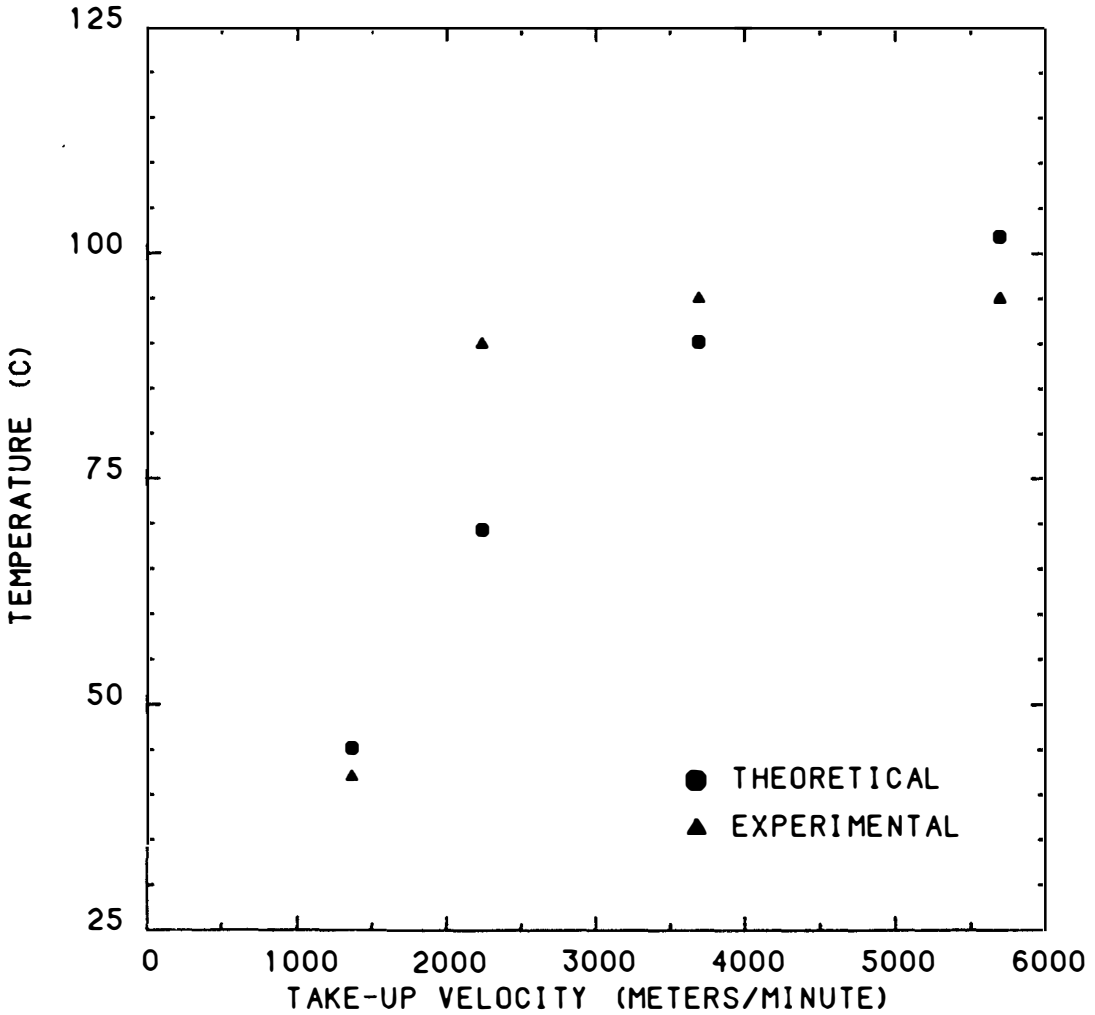


Figure 7.46 Comparison of the predicted and experimental temperatures at which crystallization is first observed for the 178,000 Mw polypropylene.

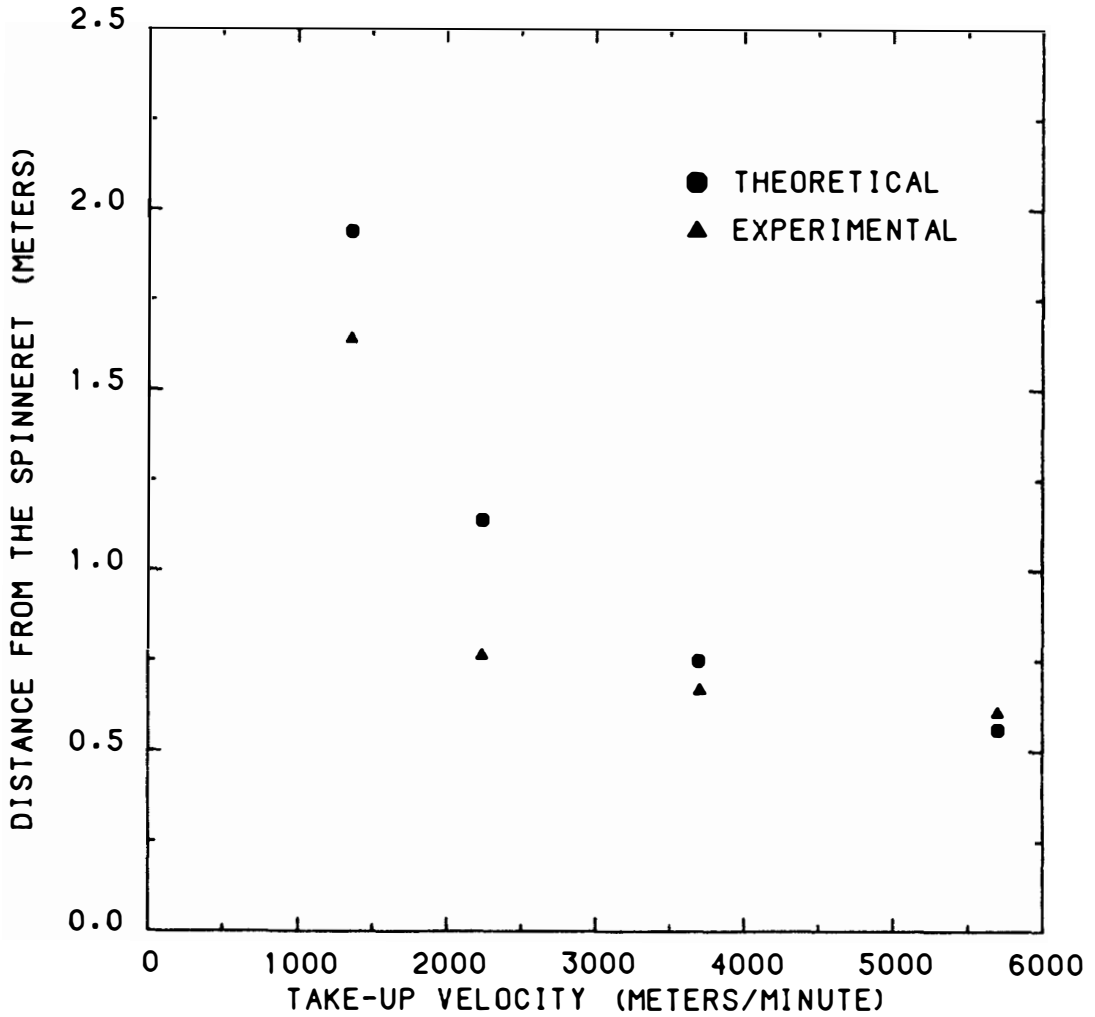


Figure 7.47 Comparison of the predicted and experimental distance from the spinneret at which crystallization is first observed for the 178,000 Mw polypropylene.

temperature. This seems to be the case for spinning speeds above 3000 meters per minute for this polypropylene.

Figure 7.48 is a comparison of the predicted and experimental diameter profiles for a polypropylene of 237,000 weight average molecular weight. The effect of the increase in molecular weight was introduced into the model through the elongational viscosity. Figure 7.49 is a comparison of the predicted and experimental birefringence profiles. As is the case for the lower molecular weight polypropylene the predicted rise is sharper than the observed increase. The predicted and experimental temperature profiles for the higher molecular weight polypropylene (Figure 7.50) are similar to those predicted and observed for the lower molecular weight material.

The model does a very good job in describing the molecular weight effect even though it is only introduced into the elongational viscosity. The effect of molecular weight on the other properties such as modulus, stress optical coefficient, etc. has been ignored yet the model qualitatively and, within reasonable limits, quantitatively predicts the diameter and birefringence profiles.

It is interesting to note that in the temperature profiles for both molecular weight materials there is a considerable amount of difference between the model and experimental profiles after crystallization has occurred yet there is good agreement of the diameter and birefringence profiles over the entire spinline. This behavior can be reconciled by considering that the crystallization process "locks" in the structure at the time it occurs. The strain hardening that takes place prevents any further reduction in the diameter and since a

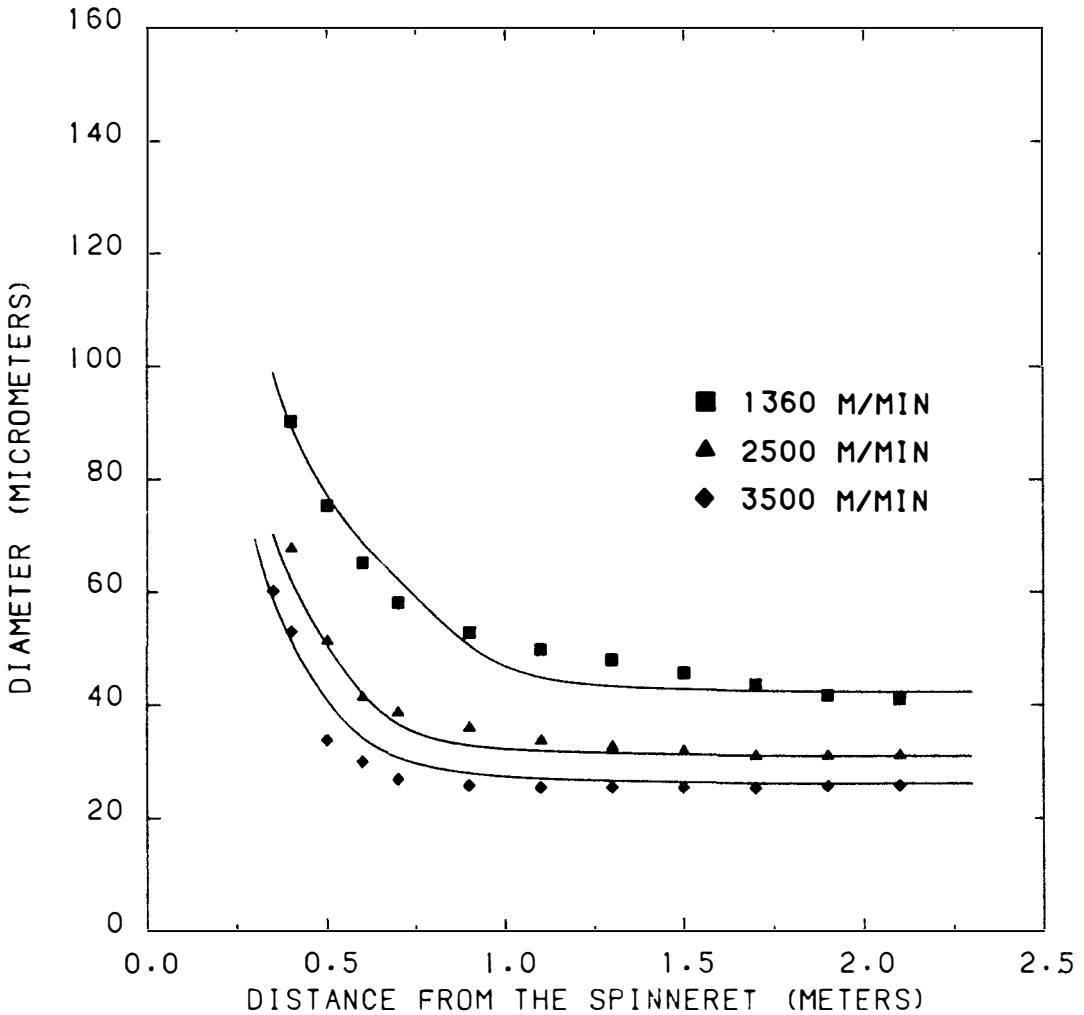


Figure 7.48 Comparison of predicted and experimental diameter profiles for a 237,000 Mw polypropylene with a mass throughput of 1.68 gm/min.

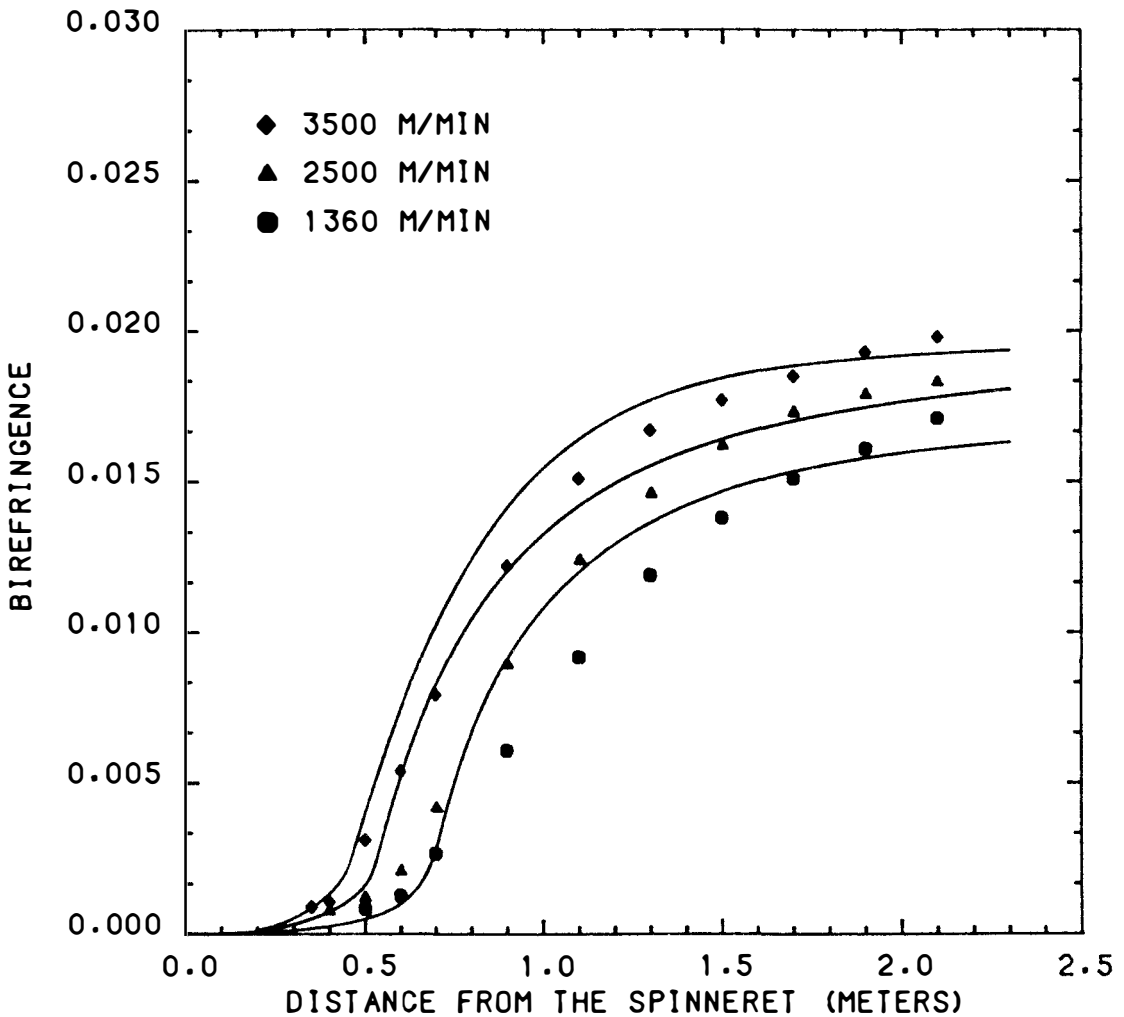


Figure 7.49 Comparison of predicted and experimental birefringence profiles for a 23700 Mw polypropylene with a mass throughput of 1.68 gm/min.

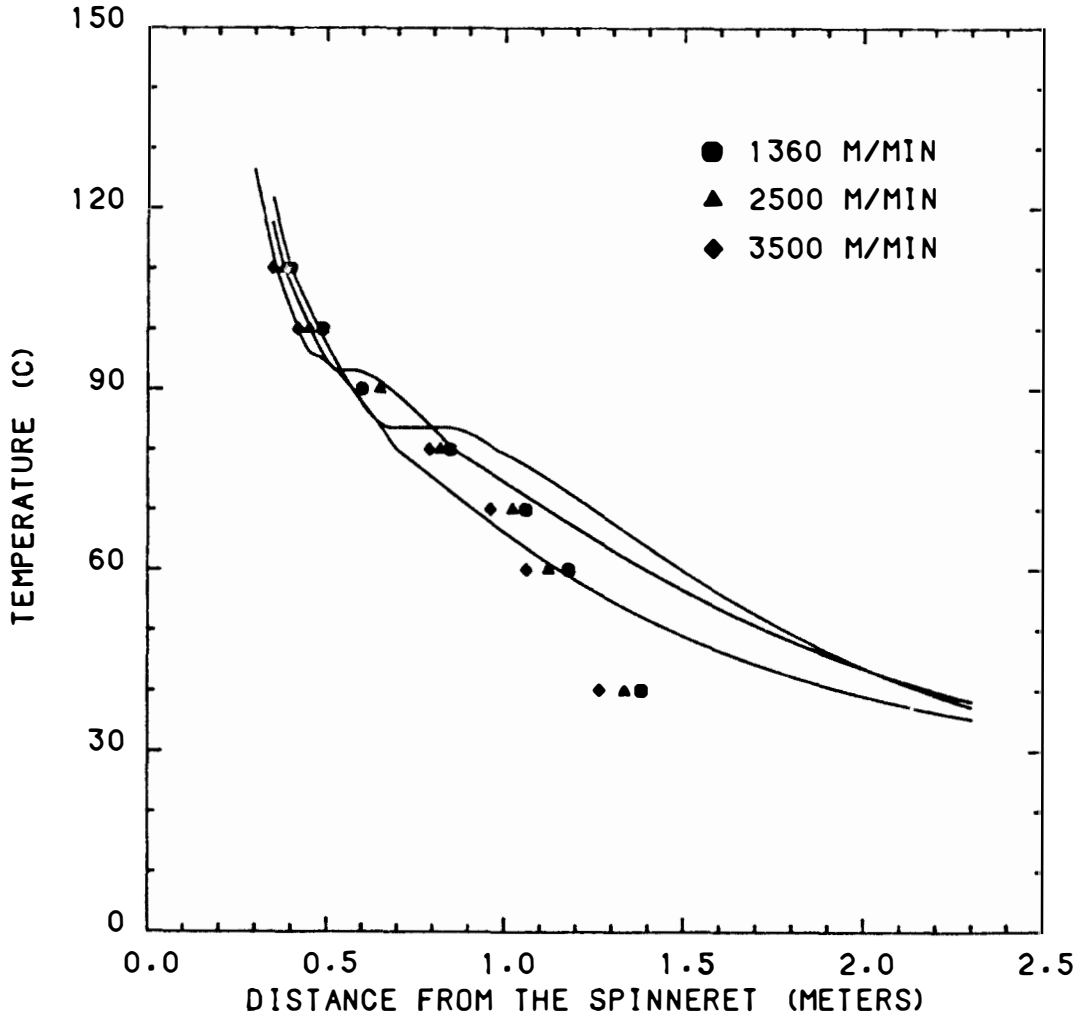


Figure 7.50 Comparison of predicted and experimental temperature profiles for a 237,000 Mw polypropylene with a mass throughput of 1.68 gm/min.

significant amount of the material consists of oriented crystallites there is little change in the birefringence.

The strain hardening in the model is manifest in the crystallinity dependence of the elongational viscosity. The form of this dependence was adapted from the form that was used by Kikutani (106) since there was no other data regarding this interaction available in the literature. The strain hardening is a key aspect in the spinning behavior during crystallization and it is important that there should be some experimental studies to investigate the effect of crystallinity on the physical properties over the wide temperature range found in melt spinning of some commonly used polymers.

In order to evaluate to what extent the molecular weight and its distribution play a role in the crystallization behavior during spinning, there is a need for more information on the variation of the physical properties of the polymer itself along with experimental online studies in which these quantities are fully characterized and carefully controlled.

The model has been applied to the high speed melt spinning of two polymers, nylon-66 and polypropylene. Nylon-66 has a much higher crystallization rate than polypropylene and a lower viscosity at the same temperature. In addition nylon-66 has a glass transition temperature above room temperature while that of polypropylene is well below room temperature. The spinning conditions were also significantly different for the two materials. Nylon-66 was processed at a temperature just above its equilibrium melting temperature while the

extrusion temperature of polypropylene was over 50 degrees above its equilibrium melting temperature.

In the online studies neither material exhibited the necking behavior reported for high speed spinning of PET, although it was observed for nylon-66 spun at very high speeds at low mass throughput and short spinlines. The nylon-66 temperature profiles did not show the plateau regions exhibited by the polypropylenes.

Since the glass transition temperature of polypropylene was well below room temperature it was found that the WLF expression for the temperature dependence was insufficient to describe the elongational viscosity from $T_m$ to $T_g$. A second Arrhenius expression using a larger activation energy was adequate. In the absence of any available data the activation energy above $T_m$ was assumed to be quite low. These are problems which are associated with the material but which have a significant impact on the performance of the model.

In spite of seemingly overwhelming complexities the model developed in this study has demonstrated that it contains the essential features needed to successfully describe, both qualitatively and quantitatively, the high speed melt spinning behavior of nylon-66 and polypropylene.

# CHAPTER 8

## CONCLUSIONS AND RECOMMENDATIONS

A mathematical model has been developed to help interpret the high speed melt spinning behavior of crystallizable polymers. This model includes the effects of inertia, drag and gravity on the dynamics as well as temperature and molecular orientation effects on the crystallization kinetics of the polymer.

This model was applied to the high speed melt spinning of nylon-66 and two different molecular weight polypropylenes, two materials which exhibit very different physical characteristics in the range of processing conditions studied.

The predicted diameter, birefringence and temperature profiles were compared to experimentally obtained profiles. They were qualitatively and reasonably quantitatively in good agreement. The model successfully predicted the effect of molecular weight on the spinning behavior of polypropylene.

The limitations of the model can be traced to two major sources. The first being the assumption of no radial variations which was necessary to reduce the mathematical complexity of the problem. The second is the lack of readily available, reliable data on the variation of various physical properties such as elongational viscosity, densities, modulus, etc. with temperature, molecular weight, molecular weight distributions, crystallinity, etc. for many common polymers.

It is recommended that further refinement and utilization of the model lies in two directions. The first area deals with improvement of the model itself with the application of different constitutive equations, introduction of orientation distributions, development of more accurate and detailed physical property relationships and a methodology of incorporating radial variation into the framework. It would also be useful to develop the model to account for multifilament spinning effects. These effects are of importance in applications to commercial operations.

The second area is the application of the model to the study of the crystallization kinetics in the spinline. The present model holds the promise, abet by trial and error, of being capable of evaluating several critical parameters in the kinetic models by using the melt spinline as an experiment in orientation induced crystallization which can not be duplicated by any other means.

REFERENCES

## REFERENCES


1. Shimizu, J., N. Okui, S. Tamaki, Y. Imai and A. Takaku, Sen-I Gakkaishi, 41, 101 (1985).

2. Chappel, F. P., M. F. Culpin, R. G. Gasden and T. C. Tranter, J. Appl. Chem. (London), 14, 12 (1964).

3. Lecluse, C., "High Speed Spinning of Polyamide 6.6", Rhone-Poulenc Fibers Company Report (1984).

4. Wigotsky, V., Plastics Engineering, 41, 37 (1985).

5. Ishizuka, O. and K. Koyama, Sen-I Gakkaishi, 32, 43 (1976).

6. Ishizuka, O. and K. Koyama, Sen-I Gakkaishi, 32, 49 (1976).

7. Ishizuka, O. and K. Koyama, Polymer, 18, 913 (1977).

8. Ishizuka, O. and K. Koyama, Polym. J., 12, 735 (1980).

9. Shimizu, J., A. Watanabe and K. Toriumi, Sen-I Gakkaishi, 30, 35 (1974).

10. Shimizu, J., K. Toriumi and Y. Imai, Sen-I Gakkaishi, 33, 255 (1977).

11. Shimizu, J., N. Okui and Y. Imai, Sen-I Gakkaishi, 35, 405 (1979).

12. Lu, F. and J. E. Spruiell, unpublished data.

13. Carothers, W. H. and J. W. Hill, J. Amer. Chem. Soc., 54, 1579 (1932).

14. Ziabicki, A., Kolloid Z., 175, 14 (1961).

15. Ziabicki, A. and K. Kedzierska, Kolloid Z., 171, 51 (1960).

16. Ziabicki, A. and K. Kedzierska, Kolloid Z., 171, 111 (1960).

17. Sakiadis, B. C., Amer. Inst. Chem. Eng. J., 7, 467 (1961).

18. Andrews, E. H. in "Fiber Structure", J. W. S. Hearle and R. H. Peters, Eds., Butterworth and the Textile Institute, Manchester, London (1962).

19. Aoki, H., Y. Suzuki and A. Ishimoto, unpublished work.

20. Sano, Y. and K.Orii, Sen-I Gakkaishi, 24, 212 (1968).

21. Hamana, I., M. Matsui and S. Kato, Melliand Textil, 50, 382 (1969).

22. Kwon, Y. D. and P. C. Prevorsek, J. Appl. Polym. Sci., 23, 3105 (1979).

23. Gould, J. and F. S. Smith, J. Text. Inst., 1, 38 (1980).

24. Han, C. D. and R. R. Lamonte, Trans. Soc. Rheo., 16, 447 (1972).

25. Han, C. D., R. R. Lamonte and T. Shah, J. Appl. Polym. Sci., 16, 3307 (1972).

26. Lamonte, R. R. and C. D. Han, J. Appl. Polym. Sci., 16, 3285 (1972).

27. Kase, S. and T. Matsuo, J. Text. Mach. Soc. Japan, 18, 188 (1965).

28. Kase, S. and T. Matsuo, J. Polym. Sci., A3, 2541 (1965).

29. Kase, S. and T. Matsuo, J. Appl. Polym. Sci., 11, 251 (1967).

30. Ishibashi, T., K. Aoki and T. Ishii, J. Appl. Polym. Sci., 14, 1597 (1970).

31. Hill, J. W. and J. A. Cuculo, J. Appl. Polym. Sci., 18, 2569 (1974).

32. Chen, I. J., G. E. Hagler, L. E. Abbott, D. C. Bogue and J. L. White, Trans. Soc. Rheo., 16, 473 (1972).

33. Spearot, J. A. and A. B. Metzner, Trans. Soc. Rheo., 16, 495 (1972).

34. Acierno, D., J. N. Dalton, J. M. Rodriguez and J. L. White, J. Appl. Polym. Sci., 15, 2395 (1971).

35. Matovich, M. A. and J. R. A. Pearson, Ind. Eng. Chem. Fund., 8, 512 (1969).

36. White, J. L., J. Appl. Polym. Sci., 8, 2339 (1964).

37. Larson, R. G., J. Rheo., 27, 475 (1983).

38. Andrews, E. H., Brit. J. Appl. Phys., 10, 39 (1959).

39. Wilhelm, V. G., Kolloid. Z.-Z. Polym., 208, 97 (1966).

40. Ziabicki, A., and K. Kedzierska, Chemie Stosowana, 3, 151 (1960).

41. Barnett, T. R., J. Amer. Chem. Soc. Div. Polym. Chem. Preprints, 7, 691 (1966).

42. Copley, M., N. H. Chamberlain and K. W. Hiller, J. Amer. Chem. Soc. Div. Polym. Chem. Preprints, 7, 679 (1966).

43. Morrison, M. E., Amer. Inst. Chem. Eng. J., 16, 57 (1970).

44. Nakamura, K., T. Watanabe, K. Katayama and T. Amano, J. Appl. Polym. Sci., 16, 1077 (1972).

45. Glicksman, L. R., Glass Technology, 9, 131 (1968).

46. Mueller, A. C., Trans. Amer. Inst. Chem. Eng., 38, 613 (1942).

47. Roberts, J. K., "Heat and Thermodynamics", Blackie and Sons, London (1940).

48. Sano, Y. and S. Nishikawa, Kagaku Kogaku, 28, 275 (1964).

49. Sano, Y. and N. Vamada, Kagaku Kogaku, 30, 997 (1966).

50. Wanger, W. H. and V. G. Fox, "Man-made Fiber Tech. Part 1", Symp. at 7th National Meeting, Amer. Inst. Chem Eng., Atlantic City, New Jersey, August (1971).

51. Ziabicki, A., Appl. Polym. Symp., 6, 1 (1967).

52. Ziabicki, A. in "Man-made Fibers", H. F. Mark, S. M. Atlas and E. Cernia, Eds., Interscience, New York (1967).

53. Nakamura, K., K. Katayama and T. Amano, J. Appl. Polym. Sci., 17, 1031 (1973).

54. Nakamura, K., T. Watanabe, T. Amano and K. Katayama, J. Appl. Polym. Sci., 18, 615 (1974).

55. Abbott, L. E. and J. L. White, Appl. Polym. Symp., 20 (1973).

56. Abhiraman, A. S., J. Polym. Sci., Polym. Phys. Ed., 21, 583 (1983).

57. Krigbaum, W. R. and R. J. Roe, J. Polym. Sci., 2, 4391 (1964).

58. Ziabicki, A., Colloid and Polym. Sci., 252, 207 (1974).

59. Hearle, J. W. S., J. Text. Inst., 53, 449 (1962).

60. Keller, A., J. Polym. Sci., 15, 13 (1955).

61. Vonk, C. G., Kolloid Z., 206,121 (1965).

62. Kruger, D. and G. S. Y. Yeh, J. Macromol. Sci., B6, 431 (1972).

63. Ziabicki, A., J. Appl. Polym. Sci., 2, 24 (1959).

64. Ziabicki, A., and K. Kedzierska, J. Appl. Polym. Sci., 2, 14 (1959).

65. Ziabicki, A. and K. Kedzierska, J. Appl. Polym. Sci., 6, 111 (1962).

66. Furukawa, J., T. Kitao, S. Yamashita and S. Ohaya, J. Polym. Sci., 9, 299 (1971).

67. Kitao, T., S. Ohaya, J. Furukawa and S. Yamashita, J. Polym. Sci, Polym. Phys. Ed., 11, 1091 (1973).

68. Spruiell, J. E. and J. L. White, Polym. Eng. Sci., 15, 660 (1975).

69. Katayama, K., T. Amano and K. Nakamura, Kolloid Z.-Z. Polym., 226, 125 (1967).

70. Dees, J. R., Ph.D. dissertation, University of Tennessee-Knoxville, June (1974).

71. Dees, J. R. and J. E. Spruiell, J. Appl. Polym. Sci., 18, 1053 (1974).

72. Nadella, H. P., M.S. thesis, University of Tennessee-Knoxville, (1976).

73. Nadella, H. P., H. Henson, J. E. Spruiell and J. L. White, J. Appl. Polym. Sci., 21, 3003 (1977).

74. Bankar, V., Ph.D. dissertation, University of Tennessee-Knoxville, (1976).

75. Bankar, V., J. E. Spruiell and J. L. White, J. Appl. Polym. Sci., 21, 2341 (1977).

76. Khokhani, M. J., M.S. thesis, University of Tennessee-Knoxville, (1975).

77. Aggarwal, S. L., G. P. Tilley and O. J. Sweeting, J. Polym. Sci., 51, 551 (1961).

78. Ishikawa, K., J. Polym. Sci., 7, 1259 (1969).

79. White, J. L., K. S. Dharod and E. S. Clark, J. Appl. Polym. Sci.,, 18, 2539 (1974).

80. Southern, J. H., N. Weeks, R. S. Porter and R. G. Crystal, Die Molekularie Chemie, 162, 19 (1972).

81. Keller, A. and M. J. Machin, J. Macromol. Sci. - Phys., B1, 41 (1967).

82. Fung, P. Y. F. and S. H. Carr, J. Macrol. Sci., B6, 621 (1972).

83. Binsbergen, F. L., Nature, 211, 516 (1966).

84. Samuels, R. J., J. Polym. Sci., 6, 2021 (1968).

85. Garber, C. and E. S. Clark, J. Macromol. Sci. - Phys., B6, 499 (1970).

86. Keller, A., J. Polym. Sci., 21, 363 (1958).

87. Hamana, I.,M. Matsui and S. Kato, Melliand Textil., 5, 409 (1969).

88. Huisman, R. and H. M. Heuval, J. Appl. Polym. Sci., 22, 943 (1978).

89. Hagler, G. E., Ph.D. dissertation, University of Tennessee-Knoxville, (1972).

90. Keller, A., J. Polym. Sci., 17, 35 (1955).

91. Kobayashi, K. in "Polymer Single Crystals", P. H. Geil, Ed., Interscience, New York (1963).

92. Nishiumi, S., J. Text. Mach. Soc. Japan, 18, 174 (1965).

93. Anderson, P. G. and S.H. Carr, J. Mater. Sci., 10, 870 (1975).

94. Clark, E. S., Bull. Amer. Phys. Soc., March (1970).

95. Clark, E. S. and J. E. Spruiell, Polym. Eng. Sci., 16, 176 (1976).

96. Sprague, B. S., J. Macromol. Sci. - Phys., B7, 157 (1973).

97. Prastaro, A. and P. Parrini, Text. Res. J., Feb., 118 (1975).

98. Gagon, D. K. and M. M. Denn, Polym. Eng. Sci., 21, 844 (1981).

99. George, H. H., unpublished data.

100. George, H. H., Polym. Eng. Sci., 22, 292 (1982).

101. Yasuda, H., H. Sugiyama and H. Yanagawa, Sen-I Gakkaishi, 35, 370 (1979).

102. Yasuda, H., H. Sugiyama and S. Hayashi, Sen-I Gakkaishi, 40, 227 (1984).

103. Yasuda, H., H. Sugiyama and S. Hayashi, Sen-I Gakkaishi, 40, 488 (1984).

104. Dutta, A., and V. M. Nadkarni, Text. Res. J., Jan., 35 (1984).

105. Shenoy, A. V. and V. M. Nadkarni, Text. Res. J., Nov., 778 (1984).

106. Kikutani, T., PhD Thesis, Tokyo Institute of Technology (1982).

107. Bai, C. C., PhD Thesis, University of Tennessee - Knoxville (1985).

108. Shimizu, J., N. Okui and Y. Imai, Sen-I Gakkaishi, 36, 166 (1980).

109. Shimizu, J., N. Okui, A. Kaneko and K. Toriumi, Sen-I Gakkaishi, 34, 65 (1978).

110. Shimizu, J., N. Okui, A. Kaneko and K. Toriumi, Sen-I Gakkaishi, 34, 93 (1978).

111. Shimizu, J., N. Okui and T. Kikutani, Sen-I Gakkaishi, 37, 135 (1981).

112. Shimizu, J., N. Okui, T. Kikutani, A. Ono and A. Takaku, Sen-I Gakkaishi, 37, 143 (1981).

113. Shimizu, J., Sen-I Gakkaishi, 38, 499 (1982).

114. Shimizu, J., N. Okui, Y. Imai, S. Nishide and A. Takaku, J. Polym. Sci., Polym. Phys. Ed., 21, 275 (1983).

115. Shimizu, J. and N. Okui, Sen-I Gakkaishi, 39, 445 (1983).

116. Shimizu, J., T. Kikutani, A. Takaku and N. Okui, Sen-I Gakkaishi, 40, 63 (1984).

117. Shimizu, J., T. Kikutani, A. Takaku and N. Okui, Sen-I Gakkaishi, 40, 177 (1984).

118. George, H. H., A. Holt and A. Buckley, Polym. Eng. Sci., 23, 95 (1983).

119. Bragato, G. and G. Gianotti, Eur. Polym. J., 19, 795 (1983).

120. Bragato, G. and G. Gianotti, Eur. Polym. J., 19, 803 (1983).

121. Colclough, M. L. and R. Baker, J. Mater. Sci., 13, 2531, (1978).

122. Ziabicki, A., Sen-I Gakkaishi, 38, 409 (1982).

123. Fisher, J. C., J. H. Hollomon and D. J. Turnbull, J. Appl. Phys., 19, 775 (1948).

124. Becker, R. and W. Doring, Ann. d. Physik., 24, 719 (1935).

125. Mandelkern, L., F. A. Quinn and P. J. Flory, J. Appl. Phys., 25, 830 (1954).

126. Mandelkern, L., "Crystallization of Polymers", McGraw-Hill, New York (1964).

127. Devoy, C. and L. Mandelkern, J. Chem. Phys., 52, 3827 (1970).

128. Turnbull, D. J., J. Chem. Phys., 18, 198 (1950).

129. Cormia, R. L., F. P. Price and D. J. Turnbull, J. Chem. Phys., 37, 1333 (1962).

130. Avrami, M., J. Chem. Phys, 7, 1103 (1939).

131. Avrami, M., J. Chem. Phys., 8, 212 (1940).

132. Avrami, M., J. Chem. Phys., 9, 177 (1941).

133. Johnson, W. A. and R. F. Mehl, Trans. Amer. Inst. Min. Met. Eng., 135, 416 (1939).

134. Evans, R. U., Trans. Faraday Soc., 41, 365 (1945).

135. Kolmogoroff, A. N., Izvestiya Akad. Nack. SSSR, Ser. Math., 1, 355 (1937).

136. Mandelkern, L., J. Appl. Phys., 26, 443 (1955).

137. Ziabicki, A., J. Chem. Phys., 48, 4374 (1968).

138. Gornick, F. and L. Mandelkern, J. Appl.Phys., 33, 907 (1962).

139. Burns, J. R. and D. Turnbull, J. Appl. Phys., 37,4021 (1966).

140. Ziabicki, A., Colloid and Polym. Sci., 252, 433 (1974).

141. Ziabicki, A., J. Chem. Phys., 48, 4368 (1968).

142. Ziabicki, A., Polimery, 12, 405 (1967).

143. Takayanagi, M. and T. Kusumoto, Kogyo Kogaku Zasshi, 62, 587 (1959).

144. Katz, J. R., Kolloid Z., 36, 300 (1925).

145. Gent, A. N., Trans. Faraday Soc., 50, 521 (1954).

146. Mitchell, J. C., Polymer, 8, 369 (1967).

147. Rabesiaka, J. and A. J. Kovacs, J. Appl. Phys., 32, 2314 (1961).

148. McCord, D. E. and J. E. Spruiell, Trans. Soc. Rheo., 16, 535 (1972).

149. Mackley, M. R. and A. Keller, Polymer, 14, 16 (1973).

150. Kobayashi, K. and T. Nagasawa, "Formation of Fibers and Development of Their Structure", edited by the Soc. Fiber Sci. and Tech., Japan, Kagaku Dojin, Kyoto (1969).

151. Kobayashi, K. and T. Nagasawa, J. Macromol. Sci. - Phys., B4, 331 (1970).

152. Smith, K. J., A. Greene and A. Ciferri, Kolloid Z., 194, 49 (1964).

153. Yamamoto, M. and J. L. White, J. Polym. Sci., 9, 1399 (1971).

154. Jarecki, L., Ph.D. dissertation, Inst. Fund. Tech. Res. Report 29, (1974).

155. Ziabicki, A., Polimery, 18, 615 (1973).

156. Andrews, E. H., Proc. Roy. Soc. London, A277, 462 (1964).

157. Ziabicki, A., "Fundamentals of Fiber Formation", Interscience, New York (1976).

158. Carothers, W. H. (to E. I. du Pont de Nemours Co.) U. S. Patent 2,130,523 (September 20, 1938).

159. Peterson, W. R. (to E. I. du Pont de Nemours Co.) U. S. Patent 2,174,527 (October 3, 1939).

160. Graves, G. D. (to E. I. du Pont de Nemours Co.) U. S. Patent 2,289,774 (July 14, 1942).

161. Johnson, W. G. (to E. I. du Ponr de Nemours Co.) U. S. Patent 3,491,177 (January 20, 1970).

162. Bannerman, D. G. and E. E. Magat in "Polymer Processing", C. E. Schlidknecht, Ed., Interscience, New York (1956).

163. Kleinert, C. J. and F. F. Hoy in "Manufacture of Plastics", W. M. Smith, Ed., Reinhold, New York (1964).

164. Hoppf, H. in "Man-made Fibers, Vol. 2", H. F. Mark, S. M. Atlas and E. Cernia, Eds., Interscience, New York (1968).

165. Kohan, M. I. in "Nylon Plastics", Interscience, New York (1973).

166. Lum, F. G. (to Califorina Research Corp.) U. S. Patent 2,987,506 (June 6, 1961).

167. Taul, H. and F. Wiloth (to Vereinigte Glanzstoff-Fabriken A.-G.) U. S. Patent 3,027,355 (March 27, 1962).

168. Anon., Chem. Eng. News, 43, 49 (June 28, 1965).

169. Sovereign, G. W. (to Monsanto Co.) U. S. Patent 3,218,297 (November 16, 1965).

170. Brill, R., Z. Physik. Chem., B53, 61 (1943).

171. Moncrieff, R. W. in "Man-made Fibers, Vol. 2", H. F. Mark, S. M. Atlas and E. Cernia, Eds., Interscience, New York (1968).

172. Sbrolli, W. in "Man-made Fibers, Vol. 2", H. F. Mark, S. M. Atlas and E. Cernia, Eds., Interscience, New York (1968).

173. Taylor, G. B., J. Amer. Chem. Soc., 69, 635 (1947).

174. Hoppf, H., Kunstsoffe, 42, 423 (1952).

175. Goldfarb, I. J. and A. C. Meeks, AFML-TR-68-347, Part 1 (1969).

176. Bruck, S.D., Polymer, 7, 231 (1966).

177. Bailey, W. J. and C. N. Bird, J. Org. Chem., 23, 996 (1958).

178. Strauss, S. and L. A. Wall, J. Res. Nat. Bur. Std., 60, 39 (1958).

179. Strauss, S. and L. A. Wall, J. Res. Nat. Bur. Std., 63A, 269 (1959).

180. Dachs, K. and E. Schwartz, Angew. Chem. Int. Ed. Eng., 1, 430 (1962).

181. Flory, P. J. (to E.I. du Pont de Nemours Co.) U. S. Patent 2,244,192 (June 4, 1941).

182. Kamerbeek, B., G. H. Kroes and W. Grolle in "Thermal Degradation of Polymers", S.C.I. Monograph No. 13, London (1961).

183. Meacock, G., J. Appl. Chem., 4, 172 (1954).

184. Indest, H. (to Vereinigte Glanzstoff-Fabriken A.-G.) U. S. Patent 3,121,763 (February 18, 1964).

185. Valko, E. I. and C. K. Chiklis, J. Appl. Polym. Sci., 9, 2855 (1965).

186. Stephenson, C. V., B. C. Moses and W. S. Wilcox, J. Polym. Sci., 55, 451 (1961).

187. Stephenson, C. V., B. C. Moses, R. E. Burks, W. C. Coburn Jr. and W. S. Wilcox, J. Polym. Sci., 55, 465 (1961).

188. Stephenson, C. V., J. C. Lacey Jr. and W. S. Wilcox, J. Polym. Sci., 55, 477 (1961).

189. Taylor, H. A., W. C. Tincher and W. F. Hammer, J. Appl. Polym. Sci., 14, 141 (1970).

190. Anton, A., J. Appl. Polym. Sci., 9, 1631 (1965).

191. Whinfield, J. R., Nature, 158, 930 (1946).

192. Slichter, W. P., J. Polym. Sci., 35, 77 (1959).

193. Greco, R. and L. Nicolais, Polymer, 17, 1049 (1976).

194. Bunn, C. W. and E. V. Garner, Proc. Roy. Soc., A189, 39 (1947).

195. Heyman, E., Soc. Plast. Eng. J., Oct., 37 (1967).

196. Kline, D. E., J. Polym. Sci, 50, 441 (1961).

197. Schaefgen, J. R., J. Polym. Sci., 38, 549 (1959).

198. Rybnikar, F., Chem. Listy, 52, 1042 (1958).

199. Kirshenbaum, I., J. Polym. Sci., 3, 1869 (1965).

200. Wunderlich, B., Polym. Eng. Sci., 18, 431 (1978).

201. Dole, M. and B. Wunderlich, Die Macromol. Chem., 34, 29 (1959).

202. Dole, M., Adv. Polym. Sci., 2, 221 (1960).

203. Trifan. D. S. and J. F. Terenzi, J. Polym. Sci., 28, 443 (1958).

204. Cannon, C. G., Spectrochim. Acta, 16, 302 (1960).

205. Starkweather, H. W., Jr., unpublished data.

206. Cannon, C. G., F. P. Chappel and J. I. Tidmarsh, J. Text. Inst., 54, 210 (1963).

207. Stein, R. S. in "Newer Methods in Polymer Characterization", B. Ke, Ed., Interscience, New York (1964).

208. Simpson, P. G., J. H. Southern and R. L. Ballman. Text. Res. J., Feb., 97 (1981).

209. Fuller, C. S. and C. J. Frosch, J. Amer. Chem. Soc., 61, 2575 (1939).

210. Keller, A. and A. Marradudin, J. Phys. Chem. Solids, 2, 301 (1957).

211. Brill, R., J. Prakt. Chem., 161, 449 (1942).

212. Baker, W. O. in "Advancing Fronts in Chemistry: High Polymers", S. B. Twiss, Ed., Reinhold, New York (1945).

213. Allen, P. W., Text. Res. J., 22, 1178 (1952).

214. Savolainen, A., J. Polym. Sci., Symp., 42, 885 (1973).

215. Magill, J. H., Polymer, 2, 221 (1961).

216. Koenig, J. L. and M. C. Agboatwalla, J. Macrolmol. Sci., B2, 391 (1968).

217. Dreyfuss, P. and A. Keller, J. Macromol. Sci., B4, 811 (1970).

218. Dismore, P. F. and W. O. Statton, J. Polym. Sci., 13, 133 (1966).

219. Dreyfuss, P., A. Keller and F. M. Willmouth, J. Polym. Sci., 10, 857 (1972).

220. Atkins, E. D. T., A. Keller and D. M. Sadler, J. Polym. Sci., 10, 863 (1972).

221. Cannon, C. G. and P. H. Harris, J. Macromol. Sci., B3, 357 (1969).

222. Khoury, F., J. Polym. Sci., 33, 389 (1958).

223. Mann, J. and L. Roldan-Gonzalez, J. Polym. Sci., 60, 1 (1962).

224. Magill, J. H., J. Polym. Sci, 4, 243 (1966).

225. Barriault, R. J. and L. F. Gronholz, J. Polym. Sci., 18, 393 (1955).

226. Lindegren, C. R., J. Polym. Sci., 50, 181 (1961).

227. Jones, C. R. and J. Porter, J. Text. Inst., 45, 498 (1956).

228. Wilholt, R. C. and M. Dole, J. Chem. Phys., 57, 14 (1953).

229. Adams, N., J. Text. Inst, 45, 530 (1956).

230. Starkweather, H. W., Jr., J. Appl. Polym. Sci., 2, 129 (1969).

231. Starkweather, H. W., Jr., J. Macromol. Sci. - Phys., B3, 727 (1969).

232. Quistwater, J. M. R. and B. A. Dunell, J. Appl. Polym. Sci.,1, 267 (1959).

233. Smith, E. G., Polymer, 17, 761 (1976).

234. Reimschuessel, H. K., J. Polym. Sci., Polym. Chem. Ed., 16, 1229 (1978).

235. McLaren, J. V., Polymer, 4, 175 (1963).

236. Hunt, D. G., Polymer, 21, 495 (1980).

237. Bird, R. B., W. E. Stewart and E. N. Lightfoot, "Transport Phenomena", John Wiley & Sons, New York (1960).

238. Han, C. D., "Rheology in Polymer Processing", Academic Press, New York (1976).

239. Welty, J. R., C. E. Wicks and R. E. Wilson, "Fundamentals of Momentum, Heat and Mass Transfer", John Wiley & Sons, New York (1969).

240. Schule, E. C. in "Enc. of Polym. Sci. and Tech.", 10, 557 (1969).

241. Starkweather, H. W., Jr. and G. A. Jones, J. Polym. Sci, Polym. Phys. Ed., 19, 467 (1981).

242. Danford, M., M.S. thesis, University of Tennessee-Knoxville, (1976).

243. Frank, F. P., "Polypropylene", Gordon and Breach Science Publishers, New York (1968).

244. Newman, S., J. Polym. Sci., 47, 111 (1960).

245. Minoshima, W., M.S. thesis, University of Tennessee-Knoxville, (1978).

246. Wilkinson, R. W. and M. Dole, J. Polym. Sci., 59, 1089 (1962).

247. Reding, F. P., J. Polym. Sci., 32, 487 (1958).

248. Oda, K., J. L. White and E. S. Clark, Polym. Eng. Sci., 18, 53 (1978).

249. Samuels, R. J., J. Polym. Sci., A3, 1741 (1965).

250. Samuels, R. J., J. Polym. Sci., A2, 1101 (1968).

251. Natta, G., M. Peraldo and G. Allegra, Makromol. Chem., 75, 215 (1964).

252. Magill, J. H., Polymer, 3, 35 (1962).

253. Speckhart, F. H. and W. L. Green, "A Guide to using CSMP - The Continuous System Modeling Program", Prentice-Hall, Inc., Englewood Cliffs, New Jersey (1976).

254. Wilchinsky, Z. W., J. Appl. Phys., 30, 792 (1959).

255. Wilchinsky, Z. W., J. Appl. Phys., 31, 1969 (1960).

256. Cullity, B. D., "Elements of X-Ray Diffraction", 2nd Ed., Addison-Wesley Publishing Company, Inc., Reading, Mass. (1978).

# APPENDIXES

APPENDIX A

CSMP program for nylon-66 melt spinning.

```
// blue job ,zieminski,group=j41241,user=p92378,
//  password =     ,time=5,region=256k
/*route print decfile
//stepl exec csmp3
//sysin dd *
title nylon-66 melt spinning simulation
initial
constant pi=3.1415926,g=980.,dna0=0.090,c1=6.85e-5,c2=0.259,c3=0.167
constant c4=3.31e-17,c5=-2.7725887,c6=0.085,c7=7548.,c8=2.6e4
constant delh=45.0,cop=1.3e-10,c11=-8.86,c12=4.605,tw=42.,c13=2.
constant tmax=150.,do=80.,tm=264.,rmax=1.64,tg=58.,n=1.,thi=0.45
constant d0=0.0635,t0=275.,ta=25.,mn=12000.,w0=2.5
constant rhoa=6.62e-5,mu=2.8e-4,vy=0.0
constant frhe0=33.7
function amod=(15.,210.),(33.,200.),(48.,200.),(63.,196.),(76.,179),..
             (84,163.),(93.,145.),(100.,124.),(107.,108.),        ...
             (111.,98.5),(116.,87.8),(121.,80.1),(128.,71.4),     ...
             (136.,65.2),(141.,59.4),(150.,56.8),(155.,51.8),     ...
             (160.,46.1),(167.,42.2),(174.,36.7),(179.,33.5),     ...
             (185.,30.5),(192.,27.9),(200.,20.4),(206.,23.2),     ...
             (213.,21.7),(218.,19.8),(224.,18.5),(231.,16.8),     ...
             (237.,15.0),(242.,13.1),(246.,11.1),(248.,9.55),     ...
             (252.,7.94),(256.,6.61),(258.,5.07),(259.,3.89),     ...
             (263.,2.57),(300.,1.0e-8)
function abeta=(-3.088,0.0005),(-2.7869,0.001),(-2.0873,0.005),    ...
              (-1.7856,0.01),(-1.0807,0.05),(-0.7724,0.1),         ...
              (-0.0113,0.5),(0.3757,1.0),(0.8781,2.0),             ...
              (1.2945,3.0),(1.6939,4.0),(2.0926,5.0),(2.4941,6.0),...
              (2.8993,7.0),(3.3076,8.),(3.7184,9.),(4.1325,10.),   ...
              (4.5464,11.),(4.9628,12.),(5.3806,13.),              ...
              (5.7995,14.0),(6.2195,15.0),(6.6403,16.0),           ...
              (7.0619,17.0),(7.4842,18.0),(7.9071,19.0),           ...
              (8.3306,20.0),(8.7546,21.0)
renam time=dist
w=w0/60.0
rho0=1./(0.000486*t+0.891)
v0=4.0*w/rho0/pi/d0/d0
bia0=cop*4.0*frhe0/pi/d0/d0
them=0.01
eta=c4*(mn**3.5)
tp=tw+tg
te=-1.0
dth=0.0
the=0.0
x0=0.0
```

```
tc=0.0
t=t0
v=v0
d=d0
bia=bia0
c9=pi/w
dynamic
procedure rho=den(t,the)
       if(t.gt.240.) rho=1/(0.000486*t+0.891)
       if(t.le.240.) bho=(1.1018-0.00151*the)/(1.0-0.128*the)
       if(t.le.240.) rho=bh0-0.000455*t
endprocedure
mod=(1.0e8)*afgen(amod,t)
cp=0.33+0.0014*t
procedure vis,cl0,kout=v(t,eta,the,thi,tp)
       if(the.le.them) fac=1.0
       if(the.gt.them) fac=exp(cl2*((the/thi)**cl3))
       if(t.ge.tp) vis=eta*exp(c7/(t+273.))*fac
       if(t.gt.tp) kout=-1
       if(kout.gt.0) go to 89
       cl0=c4*exp(c7/(tp+273.))
       if(t.le.tp) kout=1
  89   continue
       tl=alog(1.0e35/(cl0*(mn**3.5)))
       ts=(8.86*tp-tl*(101.6-tp))/(tl+8.86)
       eta2=cl0*(mn**3.5)*fac
       if(t.lt.tm.and.t.ge.ts) vis=eta2*exp(cl1*(t-tp)/(t+101.6-tp))
       if(t.lt.ts) vis=1.0e35
endprocedure
ren=rhoa*v*d/mu
finer=w*(v0-v)
dfgra=w*g/v
fgrav=intgrl(0.0,dfgra)
zeta=8.*sqrt(dist/ren/d)
procedure cd,zata,beta=t(zeta,ren)
       if(zeta.le.0.0) go to 29
       zata=alog10(zeta)
       beta=afgen(abeta,zata)
       cd=4.0/beta/ren
       go to 30
  29   cd=0.0
  30   continue
endprocedure
dfdra=pi*cd*rhoa*v*v*d
fdrag=intgrl(0.0,dfdra)
dfrhe=(w*dv+dfdra-w*g/v)
frheo=intgrl(frhe0,dfrhe)
stres=frheo*rho*v/w
procedure dv=o(stres,vis,t,tp)
       dv=stres/vis
       if(t.lt.tg) dv=0.0
endprocedure
```

```
v=intgrl(v0,dv)
vm=v*0.6
dtim=1.0/v
tim=intgrl(0.0,dtim)
d=sqrt(4.0*w/rho/pi/v)
dm=d*10000.0
h=c1((rho*v*v/w)**c2)*((1.+(8.0*vy/vm)**2.)**c3)
ratel=c9*d*h*(ta-t)/cp
procedure dth,the,dthe,rate=g(te,vfa,to,t)
       if(t.ge.tm.and.te.le.0.0) go to 10
       if(t.le.tg) go to 10
       if(to.ge.thi) go to 10
       te=1.0
       if(t.ge.tm-1.0) go to 10
       const=c8*fa*fa/(tm-t)
       bl=c5*(t-tmax)*(t-tmax)/do/do
       trob=bl+const
       if(trob.gt.174.) trob=174.
       rate=rmax*exp(trob)
       dthe=rate/v
       sum=intgrl(0.0,dthe)
       dth=thi*n*rate*(sum**(n-1.0))/exp(sum**n)
       the=thi*(1.0-1.0/exp(sum**n))
       to=the
       go to 20
 10    dth=0.0
       the=to
 20    continue
endprocedure
dt=ratel+rate2
t=intgrl(t0,dt)
xc=the*100.
dbia=cop*dv*mod/v-bia*mod/v/vis
bia=intgrl(bia0,dbia)
bic=the*c6
bit=(1.0-the)*bia+bic
fa=bia/dna0
print vm,dm,xc,bit
method stiff
nosort
timer fintim=250.0,delmin=1.0e-12,prdel=1.0
end
stop
```

APPENDIX B

CSMP program for polypropylene melt spinning.

```
// red job ,zieminski,group=j41241,user=p92378,
//  password =     ,time=5,region=256k
/*route print decfile
//stepl exec csmp3
//sysin dd *
title polypropylene melt spinning simulation
initial
constant pi=3.1415926,g=980.,dna0=0.060,cl=6.85e-5,c2=0.259,c3=0.167
constant c4=2.00e-16,c5=-2.7725887,c6=0.085,c7=500..,c8=3.8e5,tp=100.
constant delh=59.0,cop=2.5e-10,cll=-8.86,cl2=9.210,tt=180.,cl3=2.
constant tmax=65.,do=60.,tm=180.,rmax=0.55,tg=-20..,n=1.,thi=0.65
constant d0=0.0762,t0=230.,ta=25.,mn=237980.,w0=1.68
constant rhoa=6.62e-5,mu=2.8e-4,vy=0.0,c7p=4800.,c7pp=6000.
constant tw=80.,tq=110.,frhe0=50.1
function amod=(-8.3,921.),(-2.2,784.),(3.9,668.),(10.0,546.),      ...
             (16.8,484.),(22.9,446.),(28.3,396.),(33.8,351.),     ...
             (39.2,323.),(44.7,287.),(52.1,265.),(58.9,234.)),    ...
             (64.4,216.),(69.8,208.),(75.9,184.),(82.7,170.),     ...
             (88.2,157.),(95.0,151.),(100.4,128.),(107.2,114.),   ...
             (114.,96.7),(121.5,79.),(127.6,57.2),(133.7,43.2),   ...
             (137.1,32.6),(139.2,25.6),(142.6,18.5),(146.6,12.4)),...
             (150.,8.29),(152.8,5.11),(153.4,3.15),(156.2,2.19),  ...
             (156.8,1.25),(159.6,0.712),(160.2,0.331),            ...
             (160.9,0.148),(300.,1.0e-25)
function abeta=(-3.088,0.0005),(-2.7869,0.001),(-2.0873,0.005),    ...
               (-1.7856,0.01),(-1.0807,0.05),(-0.7724,0.1),        ...
               (-0.0113,0.5),(0.3757,1.0),(0.8781,2.0),            ...
               (1.2945,3.0),(1.6939,4.0),(2.0926,5.0),(2.4941,6.0),...
               (2.8993,7.0),(3.3076,8.),(3.7184,9.),(4.1325,10.),  ...
               (4.5464,11.),(4.9628,12.),(5.3806,13.),             ...
               (5.7995,14.0),(6.2195,15.0),(6.6403,16.0),          ...
               (7.0619,17.0),(7.4842,18.0),(7.9071,19.0),          ...
               (8.3306,20.0),(8.7546,21.0)
renam time=dist
w=w0/60.0
rho0=1./(1.145+0.000903*t)
v0=4.0*w/rho0/pi/d0/d0
bia0=cop*4.0*frhe0/pi/d0/d0
them=0.01
eta=c4*(mn**3.55)
te=-1.0
dth=0.0
the=0.0
x0=0.0
tc=0.0
```

```
t=t0
v=v0
d=d0
eta2=eta*exp((c7-c7p)/(tt+273.))
eta3=eta2*exp((c7p-c7pp)/(tp+273.))
bia=bia0
c9=pi/w
dynamic
procedure rho=den(t,the)
       if(t.gt.180.) rho=1/(1.145+0.000903*t)
       if(t.le.180.) rho=1./(1.148-0.102*the+0.000903*t)
endprocedure
mod=(1.0e7)*afgen(amod,t)
cp=0.3669+0.00242*t
procedure vis,fac=v(t,eta,the,thi,eta2,eta3)
       if(the.le.them) fac=1.0
       if(the.gt.them) fac=exp(c12*((the/thi)**c13))
       if(t.ge.tt) vis=eta*exp(c7/(t+273.))*fac
       if(t.lt.tt) vis=eta2*exp(c7p/(t+273.))*fac
       if(t.lt.tp) vis=eta3*exp(c7pp/(t+273.))*fac
endprocedure
ren=rhoa*v*d/mu
finer=w*(v0-v)
dfgra=w*g/v
fgrav=intgrl(0.0,dfgra)
zeta=8.*sqrt(dist/ren/d)
procedure cd,zata,beta=t(zeta,ren)
       if(zeta.le.0.0) go to 29
       zata=alog10(zeta)
       beta=afgen(abeta,zata)
       cd=4.0/beta/ren
       go to 30
  29   cd=0.0
  30   continue
endprocedure
dfdra=pi*cd*rhoa*v*v*d
fdrag=intgrl(0.0,dfdra)
dfrhe=(w*dv+dfdra-w*g/v)
frheo=intgrl(frhe0,dfrhe)
stres=frheo*rho*v/w
procedure dv=o(stres,vis,t,tp)
       dv=stres/vis
       if(t.lt.tg) dv=0.0
endprocedure
v=intgrl(v0,dv)
vm=v*0.6
dtim=1.0/v
tim=intgrl(0.0,dtim)
d=sqrt(4.0*w/rho/pi/v)
dm=d*10000.0
h=c1((rho*v*v/w)**c2)*((1.+(8.0*vy/vm)**2.)**c3)
ratel=c9*d*h*(ta-t)/cp
```

```
procedure dth,the,dthe,rate=g(te,vfa,to,t)
       if(t.ge.tm.and.te.le.0.0) go to 10
       if(t.le.tg) go to 10
       if(to.ge.thi) go to 10
       te=1.0
       if(t.ge.tm-1.0) go to 10
       const=c8*fa*fa/(tm-t)
       bl=c5*(t-tmax)*(t-tmax)/do/do
       trob=bl+const
       if(trob.gt.174.) trob=174.
       rate=rmax*exp(trob)
       dthe=rate/v
       sum=intgrl(0.0,dthe)
       dth=thi*n*rate*(sum**(n-1.0))/exp(sum**n)
       the=thi*(1.0-1.0/exp(sum**n))
       to=the
       go to 20
 10    dth=0.0
       the=to
 20    continue
endprocedure
dt=rate1+rate2
t=intgrl(t0,dt)
xc=the*100.
dbia=cop*dv*mod/v-bia*mod/v/vis
bia=intgrl(bia0,dbia)
bic=the*c6
bit=(1.0-the)*bia+bic
fa=bia/dna0
print vm,dm,xc,bit
method stiff
nosort
timer fintim=230.0,delmin=1.0e-12,prdel=1.0
end
stop
```

# VITA

Kenneth F. Zieminski received an Associate in Applied Science degree in Chemistry from Erie Community College in 1976. In 1978, he acquired a Bachelor of Science in Chemical Engineering from the State University of New York at Buffalo. Further study was conducted at Purdue University where a Master of Science in Chemical Engineering was granted in 1980. He then pursued the Doctor of Philosophy degree in Polymer Engineering at the University of Tennessee - Knoxville. This quest was successful in 1986.